NASA CONTRACTOR REPORT

NASA CR-1180

NASA CR-1180

ANALYSIS OF PERFORMANCE CHARACTERISTICS IN GROUND EFFECT OF A LARGE-SCALE V/STOL MULTI-FAN-IN-WING TRANSPORT MODEL

by R. J. Oberto, D. J. Renselaer, and D. L. Alfano

Prepared by
NORTH AMERICAN ROCKWELL CORPORATION
Los Angeles, Calif.
for

NATIONAL AERONAUTICS AND SPACE ADMINISTRATION • WASHINGTON, D. C. • OCTOBER 1968

NASA CR-1180

ANALYSIS OF PERFORMANCE CHARACTERISTICS IN GROUND EFFECT OF A LARGE-SCALE V/STOL MULTI-FAN-IN-WING TRANSPORT MODEL

By R. J. Oberto, D. J. Renselaer, and D. L. Alfano

Prepared under Contract No. NAS 2-4352 by
NORTH AMERICAN ROCKWELL CORPORATION
Los Angeles, Calif.

for

NATIONAL AERONAUTICS AND SPACE ADMINISTRATION

For sale by the Clearinghouse for Federal Scientific and Technical Information
Springfield, Virginia 22151 – CFSTI price $3.00

FOREWORD

The performance data described in this report were obtained from tests of a large-scale multi-fan-in-wing V/STOL transport model conducted at the NASA Ames Research Center VTOL Test Facility. Tests were conducted by North American Rockwell Corporation, Los Angeles Division, and NASA Ames Research Center in a cooperative program during July 1966.

The analysis of data and preparation of this report were performed under NASA Ames Research Center Contract NAS 2-4352 during the period May through November 1967.

ABSTRACT

Performance data obtained from static tests in ground effect of a large multi-fan-in-wing V/STOL Transport Model, conducted by North American Rockwell Corporation and NASA-Ames in a cooperative program, are described. The data include plots of propulsion systems performance, force and moment characteristics, and induced thermal conditions. Major test variables were height above ground plane, lift/cruise (L/C) nozzle angle, fan louver angle, fan speed, L/C engine power, and operations with L/C nozzles and fans in combination, L/C nozzles alone, and fans alone.

TABLE OF CONTENTS

LIST OF ILLUSTRATIONS

LIST OF TABLES

NOTATION

A	Area (square feet)
Btu	British thermal unit
C_L	Lift coefficient
D	Diameter (feet)
EGT	Exhaust gas temperature
F	Thrust (pounds)
L	Total lift on model (pounds)
L/C	Lift/cruise
M	Mach number or pitching moment (foot-pounds)
MAC	Mean aerodynamic chord
MPH	Miles per hour
N	Engine speed (revolutions per minute)
N_F	Fan speed (revolutions per minute)
P	Static pressure
P_T	Total pressure (pounds per square foot)
R	Gas constant for air (53.35 ft-lb_f/lb_m-°R)
rpm	Revolutions per minute
T	Temperature, °R or as noted; or total forward force on model (pounds)
V	Velocity (feet per second)
g	Gravitational constant (32.2 ft/sec^2)
h	Model Height above ground or ground distance, measured from fuselage lower surface (feet); or heat transfer coefficient (But/Hr ft^2 °F)
q	Dynamic pressure (pounds per square foot)

α	Angle of attack, measured at fuselage lower surface (degrees)
β_V	Fan exit louver angle (degrees)
γ	Ratio of specific heats = 1.4
δ	Corrected total pressure (P_T/14.696 psi)
δ_N	Lift/cruise engine nozzle angle (degrees)
η_R	Inlet total pressure recovery ($P_{T_{10}}/P_{T_O}$)
e	Corrected total temperature (T/519° R)

SUBSCRIPTS

0	Ambient
10	Fan inlet
11	Fan discharge
ave	Average
EE	Excess exhaust
e	Excess exhaust or lift/cruise nozzle exit
f, F	fan
FAN	Fan
g	Gross
Max	Maximum
Min	Minimum
N	L/C Nozzle
S	Static
GG	Gas generator

ANALYSIS OF PERFORMANCE CHARACTERISTICS IN GROUND EFFECT OF A LARGE-SCALE V/STOL MULTI-FAN-IN-WING TRANSPORT MODEL

By R. J. Oberto, D. J. Renselaer, D. L. Alfano

SUMMARY

An investigation has been conducted to determine the performance characteristics of a large-scale multi-fan-in-wing V/STOL transport model in ground effect. The model had a high-mounted 20-degree sweptback wing with three 36-inch-diameter, General Electric X-376 tip-turbine lift fans spanwise in each wing panel, and a 12.5-inch-diameter lift-cruise (L/C) nozzle extending from each side of the fuselage, slightly below and forward of the wing. Four YJ85-5 engines, mounted inside the fuselage, provided propulsion power: two in the upper-center fuselage for the fans, and two in the upper-forward fuselage for the (L/C) nozzles. Engine inlets were located on the top side of the fuselage: one above the wing, and the other above the forward fuselage.

Tests were performed at the NASA Ames Research Center VTOL Test Facility. A scissors jacking system provided height and angle-of-attack adjustments relative to the test stand's 78 x 80-foot steel ground plane, Load cells contained at three support points of the model provided force and moment measurements. Remotely controllable sets of louvers or vanes on the discharge side of each fan enabled fan exhaust to be vectored from 15 degrees forward to 80 degrees aft of vertical. Lift-cruise nozzles were manually vectorable from 15 degrees forward to 90 degrees aft of vertical.

Tests with symmetrical combinations of two, four, and six fans alone; L/C nozzles alone; and combined operation of fans and L/C nozzles were performed. Primary test variables were model height, fan louver angle, L/C nozzle angle, fan speed, L/C engine power, and angle of attack.

Test results indicate force and pitching moment characteristics, propulsion component performance, and induced thermal conditions.

INTRODUCTION

Knowledge and understanding of the operational problems of VTOL aircraft in close proximity to the ground are essential to VTOL aircraft development. Operational problems such as ingestion of hot gases by propulsion components can result in critical thrust losses, engine overtemperature, or engine stall

conditions. Improper location of multiple propulsion components in an aircraft configuration result in thrust losses due to interference effects. Downwash interactions in near-ground operation can cause negative or variable positive and negative lift effects and moment imbalance on the aircraft. These adverse effects can be minimized by the choice of aircraft configuration. Known losses which persist must be compensated for and acceptable takeoff and landing techniques must be developed to avoid the excessive development of adverse conditions.

For VTOL aircraft intended for operation from unprepared, unclean, natural sites, additional problems to be considered are foreign object ingestion, obscured vision from induced dust clouds, ground erosion, and adverse effects on surrounding facilities and personnel. These problems may be minimized by the choice of aircraft configuration and by the employment of operating techniques.

Investigation of these problems using large-scale models and propulsion components provides a realistic appraisal of performance. Test results so obtained can provide a real basis for design decision. With these advantages in mind, the North American Rockwell Corporation joined in a cooperative program with NASA-Ames to investigate the near-ground performance characteristics of the large-scale model of a multi-fan-in-wing V/STOL transport aircraft at the Ames outdoor VTOL test facility.

The model incorporated three tip-turbine fans in each wing panel and a single side-mounted lift/cruise (L/C) nozzle on each side of the forward fuselage. A total of four YJ85-5 engines mounted inside the fuselage provided propulsive power: two engines generating gas for driving the six tip-turbine lift fans and two engines for L/C nozzle operation. Engine inlets were located on top of the fuselage.

Results presented indicate model force and moment characteristics, propulsion system performance, and induced thermal conditions. Major test variables were ground height, fan louver angle, L/C nozzle angle, fan speed, L/C engine power, angle of attack, operations with fans alone, L/C nozzles alone, and combined fans and L/C nozzles.

SECTION I

MODEL AND APPARATUS

Model

A photograph of the model mounted on the outdoor static test stand at the NASA Ames Research Center is shown in figure 1. Figure 2 is a general arrangement drawing of the model with pertinent dimensions. The model, constructed of steel, had an overall length of about 48 feet, a wing span of nearly 36 feet, and a weight of approximately 37,000 pounds.

Wing. - The wing was mounted high on the fuselage. The wing had an aspect ratio of 3.43, a taper ratio of 0.47, a dihedral of -6 degrees, a 20 degree sweepback at the quarter chord line, and an area of 368.5 square feet. Wing incidence was 2.92 degrees at the root and 0.22 at the tip. The airfoil section was a NACA 65A211. An 18 percent chord single-slotted trailing edge flap extended in two 60-inch and one 56-inch segment from the fuselage to the wing tip.

Fuselage. - The fuselage, which was flat sided with rounded corners, was 427.7 inches long with a maximum depth of 88 inches and a maximum width of 69.6 inches. The inlets for the lift-cruise engines were located in the forward fuselage while the inlets for the engines driving the lift fans were located above the fuselage in the wing center section. The structure simulating the wheel fairings and wheels was detachable.

Tail. - The horizontal tail had an aspect ratio of 3.27, a taper ratio of 0.33, a dihedral of 22.5 degrees, an area of 96.07 square feet, and a span of 17.71 feet. The horizontal tail was pivoted about the 57 percent chord line. The vertical tail had an aspect ratio of 1.17, a taper ratio of 0.46, an area of 50.61 square feet, and a 7.67-foot span.

Propulsion System

Four YJ85-5 turbojet engines (two for simulating lift-cruise engines and two for driving the six General Electric X-376 lift fans in the wing) were installed in the fuselage of the model.

Lift-cruise engines. - Two YJ85-5 engines were mounted in the forward fuselage and exhausted through nozzles on each side of the fuselage. The nozzles were approximately 12.5 inches in diameter and were vectorable from

15 degrees forward of vertical to 90 degrees aft (horizontal). The center of rotation of the nozzles was at fuselage station 120.75 and waterline 160.50 as shown in figure 2.

Lift fan. - Six X-376 lift fans were completely enclosed in the wing. The fans were driven by the exhaust from two YJ85-5 turbojet engines. Each engine exhausted into a plenum chamber. Ducting ran from each plenum chamber to drive the three fans in each wing panel as illustrated in figure 3. Remotely controllable trimmer valves were located in the ducting from the plenum chamber to adjust the exhaust flow to each fan for control of fan speed and engine exhaust gas temperature. Each plenum chamber also had an exhaust tailpipe including a trimmer valve to allow excess exhaust to be dumped overboard.

The X-376 fans were high thrust-to-weight ratio, single-stage, tip-turbine-driven lift fans. The fan tip diameter was 36.1 inches with a hub diameter of 16.2 inches. Fan design speed at sea level was 4074 rpm at a pressure ratio of 1.1. The tip turbine is located radially outboard of the fan tip and absorbs power over approximately 167 degrees of the circumferential turbine arc. The turbine scroll net entrance flow area was a nominal 34 square inches. The fans rotated in a clockwise direction when viewed from above the model.

A cascade of 14 exit vanes or louvers was mounted in the exhaust of each fan. The louvers were used for vectoring the fan exhaust and for closing the wing undersurface. Each louver airfoil had a chord length of 4.06 inches, a maximum thickness of 10 percent chord at 20 percent chord, and had a maximum of 2.3 percent chord camber of the mean line at 35 percent chord. The louvers spanned the rotor and the tip turbine sections of the fan. Louver deflections of -15 degrees to 80 degrees were attainable.

The inboard fan centerlines were located at wing station 65.90 (30.7 percent semispan), fuselage station 234.44 (44 percent of local wing chord). The center fan centerlines were located at wing station 116.90 (54.4 percent semispan), fuselage station 246.53 (42 percent of local wing chord). The outboard fan centerlines were located at wing station 67.90 (78.2 percent semispan), and fuselage station 258.62 (39 percent of local wing chord). The plane of the center and outboard fan was parallel to the wing reference plane. The inboard fan was tilted 3 degrees 35 minutes front up.

Test Facility

The test program was conducted at the NASA-Ames Research Center Static Test Facility. The test facility provided a three-point support of the

model: near the midspan of each wing, and at an aft location under the tail. The three-point support system contained load cells for measurement of forces and moments. A scissors jacking system provided height and angle of attack adjustments of the model relative to the ground plane. The ground plane for the test stand was a steel deck approximately 80 feet square. Instrumentation, power, and control lines were routed from the model underneath the steel deck to control panels and data recorders located in several house trailers adjacent to the test stand.

Instrumentation

Force and Moments. - Lift, thrust, and pitching moment data were measured by the static facility support strut load cells. Mounting pads on the model provided strut tread of 187 inches under the wings, and a spacing of 158 inches between the main and tail strut attachments. The tail strut attach point was 39.6 inches below the main strut attach point at model angle of attack of 0 degrees.

Controls. - The operation of the four YJ85-5 jet engines and the six lift fans was remotely controlled. Each YJ85-5 jet engine was controlled using a remote control throttle actuator. Each engine was instrumented with a tachometer, EGT harness, fuel and oil pressure sensors, oil temperature sensors, throttle position potentiometer, and a vibration pickup. These data were displayed on the engine control panel.

The six lift fans were controlled using trimmer valves in the hot gas ducting in combination with valves in the excess exhaust ducting. These valves were remotely actuated to obtain matched operation of the fans. Each fan was instrumented to measure rpm, bearing temperature, front frame temperature, and fan vibration. These data were displayed on a control panel.

The EGT and rpm of each engine and the rpm of each fan were recorded for each data point.

The model was equipped with remote control actuation of the fan louvers. The position of the louvers of each wing fan was measured by autosyn transmitters and displayed on a control panel.

Temperature Measurement. - Thermocouples installed on the model, ground plane, and in the flow field were located as shown in figures 4 through 9. All thermocouples were chromel-alumel wire (30 gage). The calorimeters installed on the model were similar in design to that shown in figure 10. These

calorimeters were for the purpose of determining structural heating rates and heat transfer coefficients.

Temperature data recording equipment included three 30-channel oscillographs and four 24-channel Brown Recorders. Engine inlet (compressor face), lift fan inlet, and calorimeter temperatures were recorded by oscillographs to provide continuous temperature-time traces. Due to equipment malfunction, most of these results were lost. All other temperatures were recorded by Brown Recorders which provided a point reading for each thermocouple at approximately 30-second intervals.

All temperature recorders were started prior to engine start for each test run to establish a "zero" reading for each thermocouple. In the case of a cold start test or first-run-of-the-day test, the "zero" reading was essentially equivalent to ambient temperature. This method was used to establish a reference temperature line for each oscillograph temperature trace. To minimize drift or shifting of the temperature trace resulting from oscillograph warmup, the oscillographs were maintained in a standby operating (warmed up) condition between test runs. Each oscillograph channel was calibrated by measuring the amount of deflection when alternately recording the temperature of ice water and boiling water.

Estimates of engine inlet temperatures and fan inlet temperatures were provided by Brown Recorder temperature readings from the array of thermocouples located forward of the engine inlets and above the wing leading edge.

Pressure Measurement. - The model was instrumented with 398 total and static pressure taps for the purpose of measuring fuselage, wing, and fan entrance bellmouth static pressures and gas generator inlet, fan inlet and discharge, scroll entrance, L/C nozzle exit, and excess exhaust nozzle total pressures. Additional pressure instrumentation included 10 total pressure probes mounted on the model and 38 flow field rake pressure probes. Pressures were recorded during each test point by means of 48-port scanivalves. The scanivalves were installed in the forward fuselage of the model, and each scanivalve used a pressure transducer of a given pressure range. The pressure transducer ranges were $\pm$2-1/2, $\pm$5, and $\pm$25 psid depending on the measurements of the particular scanivalve.

The 10 total pressure probes which were directionally adjustable were mounted on the fuselage to measure surface velocities in the vicinity of the calorimeters for the purpose of further defining the structural thermal environment. The 38 rake-pressure probes were contained in four total head rakes. Two of these rakes were 6-foot horizontal rakes with adjustable height for the purpose of measuring the model propulsion downwash. The other two rakes were 2-foot vertical rakes, with adjustable height, for measuring ground velocity profiles. Locations of these rakes and probes are shown in figure 8.

The pressure instrumentation of the lift fans were restricted to the three fans installed in the right-hand wing panel. These fans were designated and referred to as inboard, center, and outboard with respect to wing station location.

Total pressure instrumentation was provided at the fan face (rotor inlet) on the center and outboard fans, but not on the inboard fan since this fan, as well as the left-hand inboard fan, was on loan to the test program from another agency.

Fan discharge total pressure instrumentation (downstream of fan stators) was provided for all three fans. In addition, static pressure taps at the fan discharge were located at the hub and perimeter.

The fan bellmouth inlets of the three right-hand wing fans were instrumented with static pressure taps at circumferential locations along various fan radian lines. At each radian line, there were from one to four static taps located angularly on the bellmouth, from zero degrees at the top to 90 degrees in the plane of the fan face.

Hub static pressure taps were provided at the fan inlets of the center and outboard fans. These taps were placed in the plane of the rakes circumferentially to correspond with the total pressure rake positions.

Other static and total pressure instrumentation was provided at the fan scroll entrance to the center and outboard fans, at the L/C nozzle exit on the right side, and in the air inlet and exhaust plenum of the right-hand gas generator. Both right- and left-side excess exhaust nozzles incorporated pressure rakes.

Pressure measurements were recorded by an automatic data gathering system which stored the data on punched cards. In addition, eight strip chart recorders were provided for visual monitoring of the individual pressures. The automatic data system was capable of reading and recording all pressures in about 50 seconds.

SECTION II

TEST PROGRAM

A total of 55 test runs, as described in table I, were performed at the NASA-Ames Static Test Facility. Each test run comprised a series of data points. Test run number 10, for example, consisted of data points 10.1 through 10.8. Data points 10.1 through 10.4 correspond respectively to variations in fan louver angle, βv, of 0, 10, 20, and 30 degrees in the order listed in table I. Data points 10.5 through 10.8 correspond respectively to settings in L/C power of 80, 85, and 90 percent as listed. Wind direction listed in table I was measured clockwise from the heading of model such that 0 degrees indicates a head wind.

The 55 test runs required 10 days of testing. The testing period during each day was usually limited to the early morning hours when wind velocities were less than 6 miles per hour. Wind velocities during late morning hours usually increased to levels above 10 miles per hour and persisted for the remainder of the day.

The test procedure was to start the YJ85-5 engines one at a time and to increase power to 50 percent. The engine starting began with the left-hand L/C engine and was followed sequentially by the right-hand L/C engine, left-hand fan engine and fans, and right-hand fan engine and fans. Each engine start to 50 percent power required from 30 to 60 seconds. After observing all engines to be functioning properly, the L/C engines were set to test power conditions. This was followed by increasing power on the fan engines and setting fan speed to the required level. Each of these operations required approximately 30 seconds. The subsequent test run data points involving a change in the test variable, such as positioning of fan louver angle at settings of 0, 10, 20, and 30 degrees, were allowed a time interval of approximately 60 seconds for data recording. The shutdown time between test runs varied from 20 minutes to one hour, allowing for adjustment in model height, angle of attack, L/C nozzle angle, and servicing of the model and test equipment.

Minimum and maximum model heights of 2.65 feet and 9.0 feet represent the physical constraints of the test facility. The model's wheels when at the lowest model height of 2.65 feet were approximately 13.8 inches above ground plane as shown in figure 7.

Note that percent engine or L/C nozzle power as used herein is in actuality percent engine speed. For example, to set L/C engine power at 90 percent means that the engine speed is 90 percent of maximum rated rpm.

It should also be noted that test conditions in constrained hover with fan louvers and L/C nozzles vectored aft are not generally compatible with real hovering situations. Vectoring the nozzles and louvers aft would result in forward motion. The test performed in the program at the lowest model height at various vectored angles of the nozzles and fan louvers may be considered representative of an engine test, a power buildup prior to takeoff, and of the beginning of a short runway takeoff. Operations at other model heights with vectored nozzles and fan louvers may represent momentary conditions at the start of forward flight after a vertical takeoff.

SECTION III

TEST DATA AND RESULTS

Test data and results as presented cover three main areas of interest: force and moment characteristics, propulsion system component performance, and induced thermal conditions.

Force and moment characteristics include lift, forward thrust, and pitching moment data as a function of fan speed, engine power, fan louver angle, angle of attack, model height, L/C nozzle angle; and various propulsion configuration such as two, four, and six fans alone, L/C nozzles alone, and combined operation of fans and L/C nozzles.

The data relating to induced thermal condition concern hot gas ingestion, flow field air temperatures, structure temperatures, ground surface temperatures, and heating rates. Some flow field pressure data are also presented. Propulsion system component performance data indicates fan inlet and discharge pressure distributions, fan characteristics, L/C engine thrust, and fan gas generator inlet performance.

Force and Moment Characteristics

Operations with Lift Fans Alone. - The effect of fan speed on lift, forward thrust, and pitching moment is shown in figure 11 for model heights of 2.65, 4.45, and 9.00 feet and a fan exit louver angle of zero degrees (vertical position). Figure 11 also shows the effect of fan speed at a ground height of 2.65 and fan exit louver angle of 30 degrees. In all cases, the variation of lift, forward thrust, and pitching moment is nearly linear with the fan speed squared.

The variation in lift, forward thrust, and pitching moment with fan exit louver angle is shown in figure 12 for model heights of 2.65, 4.45, and 9.0 feet. Also shown are cos β_V and sin β_V relations which indicate the variations in lift and forward thrust which would be obtained by resolving the lift obtained at β_V = 0 degrees into components. With these relations, it is assumed that there is no loss in the magnitude of the fan thrust vector as the exit louver angle is changed and that the direction of this vector is equal to the louver angle setting. Figure 12 indicates lift to be less than the cos β_V relation and forward thrust to be slightly greater than the sin β_V relation. The reason for these differences has not been isolated. A possible explanation could be that aerodynamic interference effects caused the total fan force vector to be vectored through a greater angle than indicated by the physical deflection of the fan louvers. Calculations also show

that total fan force vector is approximately 10 to 15 percent less at $\beta_V = 30$ degrees than at $\beta_V = 0$ degrees which may be attributed perhaps to a decrease in fan exit flow area as the louvers are moved aft. A small forward thrust existed at $\beta_V = 0$ amounting to approximately 10 percent of the lift. This thrust is believed to result from the asymmetric air-foil section of the louvers which have a positive C_L value in forward direction at $\beta_V = 0$.

The pitching moment is varied by the louver angle changes from a nose-down value at $\beta_V = 0$ to nose-up value at higher angles about the test reference point of 15.65 percent MAC. This is especially the case at a model height of 2.65 feet, where the center of pressure varies from M/L = 1.0 foot aft of the reference point to 0.2 foot forward of this point. This represents a total travel in excess of 11 percent MAC.

Figure 13 shows the effect of angle of attack of the fuselage at model heights of 4.45 and 9.00 feet. Computed slopes are used for the fairings of the lift and the forward thrust change with α. Equations used are, expressed in radians:

$$\frac{\left(\frac{dL}{d\alpha}\right)}{L_{\alpha=0}} = \frac{L_{\alpha=0,\beta_V=0} \frac{d\cos(\beta_V - \alpha)}{d\alpha}}{L_{\alpha=0,\beta_V=0} \cos\beta_V} = \frac{\sin(\beta_V - \alpha)}{\cos\beta_V} \approx \tan\beta_V$$

$$\frac{\left(\frac{dT}{d\alpha}\right)}{L_{\alpha=0}} = \frac{L_{\alpha=0,\beta_V=0} \frac{d \sin(\beta_V - \alpha)}{d\alpha}}{L_{\alpha=0,\beta_V=0} \cos\beta_V} = \frac{-\cos(\beta_V - \alpha)}{\cos\beta_V} \approx -1$$

Reasonable agreement between the estimates and the test data exists.

The pitching moment variation with angle of attack is less stable at a model height of 4.45 than at 9.00 feet. For the reference point used in this presentation, $dM/d\alpha$ actually reverses sign from negative (stable) to positive (unstable) as the model height is decreased. The fact that the pitching moment derivative was not zero at the 9-foot height at zero forward velocity indicates that ground interference is still present.

The lift, forward thrust, and pitching moment versus number of fans operating is presented in figure 14 for louver angles β_V of 0 degrees and 30 degrees. In each case, the variations of the forces and the moment can be presented by straight lines as a function of number of fans operating. Thus, no significant mutual interference effects between the fans are evident on the basis of balance data.

The effects of excess nozzle thrust, F_{gEE}, resulting from the excess exhaust nozzles located at the rear of the model have been subtracted from all of the lift, thrust, and pitching moment data.

Decreasing model height from 9.0 to 2.65 feet, when all six fans are operating, results in approximately a 5 percent increase in the lift at a model height of 6 feet (figure 15), and about a 3 percent decrease below the lift of the 9-foot height at heights below 6 feet. With two or four fans operating, the peak at the 6-foot height does not occur.

When the model height was decreased with two and four fans operating, the pitching moment first changed to nose-up direction and was then followed by a nose-down direction at an angle of attack of 0 degrees. For a six-fan operation, the pitching moment tends to change more rapidly in the nose-down direction.

A comparison of lift, forward thrust, and pitching moment data is made in figure 16 for wheel fairings (includes wheels) on and off. The trend of the lift variation with model height for β_V of 0 degrees is about the same with and without the fairings; however, the magnitudes are different. At model heights of 2.65 and 9.0 feet, the lift is approximately 3 percent higher with the fairings off. The peak lift values at the 6-foot distance appear unchanged whether the fairings are on or off.

The forward thrust increases slightly when the wheel fairings are removed from the model except at the lowest model height.

Removal of the wheel fairings did not significantly change the pitching moment characteristics at angles of attack of 0 degrees and 5 degrees.

Operation with L/C Nozzles Only. - Lift, forward thrust, and pitching moment characteristics due to operation of L/C nozzles only are presented in figure 17 on a logarithmic scale as a function of L/C engine rpm for two model heights. The logarithmic scale was used for easier presentation of the data. The curves are nearly straight lines and proportionality is indicated by parallel shifts in the curves.

All curves shown are parallel for varying L/C engine power. Thus proportionality is indicated between lift, forward thrust, and pitching moments for single and dual nozzle operation throughout the L/C engine power range and for the ground distances shown.

The effect of varying model height can also be discussed on the basis of figure 17. At the model height of 9.00 feet, the lift from both nozzles together was equal to the sum of the single nozzle lifts measured. This indicates no interference effects between the nozzles. At the 2.65-foot height, however, the lift from the left-hand and right-hand nozzle at constant engine rpm is less than at the 9.0-foot height, indicating either a negative lift (suck-down) or a thrust loss at the lower height. The pitching moment for both nozzles operating was equal to model heights of 2.65 and 9.00 feet, indicating no interference effects on the pitching moment as a function of model height. The difference in forward thrust between these two ground distances is small. A presentation of the effect of varying model height with a nozzle angle of δ_N = 15 degrees is shown in figure 18. The above trends appear to apply also for this nozzle angle.

Test data as a function of nozzle angle are presented in figure 19 for 90 and 85 percent L/C engine rpm. As expected, lift follows a cos δ_N relation and the forward thrust a sin δ_N relation.

The effect of angle of attack on lift, forward thrust, and pitching moment is shown in figure 20 for a model height of 9.0 feet and a L/C nozzle angle of 15 degrees. The lift and thrust curves have slopes computed from:

$$\frac{\frac{dL}{d\alpha}}{L_{\alpha=0}} = \frac{\sin(\delta_N - \alpha)}{\cos \delta_N} \approx \tan \delta_N$$

$$\frac{\frac{dT}{d\alpha}}{L_{\alpha=0}} = \frac{-\cos(\delta_N - \alpha)}{\cos \delta_N} \approx -1$$

The small deviation of the test points from these curves is considered normal scatter.

The pitching moment variation with angle of attack was stable at a model height of 9.0 feet, similar to the pitching moment behavior when only wing fans were operating. Again, the fact that the pitching moment varies with angle of attack at this zero forward velocity of the airplane indicates that ground effect is still existing at this model height.

Simultaneous Operation of Fans and L/C Nozzles. - Lift, forward thrust, and pitching moment data for combined operation of fans and the L/C nozzles is presented in figure 21. These data are also compared with corresponding data for six fans operating alone.

Force and moment increments due to L/C nozzles as obtained from the differences between the curves in figure 21 are listed in the following table. The table also lists for comparison purposes the force and moment data obtained from tests with L/C nozzles alone.

h	δ_N	β_V		(L/C Nozzles + Fans) Minus Fans Alone	L/C Nozzles Alone
2.65	45	0	Lift	2350 lb	2050 lb
			Thrust	1950 lb	2400 lb
			Moment	2300 ft-lb	4000 ft-lb
6.00	15	0	Lift	3250 lb	3800 lb
			Thrust	1050 lb	1000 lb
			Moment	(no data)	7000 ft-lb
9.00	15	0	Lift	3250 lb	3600 lb
			Thrust	800 lb	950 lb
			Moment	6200 ft-lb	7500 ft-lb

Except for the pitching moment at a nozzle angle of 45 degrees, the differences shown between the two last columns of the above table may be considered test scatter rather than interference effects.

Deflection of the louvers result in an overall lift loss that follows approximately a $\cos \beta_V$ relation (figure 22). A fan thrust of 6700 pounds was used in the presentation of the computed $\cos \beta_V$ relation, based on the lift measured when the fans were operated alone. The lift loss was less than for the fans operating alone. This reduced lift loss may have been caused by a positive interference lift from the L/C nozzles.

The forward thrust increase with increasing louver angle is slightly in excess of a sin β_V relation. This is similar to operation with fans alone. Also, the moment variation with louver angle is similar to operation with fans alone.

The effect of L/C nozzle rotation on lift and forward thrust can be presented approximately by a cos δ_N and sin δ_N relation (figure 23). The computed cosine and sine relations are based on a L/C nozzle force of 3700 pounds based on test data obtained with L/C nozzles alone.

Moment characteristics show a similar trend with and without lift fans operating; i.e., a slight increase in nose-up pitching moment is found when the nozzle angle δ_N is increased from zero to 20 degrees, followed by a gradual decrease of the moment for greater values of δ_N.

Data pertaining to an angle of attack change from 0 degrees to 5 degrees are given in figure 24. The slopes of the curves shown for lift and forward thrust were computed. Equations used were derived from:

$$\frac{\frac{dL}{d\alpha}}{L_{\alpha=0}} = \frac{\left[L_{F_{\alpha=0,\beta_V=0}}\right]\left[\frac{d\cos(\beta_V - \alpha)}{d\alpha}\right] + \left[L_{N_{\alpha=0,\delta_N=0}}\right]\left[\frac{d\cos(\delta_N - \alpha)}{d\alpha}\right]}{L_{F_{\alpha=0,\beta_V=0}}\cos\beta_V + L_{N_{\alpha=0,\delta_N=0}}\cos\delta_N}$$

$$\frac{\frac{dT}{d\alpha}}{L_{\alpha=0}} = \frac{\left[L_{F_{\alpha=0,\beta_V=0}}\right]\left[\frac{d\sin(\beta_V - \alpha)}{d\alpha}\right] + \left[L_{N_{\alpha=0,\delta_N=0}}\right]\left[\frac{d\sin(\delta_N - \alpha)}{d\alpha}\right]}{L_{F_{\alpha=0,\beta_V=0}}\cos\beta_V + L_{N_{\alpha=0,\delta_N=0}}\cos\delta_N}$$

Differentiation of the appropriate terms and then setting $\alpha = 0$ results in the following expressions for $\delta_N = 0$:

$$\frac{\frac{dL}{d\alpha}}{L_{\alpha=0}} = \frac{\sin\beta_V + \left(\frac{L_N}{L_F}\right)_{\alpha=0,\beta_V=0,\delta_N=0}}{\cos\beta_V + \left(\frac{L_N}{L_F}\right)_{\alpha=0,\beta_V=0,\delta_N=0}} \quad \text{(per radian)}$$

$$\frac{\frac{dT}{d\alpha}}{L_{\alpha=0}} = -1$$

In these equations, L_N is the lift from the cruise nozzles alone, and L_F is the lift from fans alone.

These values of L_N and L_F are derived from tests with L/C nozzle operations alone and operation of fans alone, i.e.,

$$\left(\frac{L_N}{L_F}\right)_{\alpha = 0,\ \beta_V = 0,\ \delta_N = 0} = \frac{3700}{6700}$$

The test data shows only small deviations from these computed slopes, which are attributable to normal scatter.

The pitching moment variation with angle of attack has an unstable slope at the low model heights similar to operation with fans alone or L/C nozzles alone. At increased model heights, the slope tends to reverse again in a manner similar to the operation with fans alone or L/C nozzles alone.

Decreasing the model height below 6 feet with wheel fairings installed increases lift as shown in figure 25. The lift loss that was shown previously with the fans operating alone does not materialize as soon when the L/C nozzles are operated in combination with the fans.

The forward thrust is relatively unaffected by model height similar to data shown before for the fans or L/C nozzles operating alone. Also, the pitching moment characteristics were similar except that the nose-down moment change with decreasing model height occurs at a lower model height.

Removal of the wheel fairings increased lift at the model height of 9.00 feet, but caused a decrease of lift at lower model heights (figure 25). This trend differs from that found previously for operation with fans alone where removal of wheel fairing resulted in a lift increase at both high and low model heights.

Removal of the wheel fairings resulted in an increase of forward thrust similar to operation with fans alone. The pitching moment is relatively unaffected by removal of wheel fairings except at the lowest ground distance.

Propulsion System Component Performance

Fan Inlet Pressure Recovery and Distortion. - Excellent fan inlet performance is indicated by the high total pressure recovery and low total pressure distortion levels at the fan face. Distortion is defined as the ratio of the difference between maximum and minimum total pressure to the average total pressure at the fan face. Total pressure recovery was above 99 percent for all test points investigated and total pressure distortion did not exceed 2-1/2 percent. Plots of recovery and distortion versus corrected fan speed are shown in figure 27 for both four- and six-fan

operation. The slight reduction in inlet performance with fan speed is due to the losses associated with the increasing flow velocity. The consistently high levels of total pressure recovery and low levels of distortion for all test runs indicate that changes in ground height and fan exit louver angle are insignificant in affecting inlet performance.

Fan Inlet Static Pressure Distributions. - The three right-hand wing fan bellmouth inlets were instrumented with static pressure taps as shown in table III to aid the investigation of flow behavior at the fan face. Pressure taps were located along the inlet surface from the top of the inlet near the junction of the bellmouth and upper surface of the wing (0-degree position) to the plane of the fan inlet pressure rakes (90-degree position). The center fan had four taps at each of five circumferential positions. The number of pressure taps at the inboard and outboard fans were more limited so that only cursory data analysis and comparisons were made with the inlet flow field at the center fan. The fan bellmouth static pressure distribution plots are shown in figures 28 through 32.

Increasing fan speed increases air velocity into the fan, resulting in a decrease in the bellmouth static pressure level. Figures 28 and 29 show the center fan bellmouth static pressure distributions for four- and six-fan operation for fan speeds of 2000 to 3600 rpm. Four-fan operation involved the center and inboard fans only. Data for four- and six-fan operation show similar trends.

Ideally, for a fan operating in a stationary vehicle, the flow into the inlet should reach a maximum velocity at the fan face where the physical flow area is a minimum. This would result in continuously decreasing static pressures over the bellmouth lip. However, for both the 0-degree and 290-degree circumferential positions, the static pressure reaches a minimum slightly above the fan face. This deviation from expected static pressures may be caused by leakage of hot gases from the tip turbine scroll into the fan face. The scroll for each fan covers approximately 180 degrees of the fan perimeter as shown in figure 26. For the center fan, this arc includes the 0-degree, 20-degree, and 290-degree radial positions. The high static pressure readings at the fan face for the 0-degree and 290-degree radians may be attributed to the disturbing effect of tip turbine leakage gases in the vicinity of these pressure taps. The 20-degree radial position, which is at the extremity of the tip turbine scroll arc, shows that static pressures are not affected by leakage.

The static pressure distributions at the 110- and 200-degree radians show a continual decrease into the fan face and are similar to the distributions occuring at the 20-degree fan radian. This implies that the portion of the inlet flow field which is not influenced by turbine scroll leakage is very nearly uniform. Further inspection of these data indicates that at the perimeter of the fan face, the maximum velocity probably occurs at about the 90-degree fan radian.

A comparison of the right-hand center fan bellmouth pressures between four- and six-fan operation shows a generally slightly lower pressure level at the plane of the fan face in four-fan operation. Since inlet total pressure recoveries are equal in the two cases, the outboard fan represents a "sink" which detracts slightly from the center fan performance in six-fan operation.

Bellmouth static pressure data for the inboard and outboard fans (figures 30 and 31) which lack static pressure data at the 60-degree position limits interpretation of performance. The data, however, appear to follow a pattern similar to that of the center fan. For the inboard fan, the possibility of turbine scroll leakage is apparent at the 0- and 270-degree fan radians.

A comparison of the bellmouth static pressure distributions at the inboard fan for four- and six-fan operation (figure 30) indicates that operation of an adjacent fan (center fan) has an influence on the flow field of the inboard fan similar to that encountered with the center fan during four- and six-fan operation.

Figure 32 shows bellmouth static pressure distributions to be essentially unaffected by changes in ground height. Likewise, changes in fan louver and L/C nozzle angles had little effect on the fan inlet flow field.

Fan Exit Total Pressure Distributions. - Total pressure distributions at the fan discharge (downstream of fan stators) are shown in figures 33 and 34 for four- and six-fan operation, respectively. The data are for the right-hand center fan at a ground height of 2.65 feet and encompass fan speeds from 2000 rpm to 3600 rpm. Instrumentation is described in table IV.

At intermediate radial distances, the discharge total pressures are greatest; while near the fan perimeter, pressures are significantly lower, particularly at the higher fan speeds. This may be attributed to two conditions. First, the poor performance of the fan bellmouth is transmitted across the fan and, second, the proximity of the tip-turbine discharge may influence the fan discharge through viscous interactions. Further inspection of these data indicate that the discharge pressures near the perimeter of the fan continually decay in the direction of the fan rotation from the 0- to the 270-degree radian.

For the 270-degree circumferential position, the total pressure readings near the hub (9.36-inch radius) were extremely low ($P_{T_{11}}/P_{T_0}<1.0$). This was considered questionable and was disregarded in fairing the distribution curves.

Total pressure distributions for the center fan in four-fan operation are qualitatively similar to those for six-fan operation. A comparison of

discharge total pressure distributions at 0-, 10-, and 20-degree louver angles indicated essentially no change in total pressure level as a function of louver angle position.

Fan Performance. - Fan performance characteristics in terms of gross thrust, fan pressure ratio, corrected airflow and corrected fan speed are shown in figures 35 and 36.

Fan performance was computed using ambient air temperature since reliable data from thermocouples located at the fan face were not available. The margin of error due to lack of real fan inlet temperature data is believed to be small. For example, an excursion in fan inlet air temperature from 70° F to 140° F, if not corrected, would result in an error in corrected fan speed of approximately 6 percent. A survey of wing leading edge air temperature data shown in table V indicates the probable magnitude of the temperature rise to be generally less than 30° F. The computation of fan thrust exclusive of the fan-tip-turbine thrust contribution is dependent upon actual fan pressure data measurements. The effect of inlet air temperature changes on fan thrust is inherently manifested in fan pressure data. Ambient pressure was assumed at the fan exit.

Overall fan pressure ratio and corrected fan airflow are presented in figure 35 for the right-hand center fan. As shown, fan pressure ratio increases with increasing fan speed approaching a value of 1.1 at 100 percent fan speed. The variation in fan pressure ratio with fan speed was essentially the same for both four- and six-fan operation.

However, fan airflow is slightly greater during four-fan operation than six-fan operation. This indicates that the outboard fan probably influences the center fan flow field, although this proximity effect is quite small.

Also shown in figure 35 is the fan system thrust of the right-hand center fan for both four- and six-fan operation. These thrust data include the thrust contribution of the tip turbine system which is in the order of 10 percent of the actual fan thrust and are correlated with the square of fan speed. As noted, the thrust during four-fan operation is slightly higher than under six-fan operation which is attributable to the higher fan airflows for four-fan operation.

The fan thrust was calculated on the basis of the exit momentum at the fan stator discharge just upstream of the fan exit louvers in conjunction with a fan efficiency of 88 percent. The fan airflow, however, was calculated from pressure measurements taken at the fan rotor inlet since it provided a more accurate determination from the standpoint of a more uniform flow field. It should be realized that the noted thrust levels represent a gross thrust and no account for fan recirculation, if it existed, in the form of ram drag

was considered. Furthermore, the thrust data do not reflect losses associated with the exit louvers and do not consider the losses due to the fan hub base.

At a nominal corrected fan speed of 3600 rpm under six-fan operation, the calculated thrust is approximately 1800 pounds. An estimate of the losses due to the fan hub base and louvers was shown to account for 170 and 90 pounds, respectively, resulting in a net thrust of 1540 pounds. No attempt was made to extrapolate and correlate this thrust calculation with thrust measurements obtained from force balance system. This was due to several factors. First, the inboard fan was not the same design as the center and outboard fans and, second, the test conditions did not permit a direct comparison since the center fan was not run independently. Furthermore, the inadequacy of the instrumentation system resulted in a low level of confidence in the thrust calculations.

Fan thrust versus ground height is shown in figure 36. This plot indicates only slight changes in center fan thrust with variation in ground height when L/C engine power is off. Similarly, operation with L/C engine power on produces essentially no change in center fan thrust with changes in ground height. The negligible effect of fan exit louver angle on thrust is also indicated in figure 36.

An inspection of the data at two test points involving ground heights of 2.65 and 9.0 feet at a L/C nozzle angle of 15 degrees indicated 8 percent less thrust than at a 0-degree nozzle angle.

L/C Engine Performance. - L/C engine thrust was calculated using measured values of EGT and static and total pressures at the nozzle exit. Nozzle exit pressure measurements were taken at the right-hand L/C nozzle only. L/C engine thrust is shown in figure 37.

Lift-Fan Gas Generator Inlet Performance. - A check of total pressure recovery for the lift-fan gas generator inlets showed recoveries exceeding 98 percent for all points investigated. This verifies that the inlets were operating as designed.

Induced Thermal Conditions

Hot Gas Ingestion. - An estimate of hot gas ingestion is indicated in both tabulated and curve formats.

Table V indicates the air temperature rise above ambient in the immediate vicinity of the L/C engine inlet, gas generator (fan engine) inlet, and above the leading edge of the wing for a wide range of test conditions.

The air temperature rise at the L/C engine inlet is represented by averaging the temperature readings from a group of thermocouples located forward of the L/C engine inlet. An indication of fan engine inlet temperature rise above ambient is provided by temperature readings from thermocouples 15, 16, 17 which were located forward of the inlet. The temperature reading from these three thermocouples were not averaged due to the large variations in temperature levels which appeared to exist. Estimates of hot gas ingestion into the wing fans are unavailable due to faulty oscillograph recordings of fan inlet temperature data. However, an indication of the probable occurrence of some hot gas ingestion into the fans is given by air temperature readings from thermocouples located above the leading edge of the wing.

Figure 38 summarizes L/C engine inlet hot gas ingestion data indicating the magnitudes of air temperature rise above ambient as a function of fan louver angle, nozzle angle, and model height. The air temperature rise data are based upon the averaging of temperature readings from the group of thermocouples located forward of the L/C engine inlet.

Figure 39 through 47 present the average air temperature forward of the L/C engine inlet and the air temperatures readings from three thermocouples located forward of the fan engine inlet as a function of time. These data were obtained using a Brown Recorder that had a reading cycle time of 24 seconds.

Inspection of data in table V and figures 38 through 47 reveals that engine inlet air temperature rise occurs over the full range of model heights, nozzle angles, and louver angles. Increasing model height from 2.65 to 9.0 feet does not necessarily lessen the magnitude of hot gas ingestion. In some instances hot gas ingestion appears to be greater at the model height of 9.0 feet than at 2.65 feet. Varying louver angle positions from 0 through 10 degrees does not appear to reduce ingestion, however; increasing of fan exit louver angle to 20 or 30 degrees generally results in a reduction of ingestion. Increasing L/C nozzle angle to 30 or 45 degrees also results in appreciable reduction of hot gas ingestion when coupled with fan exit louver angles of 20 or 30 degrees. Engine inlet air temperature rise during operations with an L/C nozzle angles of 30 or 45 degrees and fan louver angles of 20 or 30 degrees is generally less than 5° F.

Hot gas ingestion when operating with L/C nozzles alone appears to involve an air temperature rise of generally less than 10° F at the L/C engine inlet. For operations with wing fans alone, fan engine inlet air temperature rise appears to vary considerably from values less than 10° F to over 40° F.

Flow Field Temperatures. - Flow field temperatures were obtained with a 6-foot vertical rake and several 6-foot horizontal rakes which were positioned as shown in figure 8. These rakes were intended to be moved throughout the flow field to obtain overall temperature map of flow field; however, the installation of the rakes and the securing of the bundles of thermocouple leads to the steel ground plane proved to be so consuming of manpower and time during the first change that the plan was abandoned.

A sampling of flow field temperature data taken with the six-foot vertical rake is shown in figure 48 which also depicts rake location. These data indicate air temperature profiles as a function of model heights, and L/C nozzle and fan louver angles. For operations with L/C nozzles alone, high-temperature exhaust gas flowed undisturbed near the ground as expected. Temperatures at elevations above 40 inches appear to be only slightly affected and are approximately equivalent to the ambient air temperature. This was not the case for combined operations of fans and L/C nozzles where downwash interactions resulted in upward flow, turbulence, and mixing. Air temperatures in excess of 150° F were indicated up to the full extent of the rake. This upward flow of hot gases would suggest the primary cause for hot gas ingestion. Figure 48 also indicates that the higher elevation rake temperatures decrease with increasing nozzle and fan exit louver angles. These rake temperature reductions are caused by an outward shifting of the fan and L/C nozzle downwash interference zones. This outward or rearward shift of hot gas upwash may account for the reduction in air temperature rise at the engine and fan inlets when L/C nozzle and fan louver angles are increased to 20 or 30 degrees.

Maximum temperatures indicated by the 6-foot horizontal temperature rake located below the L/C nozzle (figure 8) at 90 percent L/C engine power at model heights of 2.65, 4.45, 6.0, and 9.0 feet were 530°, 475°, 485°, and 405° F, respectively. Corresponding exhaust gas temperatures at the nozzles were approximately 1140° F. A temperature attenuation of 600° to 700° F is indicated. Attenuation of fan tip turbine exhaust temperature near the ground plane was indicated by the 6-foot horizontal temperature rake located beneath the center and outboard lift fans (figure 8). The maximum temperature observed was approximately 200° F which implies that only moderate localized ground heating occurs beneath the fans.

Near-Structure Air Temperatures. - Thermocouples were installed on the model to measure air temperatures 1/4-inch from the structure at locations on the fuselage and landing gear as shown in figures 4 and 7. The purpose of these temperature measurements is to indicate the probable location of hot

spots and to identify the relatively cool areas. This information may be useful, for example, in the selection of locations for air scoops and vents.

Figure 49 lists the prevailing air temperatures near the landing gear, forward fuselage, center fuselage below the wing and aft fuselage in the vicinity of the tail section.

The center fuselage area below the wing appears to be a hot spot with near-structure air temperatures ranging from 350° to 400° F. These temperature levels exist at all model heights and fan louver and L/C nozzle angles. This condition is caused by the inboard fan, tip-turbine exhaust gases which eject adjacent to the fuselage structure (figure 26).

Temperatures adjacent to the landing gear (tires) as high as 250° to 300° F are indicated.

Figure 49 indicates air temperature levels adjacent to the side of the aft fuselage which are generally less than 140° F. Temperature levels near the forward fuselage appear in the 100° to 120° F range.

Ground Surface Heating. - Thermocouples were imbedded in the steel ground plane in an area below the L/C nozzles where maximum ground heating rates were expected to occur (figure 6). A companion thermocouple for measurement of hot gas temperatures 1/4-inch above the ground plane was also provided near each imbedded thermocouple. These thermocouples were intended to indicate the ground heating rates and temperatures.

Typical ground heating conditions which are based on temperature readings from thermocouples 109 and 114, are shown in figure 50, representing model heights from 2.65 to 9.0 feet. Maximum near-surface hot gas temperatures midway between the L/C nozzles (thermocouple 114's location) were approximately 400° F. Corresponding maximum ground surface temperatures were approximately 350° F. At the model height of 9.0 feet, maximum temperatures were less than 300° F.

Computed heat transfer coefficients ranging from 39 to 95 Btu/hr ft^{2}° F are shown in figure 50. These coefficients are at best only rough approximations of the average heat transfer rates for the time intervals selected. Heat transfer to or from the ground plane was assumed to occur only at the top surface of steel ground plane and to be entirely convective. The temperatures of the ground plane (steel plate) and hot gas above the surface were assumed to be uniformly equal to the temperature readings derived from the installed thermocouples.

Heat transfer coefficients were computed from the energy balance:

$$WC_p \frac{dT}{d\tau} = hA(T_\infty - T)$$

intergrating this expression and solving gives

$$h = \left[\frac{\ln\left(\frac{T_\infty - T_1}{T_\infty - T_2}\right)}{\Delta\tau}\right] \frac{W}{A} C_p$$

where:

h = heat transfer coefficient (Btu/hr ft^2° F)

T_∞ = average near-structure air temperature during time interval (° F)

T_1 = structure temperature at beginning of time interval, (° F)

T_2 = structure temperature at end of time interval (° F)

$\Delta\tau$ = time interval (hours)

W/A = weight of ground plate per unit area (lb/ft^2)

C_p = specific heat of ground plate (Btu/lb° F)

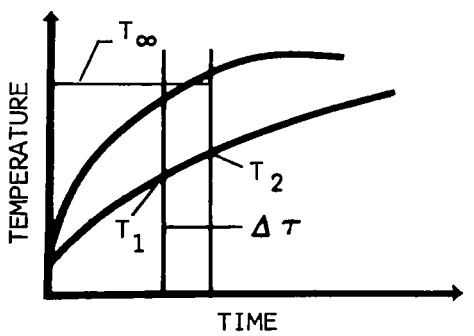

For the steel plate:

$W/A = 12.7$ lb/ft^2

$C_p = 0.12$ Btu/lb ° F

So that

$$h = 1.523 \left[\frac{\ln\left(\frac{T_\infty - T_1}{T_\infty - T_2}\right)}{\Delta\tau}\right]$$

For the calorimeter (figure 10) the expression for heat transfer coefficient is

$$h = \frac{WC_p}{A}\left[\frac{\ln\left(\frac{T_\infty - T_1}{T_\infty - T_2}\right)}{\Delta\tau}\right]$$

For this calorimeter:

$$\frac{WC_p}{A} = 0.31$$

Flow Field Pressures. - Flow field pressures are shown in table VI. These readings represent the difference between total pressure probe measurements and an atmospheric reference pressure. Each of the pressure readings are approximated to the nearest integer. Positive readings indicate a frontal velocity component at the probe. A negative reading is assumed to indicate that the flow field velocity at the probe has a velocity vector which is devoid of a frontal velocity component. These pressure readings, therefore, provide an indication of flow direction. The magnitude of positive readings indicates approximately the dynamic pressures in the flow field where the probes are known to be facing directly into the flow stream. The accuracy of the low magnitude pressure readings were compromised by the use of a 25 psid pressure transducer such that many of the pressure readings are within the noise level of the transducer.

Plots of fan dynamic pressure obtained under the outboard wing fan are shown in figures 51 and 52 for rake location 12 inches above the ground plane (figure 8).

Figure 51 indicates dynamic pressure profiles in the fan efflux for two fan heights above the pressure rake. A comparison of the curves indicates a peak pressure decay from approximately 145 to 115 psf as fan height above the pressure rake is increased from 2.2 to 3.3 fan diameters.

Figure 52 compares fan dynamic pressure for fan speeds of 2000, 3000, and 3600 rpm. Maximum fan dynamic pressures at fan speeds of 2000, 3000, and 3600 rpm are approximately 145, 95, and 40 psf, respectively. Fan dynamic pressure data shown in figure 52 for fan speeds of 2000, 3000, and 3600 rpm appear to be compatible with fan pressure ratios of figure 33.

Additional pressure data from table VI, shown in figures 53 and 54, indicate dynamic pressure parallel to the ground plane at two locations: one near the outboard fan, and the other near the L/C nozzle. Maximum dynamic pressures or velocities occur within several inches of the ground.

Relatively cool fan air temperatures and near-ground maximum dynamic pressures of approximately 60 psf permitted personnel to approach the outboard

fan with ease. Ground flow conditions in the vicinity of the L/C nozzles exceeded temperatures of 400° F and dynamic pressures of approximately 230 psf. Personnel approaches into the L/C nozzle area were not attempted.

The 6-foot horizontal pressure rake under the L/C nozzle was limited to the location shown in figure 9. The intersection of the nozzle centerline with the ground plane is indicated for L/C nozzle angles of 0 and 15 degrees. Maximum dynamic pressure readings listed in table VI appear to be less than 400 psf for model height of 2.65 feet. Corresponding dynamic pressures at the nozzle exit were approximately 1000 psf. Comparison of tabulated pressure data for test run data points 6.1 and 6.4, and 8.3 and 8.4 indicates an increase in rake pressure readings as fan louver angles increases from 0 and 10 degrees. This pressure change may be due to a reduction in forward flow of fan exhaust gas as fan louver angle is increased.

Oscillograph Temperature Traces. - Oscillograph temperatures traces from calorimeters (figure 10) and ground surface thermocouples are shown in figures 55 through 63. The origin of each curve at zero time is considered to be equivalent to ambient temperature or approximately 60° F. Each temperature trace is identified by its thermocouple number. Air and structure temperatures at the various point locations shown in figures 4, 5, and 6 are plotted in pairs.

Highest structural temperatures on the model occur on the side of the fuselage below the inboard fan. Temperatures exceeding 300° F are indicated in figure 55. Structure temperatures in excess of 100° F above ambient also occur on bottom of fuselage (figure 58). Structure temperatures on the forward fuselage and at under wing locations aft of the wing fans indicate only slight heating effects.

Ground surface temperatures and corresponding near-surface air temperatures in figure 57 exceed 250° F and 350° F, respectively.

Several sample indications of heat transfer coefficients are shown in figures 55 through 60. The ground plane heat transfer coefficients appear to be considerably higher than at locations on the surface of the model.

CONCLUSIONS

1. Lift was found to increase as model height was decreased (indicating a positive lift contribution due to ground effect) during full power lift from the L/C nozzles in combination with fans for the model configuration having wheel fairings installed.

2. No mutual interference effects on lift are evident at the model height of 9.0 feet when operating two, four, or six fans alone. Lift was found to be directly proportional to the number of fans operating. Total lift produced by the combined operation of fans and L/C nozzles was essentially equal to the sum of the lifts produced by the L/C nozzles and fans when operated alone.

3. During operations with fans alone, aft deflection of fan louvers caused lift reductions which were greater than would have been expected from a $\cos \beta_V$ relationship. However, with simultaneous operation of fans and L/C nozzles, the fan lift reductions were less and tended to follow the $\cos \beta_V$ relation.

4. At the model height of 9.0 feet for fan operations alone (wheel fairings on), ground effect was evident only in terms of pitching moment characteristics. At lower model heights, ground effect was indicated by effects on lift as well as pitching moment. Decreasing model height from 9.0 feet to 6.0 feet resulted in an increase of lift to a maximum of approximately five percent, thereafter decreasing to about three percent below the initial lift at the 9-foot level as the model was moved to 2.65 feet. Removal of the wheel fairings caused the lift to increase at the high and low model heights and tended to reduce the variations of lift with model height.

5. Operations with L/C nozzles alone appeared to exhibit losses in lift as model height was decreased.

6. Fan bellmouth inlet performance was satisfactory under all test conditions investigated. Total pressure recovery was above 99 percent, and total pressure distortion did not exceed 2-1/2 percent.

7. Hot gas ingestion (engine inlet air temperature rise above ambient) occurred in varying amounts at all model heights tested. Increasing model height from 2.65 feet to 9.0 feet did not result in a reduction of hot gas ingestion. Engine inlet air temperature increases of 10 to 50° F above ambient were not uncommon.

8. Hot gas ingestion by the engines and fans could be reduced substantially by vectoring fan louver angles aft to approximately 20 degrees. Combined vectoring of L/C nozzles and fan louver angles to aft positions of 30 degrees resulted in engine inlet temperature rises generally less than 5° F above ambient. Aft vectoring of nozzles and louvers to only 10 or 15 degrees did not appear to reduce ingestion.

9. Major hot spots on the model occurred on the fuselage below the wings due to close proximity to the inboard fan tip-turbine exhaust. Near-structure air temperatures and structure temperatures exceeding 400° and 300° F, respectively, were recorded. Structure temperatures on the bottom of the fuselage were generally less than 200° F.

REFERENCES

1. X376 Pitch Fan Specification. Lift Fan Flight Research Aircraft Program (DA44-177-TC-715), Specification No. 113, Flight Propulsion Laboratory Department, General Electric Co, 1 March 1962.

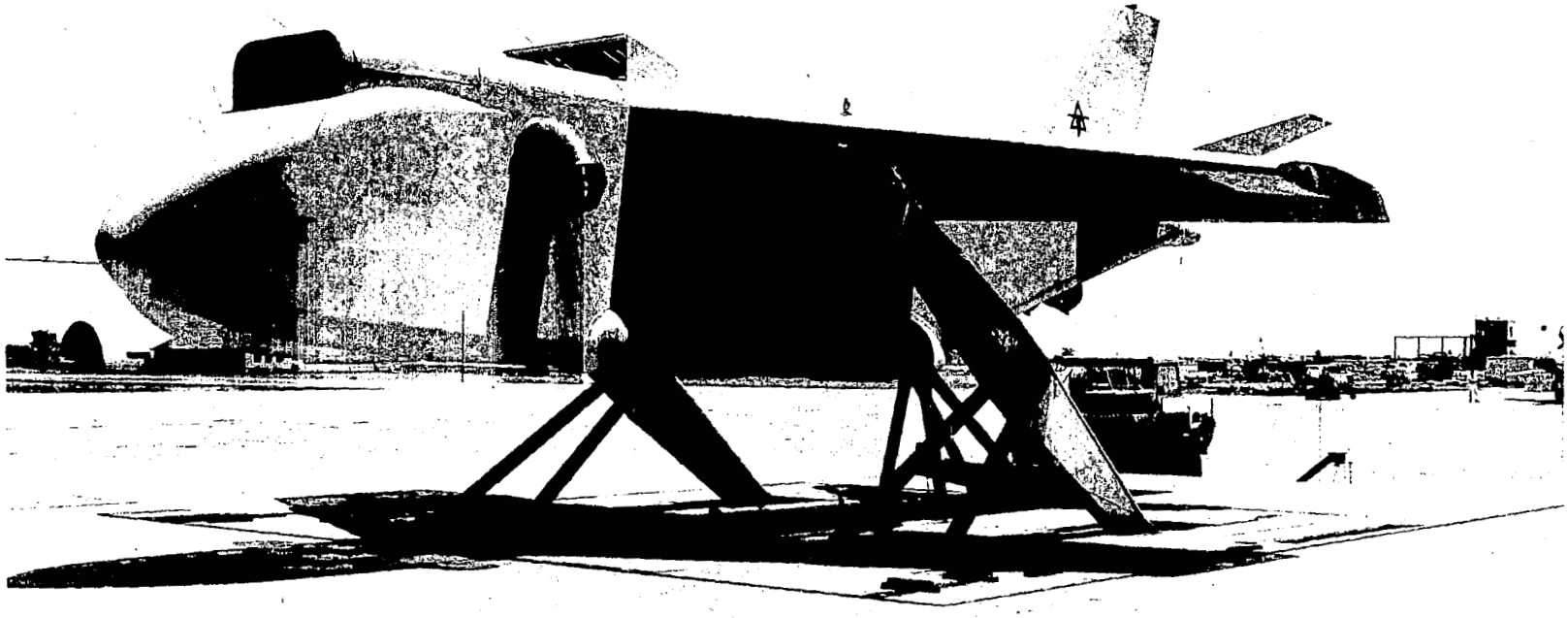

Figure 1. - Test Model Mounted on VTOL Test Stand.

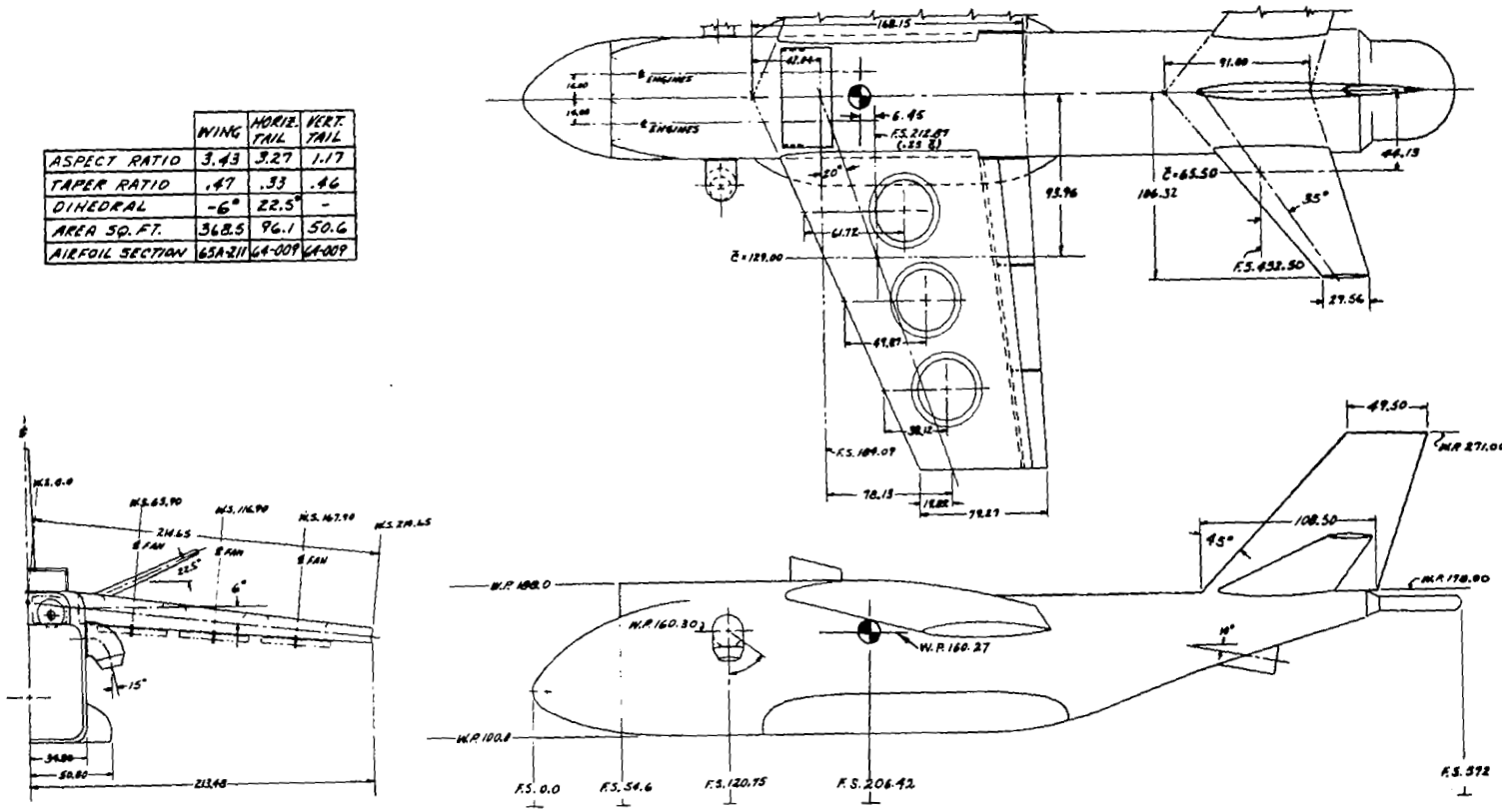

Figure 2. - Test Model General Arrangement.

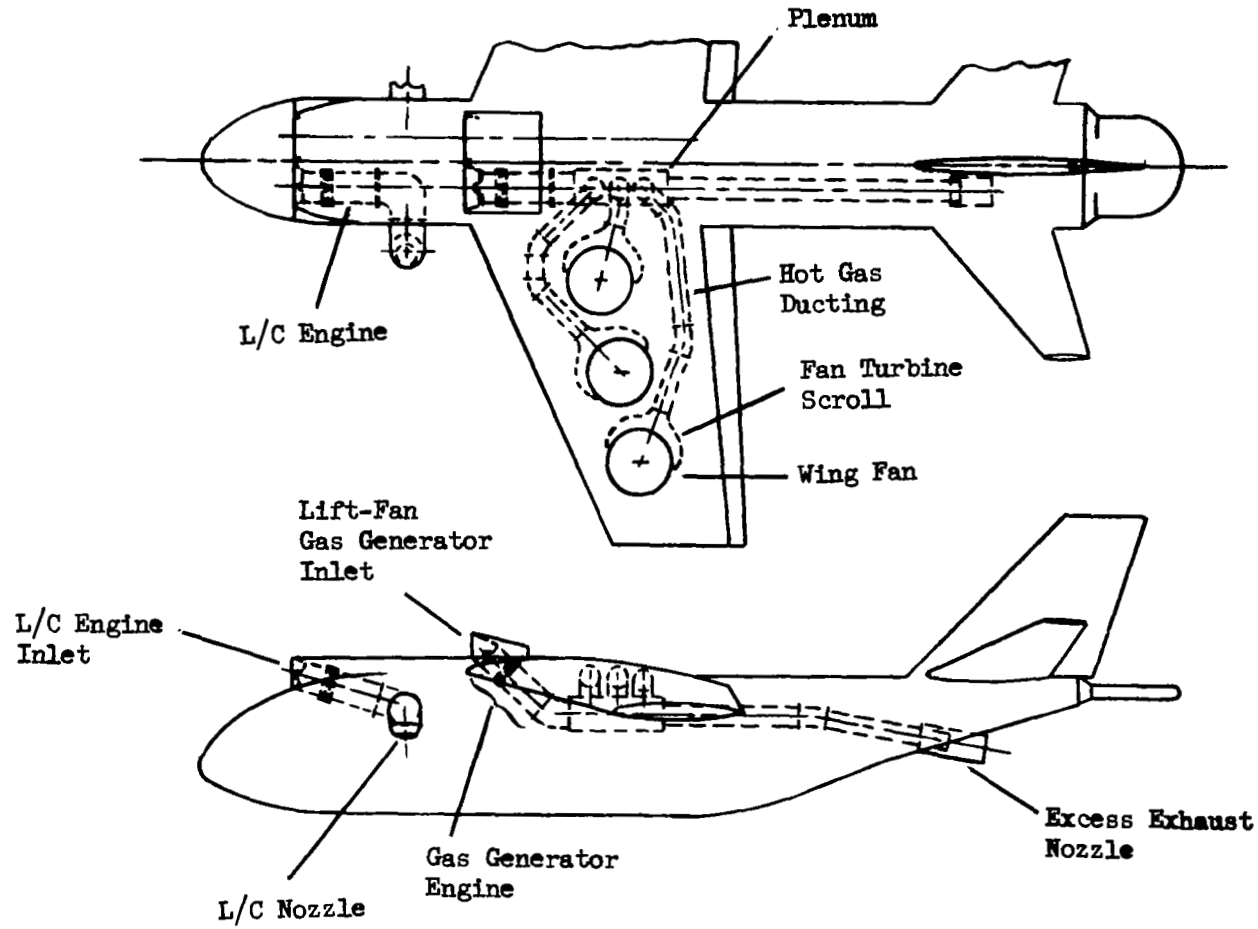

Figure 3. - Propulsion System Ducting Arrangement.

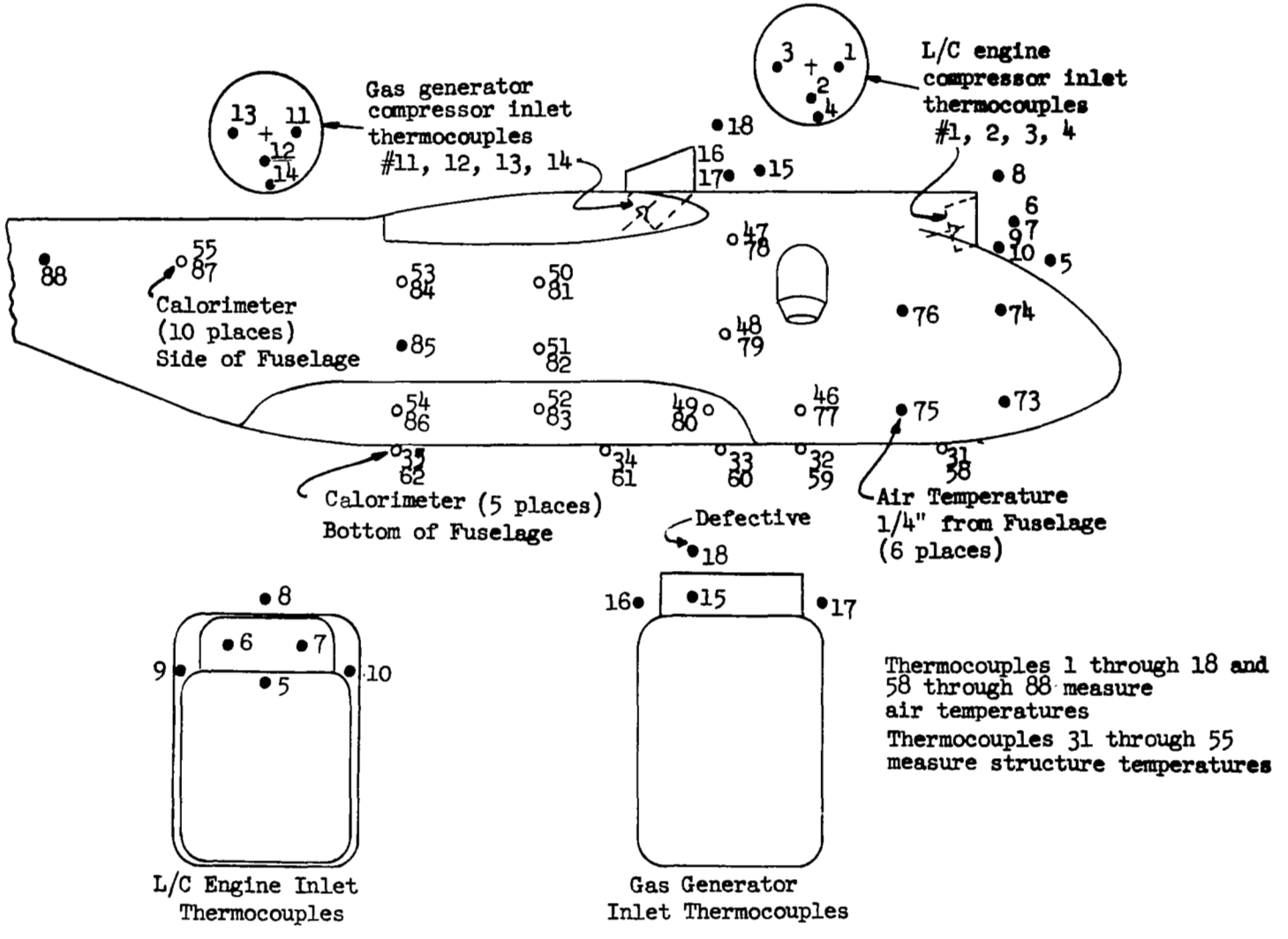

Figure 4. - Fuselage and Engine Inlet Thermocouples.

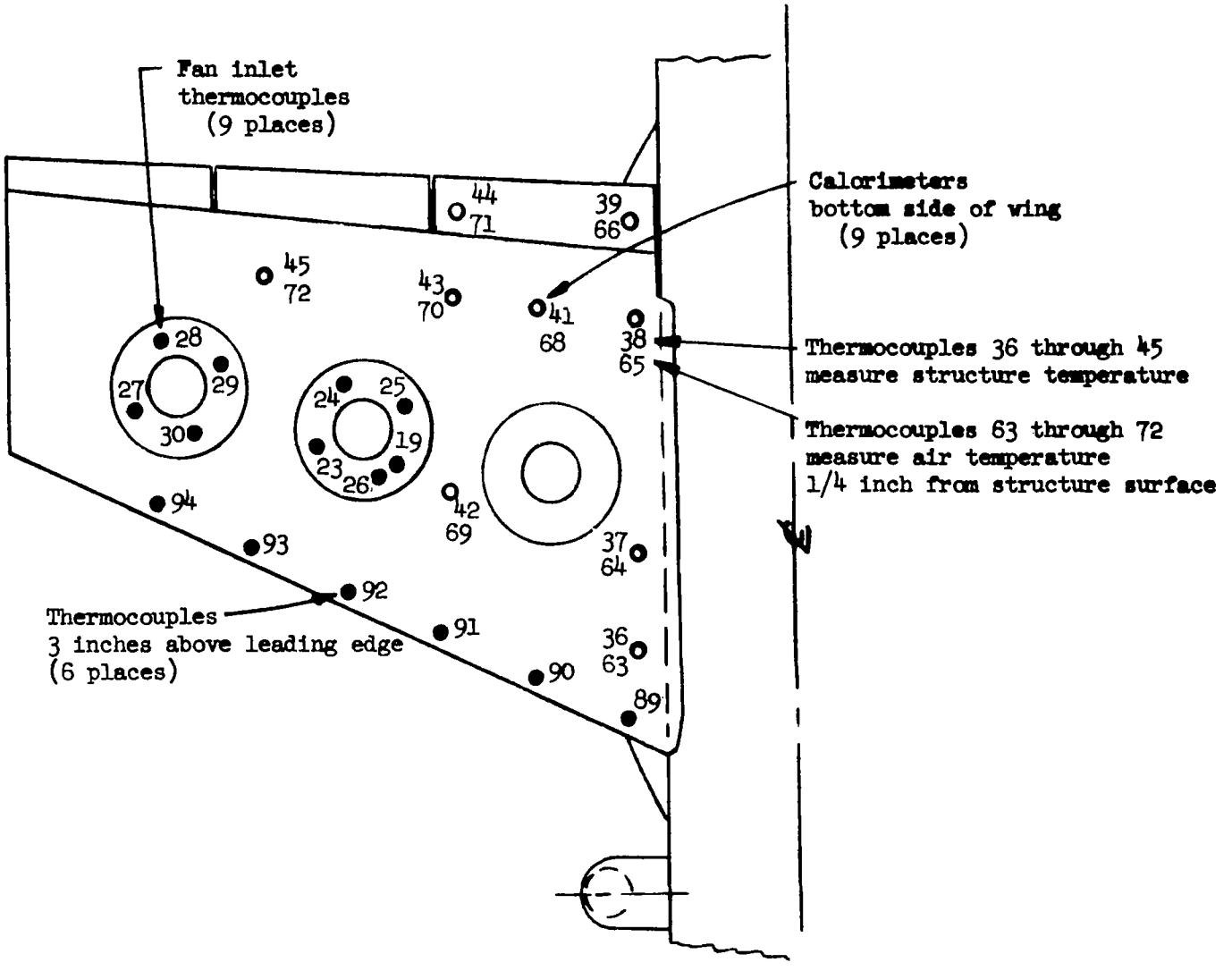

Figure 5. - Wing and Fan Inlet Thermocouples.

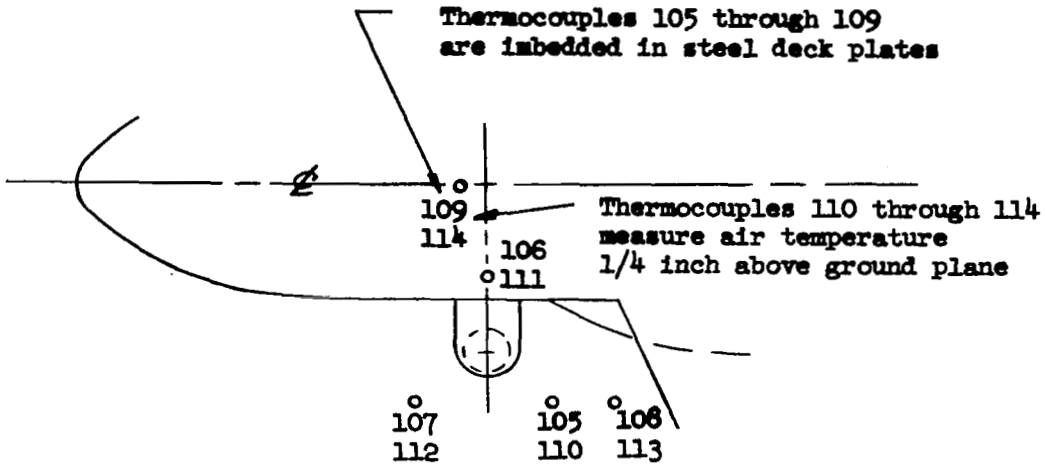

Figure 6. - Ground Plane Thermocouples.

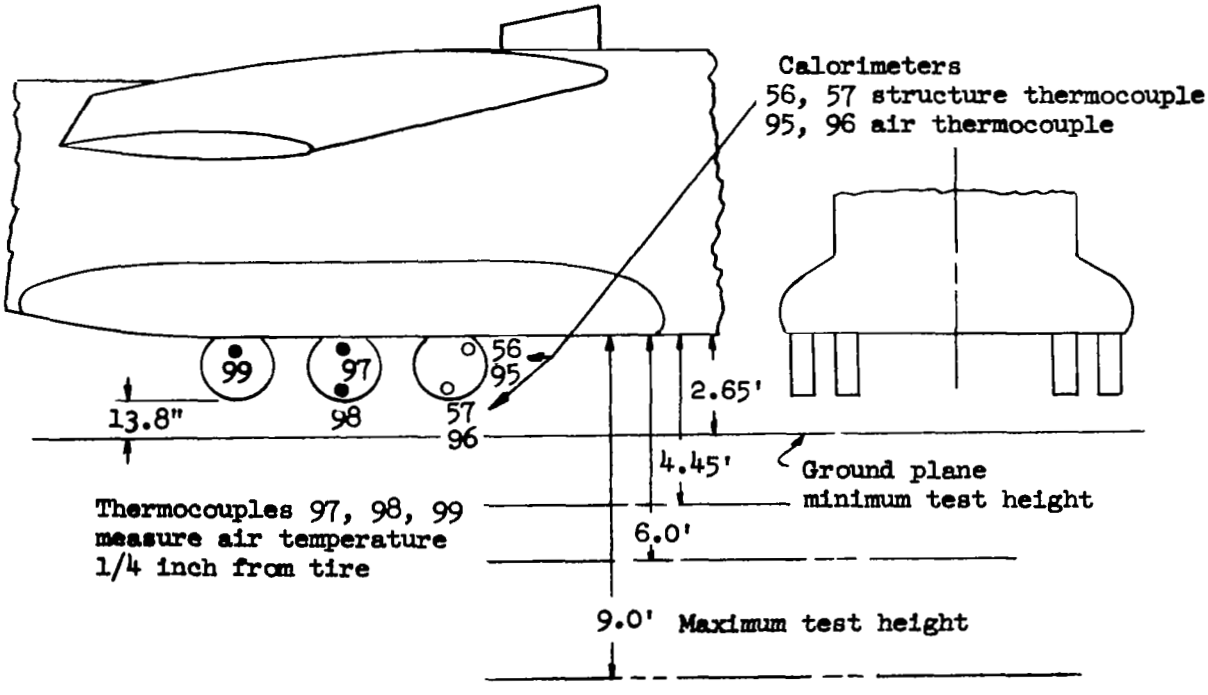

Figure 7. - Landing Gear Thermocouples.

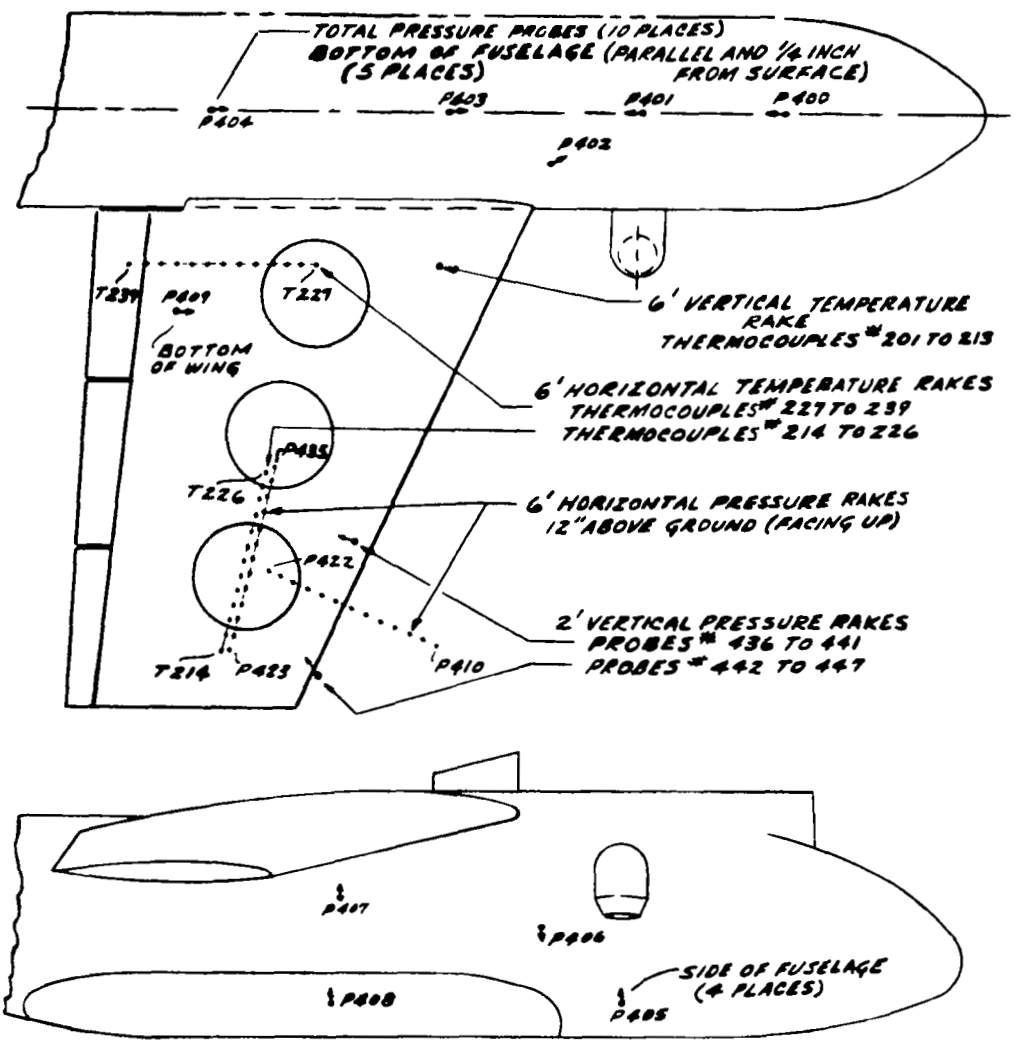

(a) Rake locations for Test Runs 1 through 5

Figure 8. Flow Field Pressure Probes and Thermocouples.

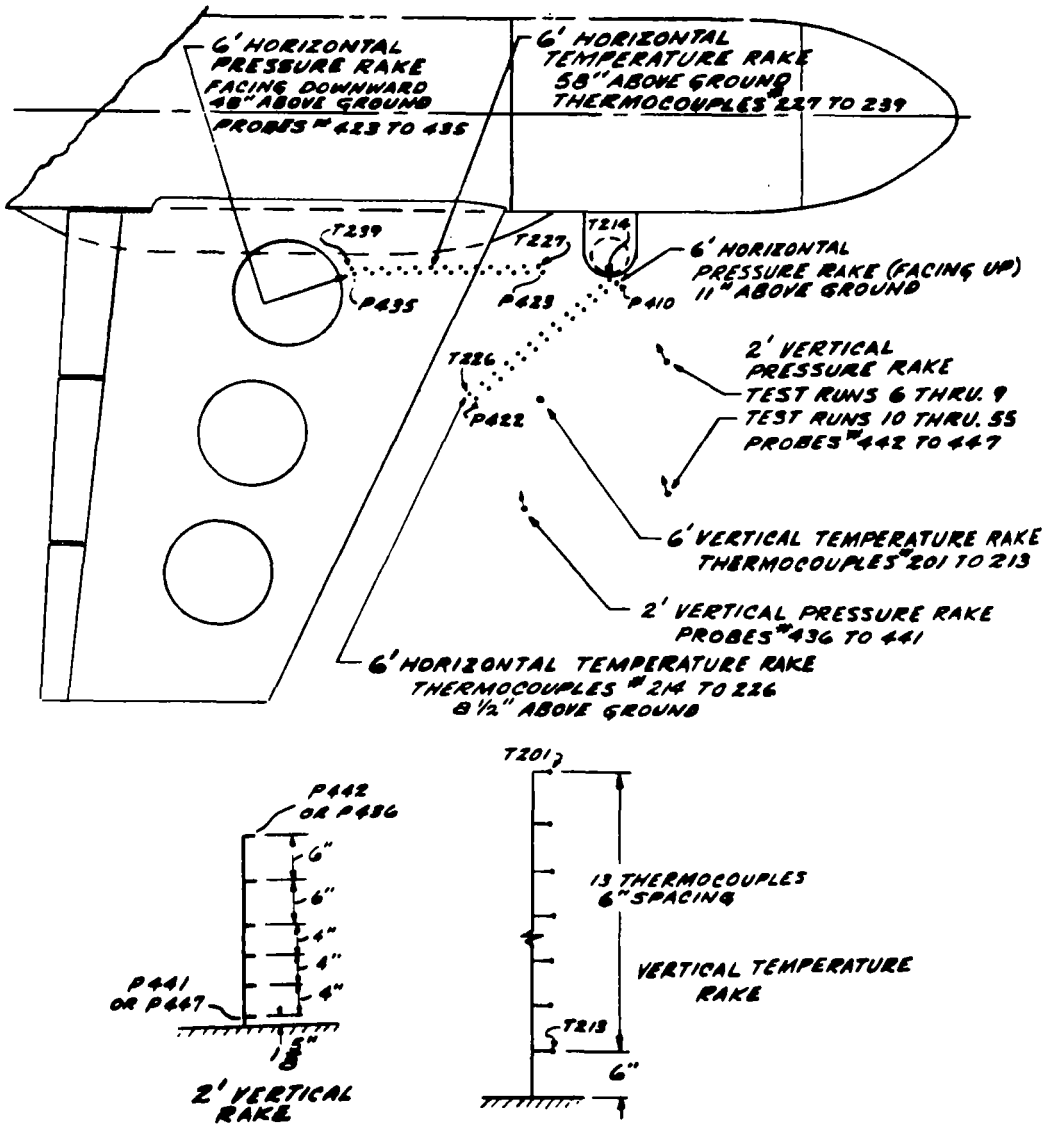

(b) Rake locations for Test Runs 6 through 55

Figure 8. Flow Field Pressure Probes and Thermocouples. (Concluded)

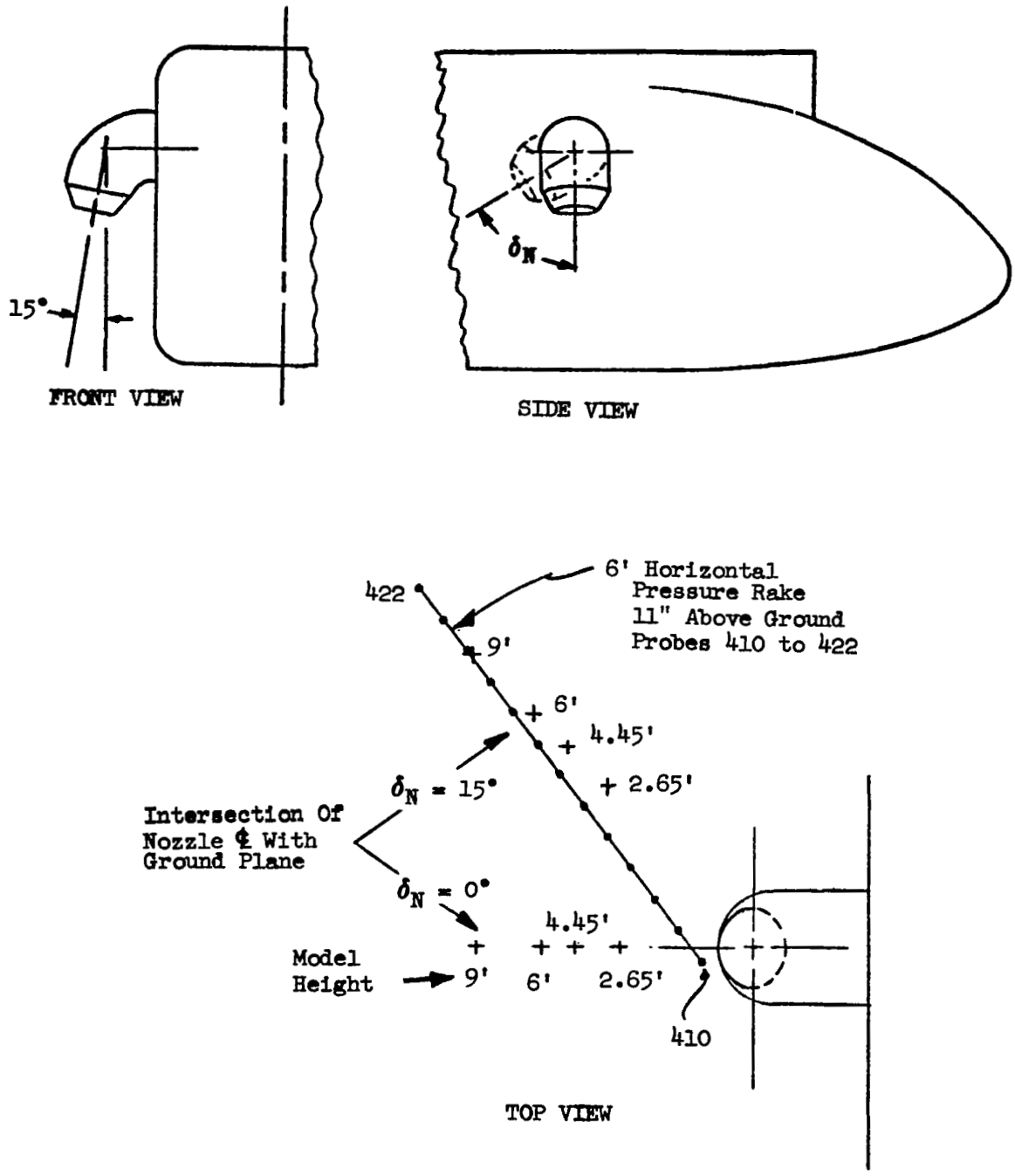

Figure 9. L/C Nozzle Horizontal Pressure Rake Location

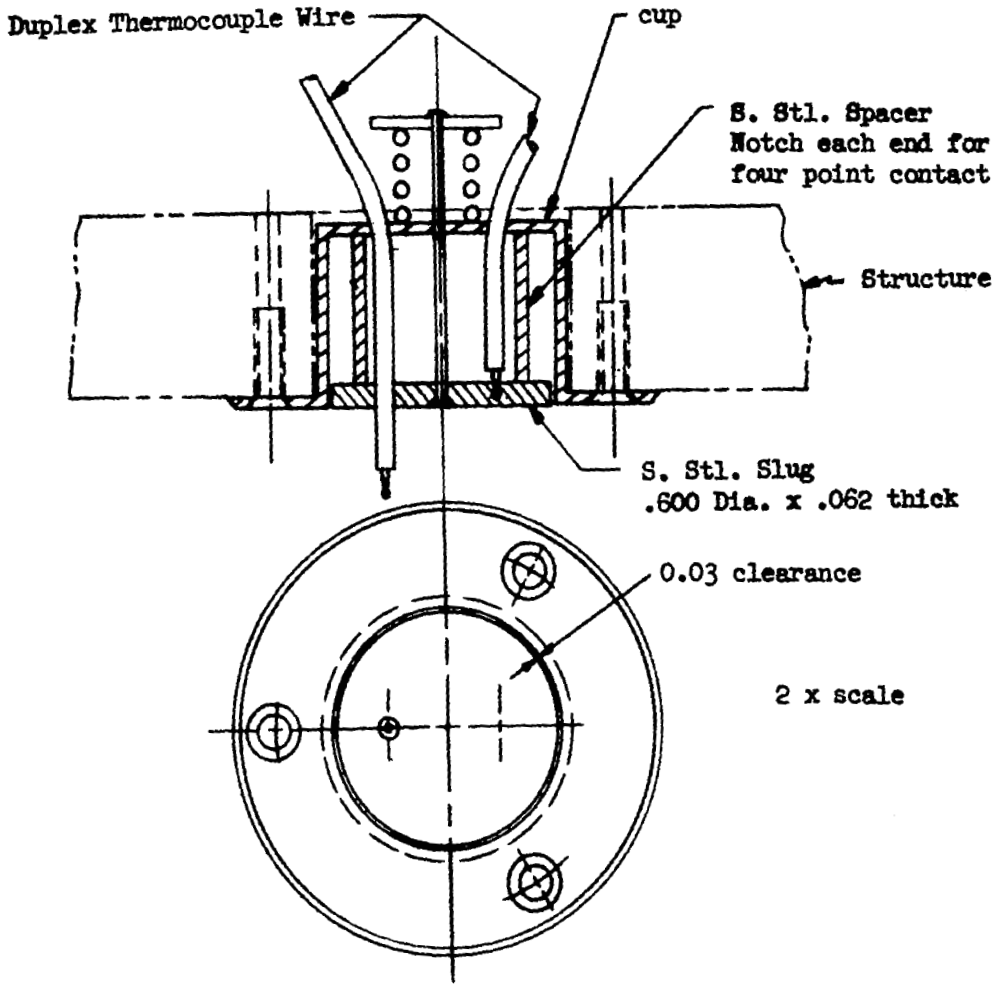

Figure 10. - Calorimeter Design.

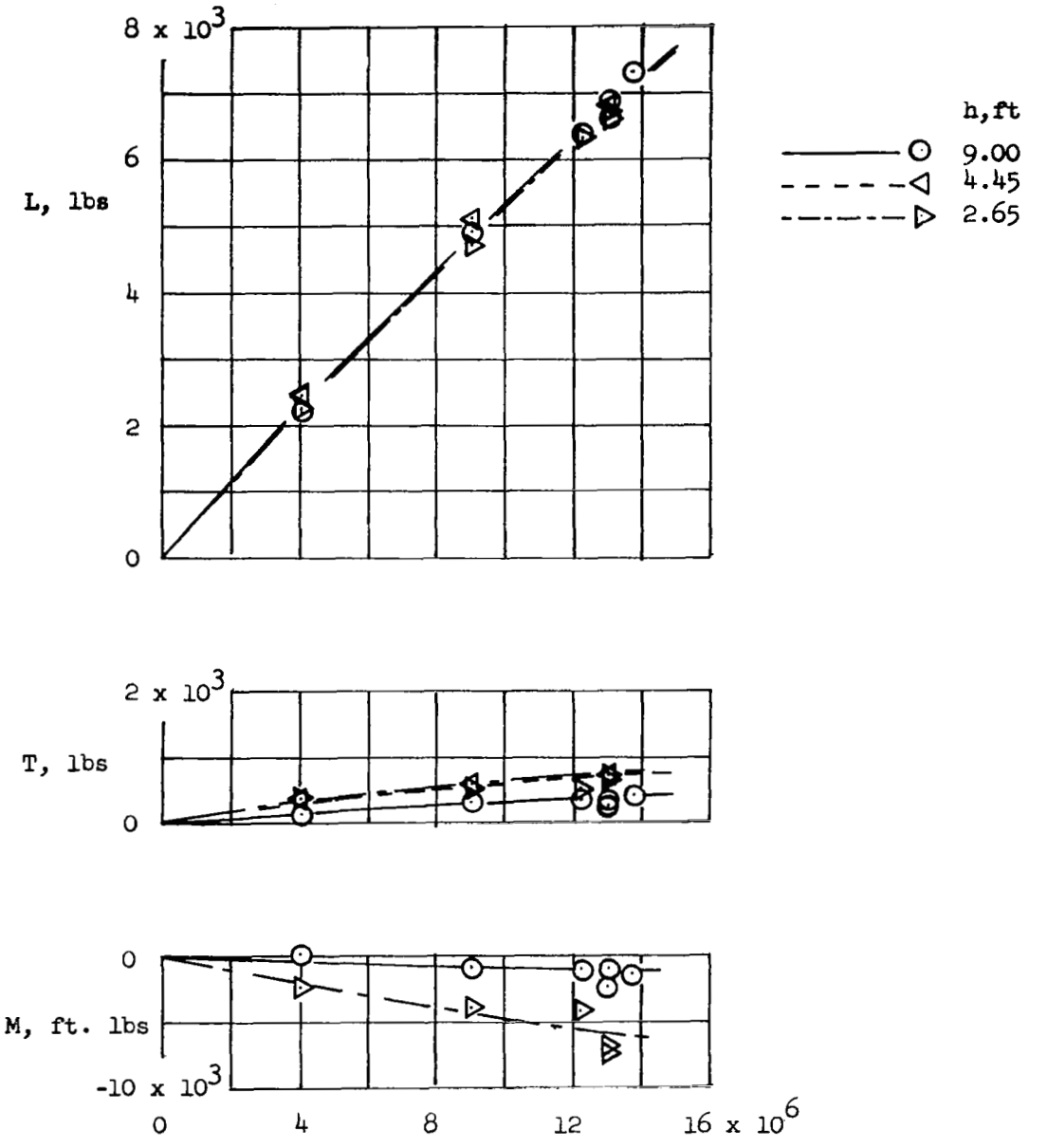

(a) $\beta_v = 0^\circ$.

Figure 11. Effect of Fan Speed with Six Fans, L/C Power Off, Wheel Fairings On, $\alpha = 0$

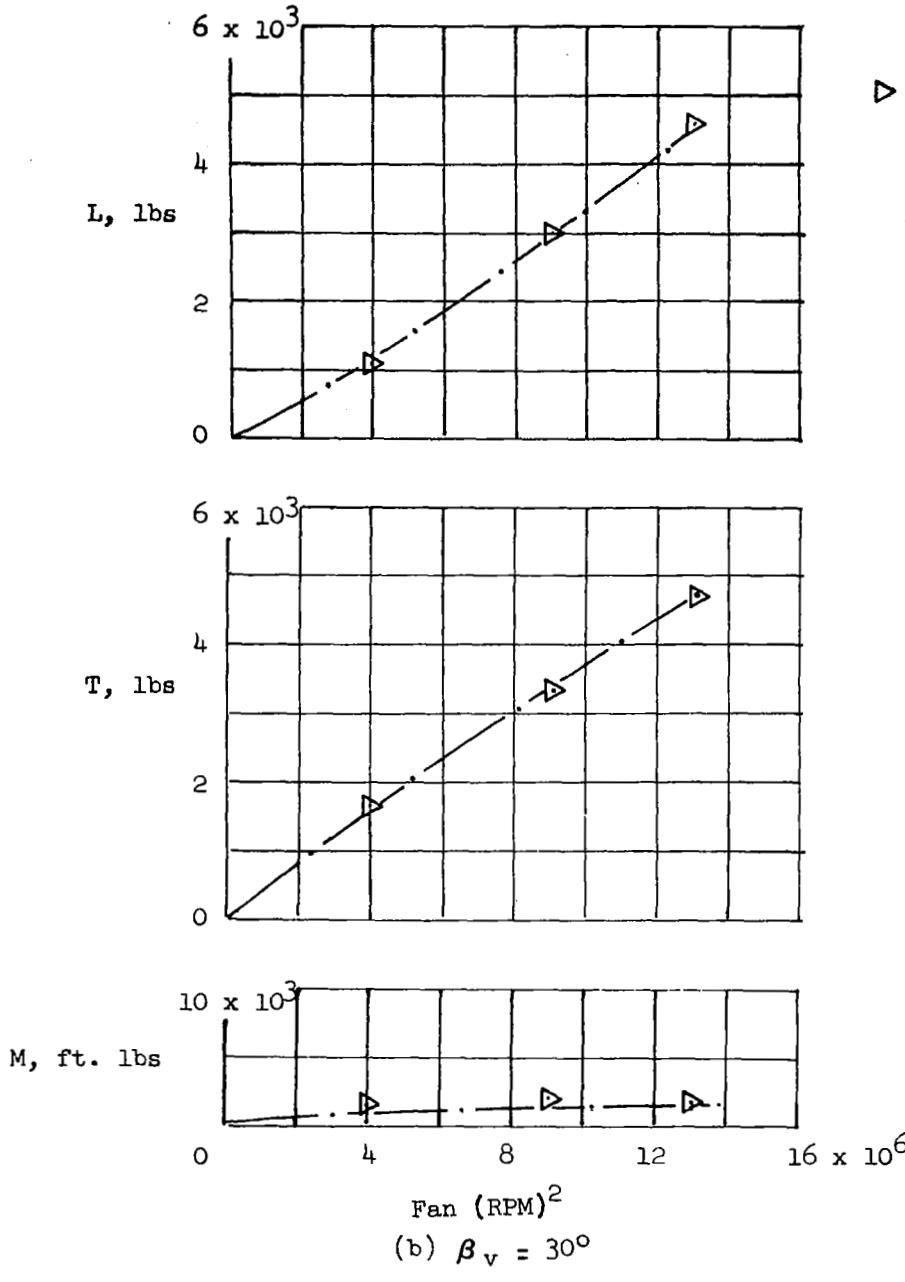

Figure 11. Effect of Fan Speed with Six Fans, L/C Power Off, Wheel Fairings On, $\alpha = 0$ (Concluded)

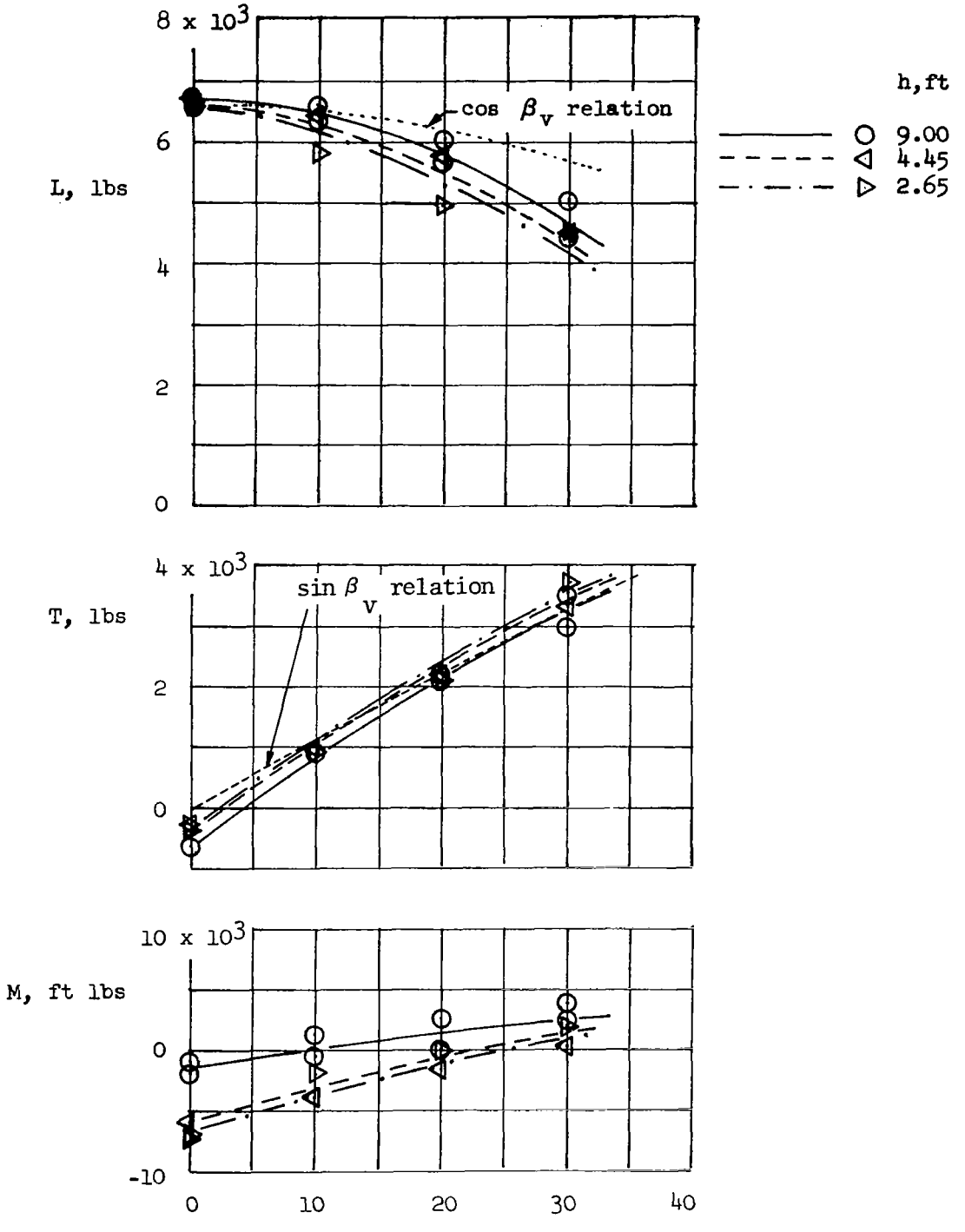

Figure 12. Effect of Fan Louver Deflection, Six Fans at 3600 RPM, L/C Power Off, Wheel Fairings On, $\alpha = 0$

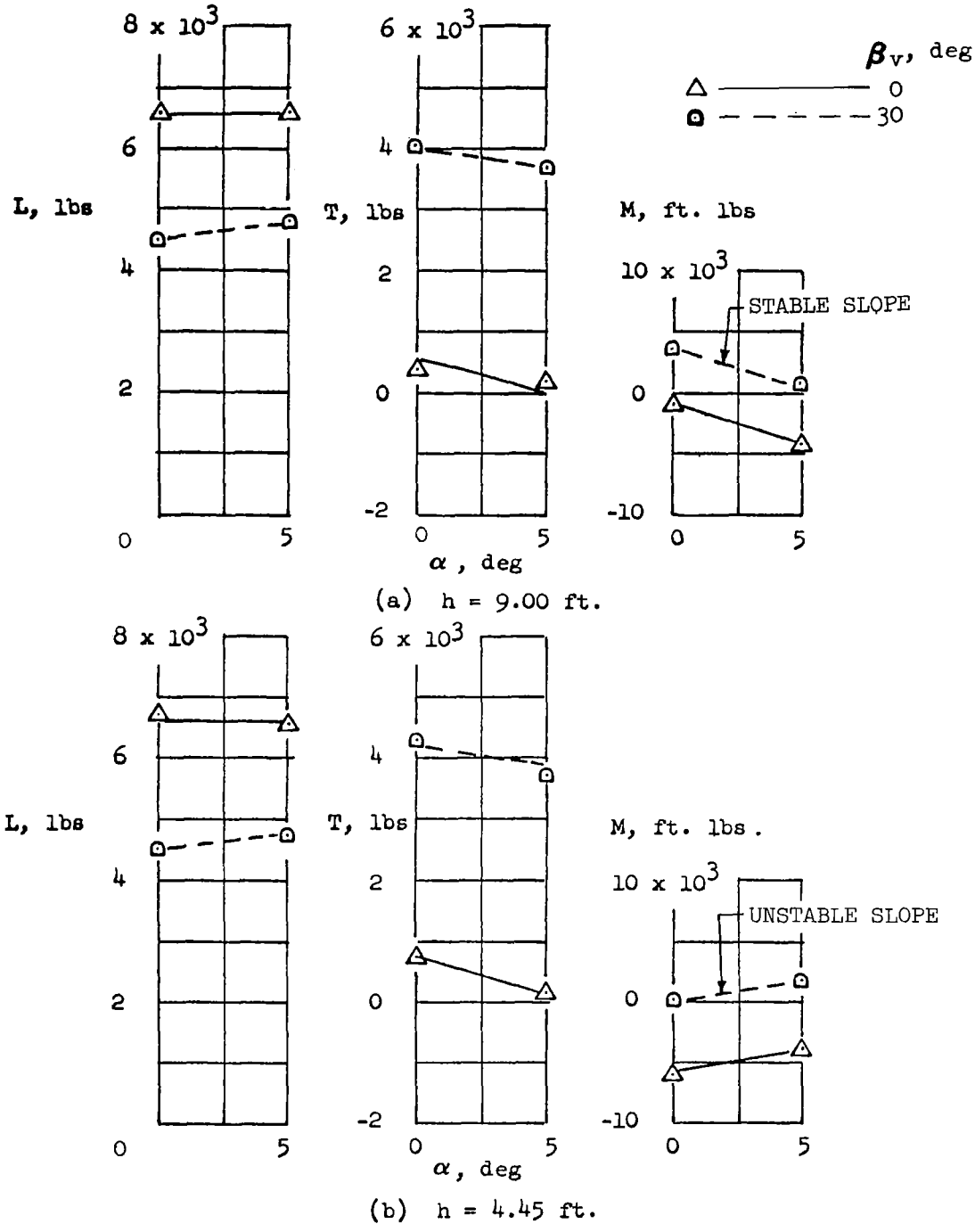

Figure 13. Effect of Angle of Attack, Six Fans at 3600 RPM, L/C Power Off, Wheel Fairings On

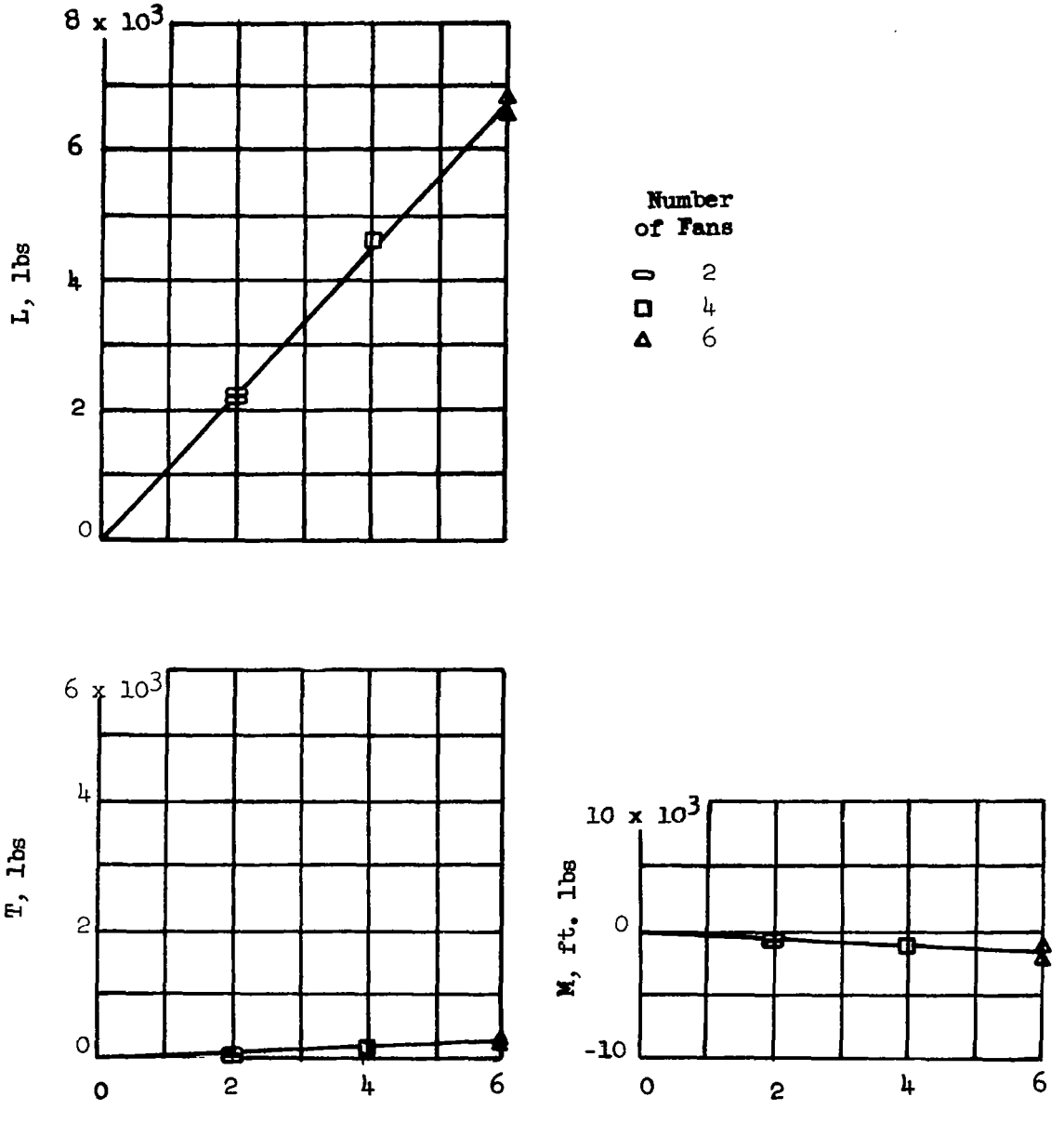

Figure 14. Effect of Number of Fans Operating, 3600 RPM, L/C Power Off, Wheel Fairings On, h = 9.0', α = 0°

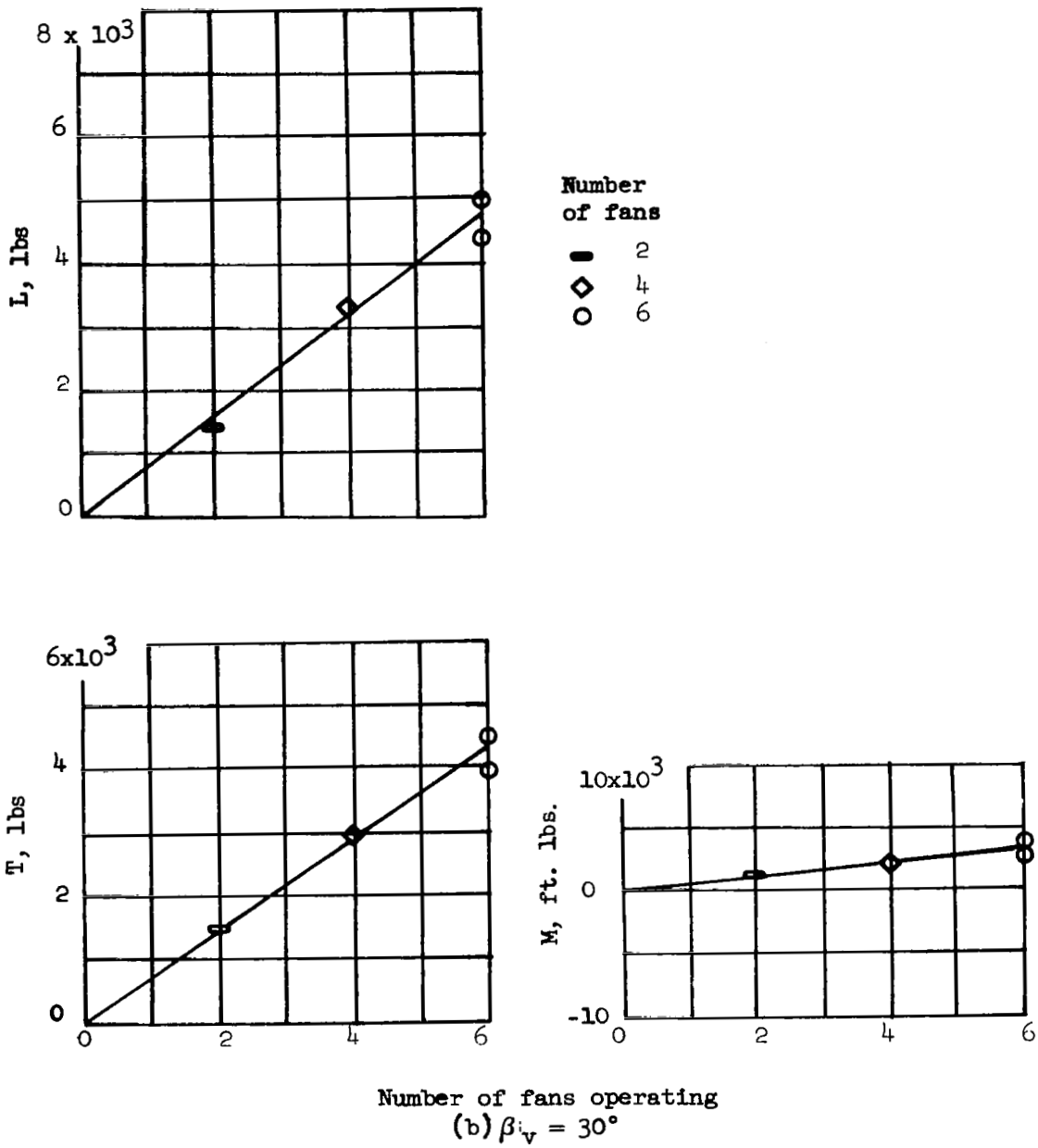

Figure 14. Effect of Number of Fans Operating, 3600 RPM, L/C Power Off, Wheel Fairings On, h = 9.0', α = 0° (Concluded)

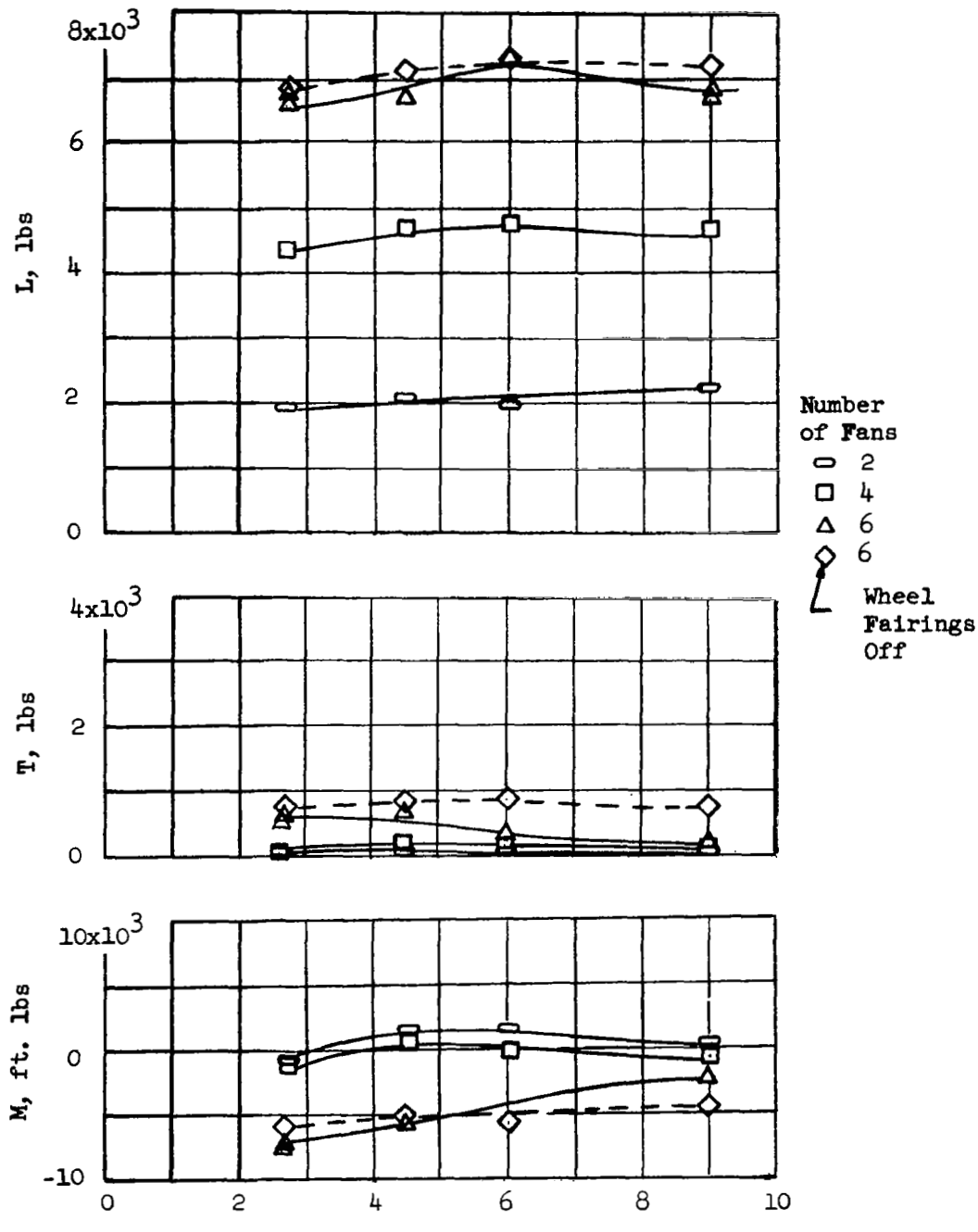

(a) $\beta_v = 0^\circ$.

Figure 15. Effect of Model Height with Two, Four, and Six Fans; 3600 RPM, L/C Power Off, Wheel Fairings on, $\alpha = 0$

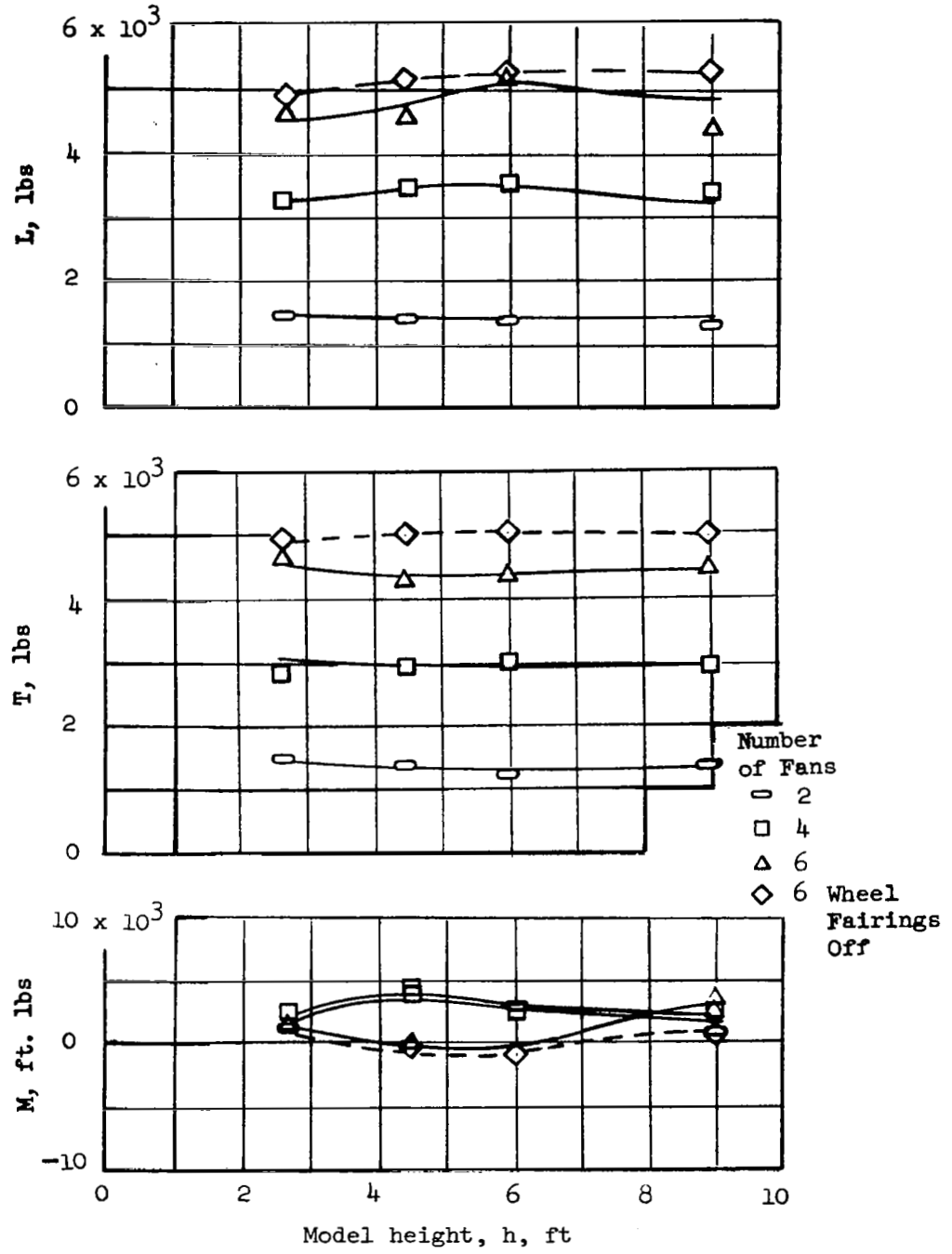

(b) $\beta_v = 30^\circ$.

Figure 15. Effect of Model Height with Two, Four, and Six Fans; 3600 RPM, L/C Power Off, Wheel Fairings on, $\alpha = 0$ (Concluded)

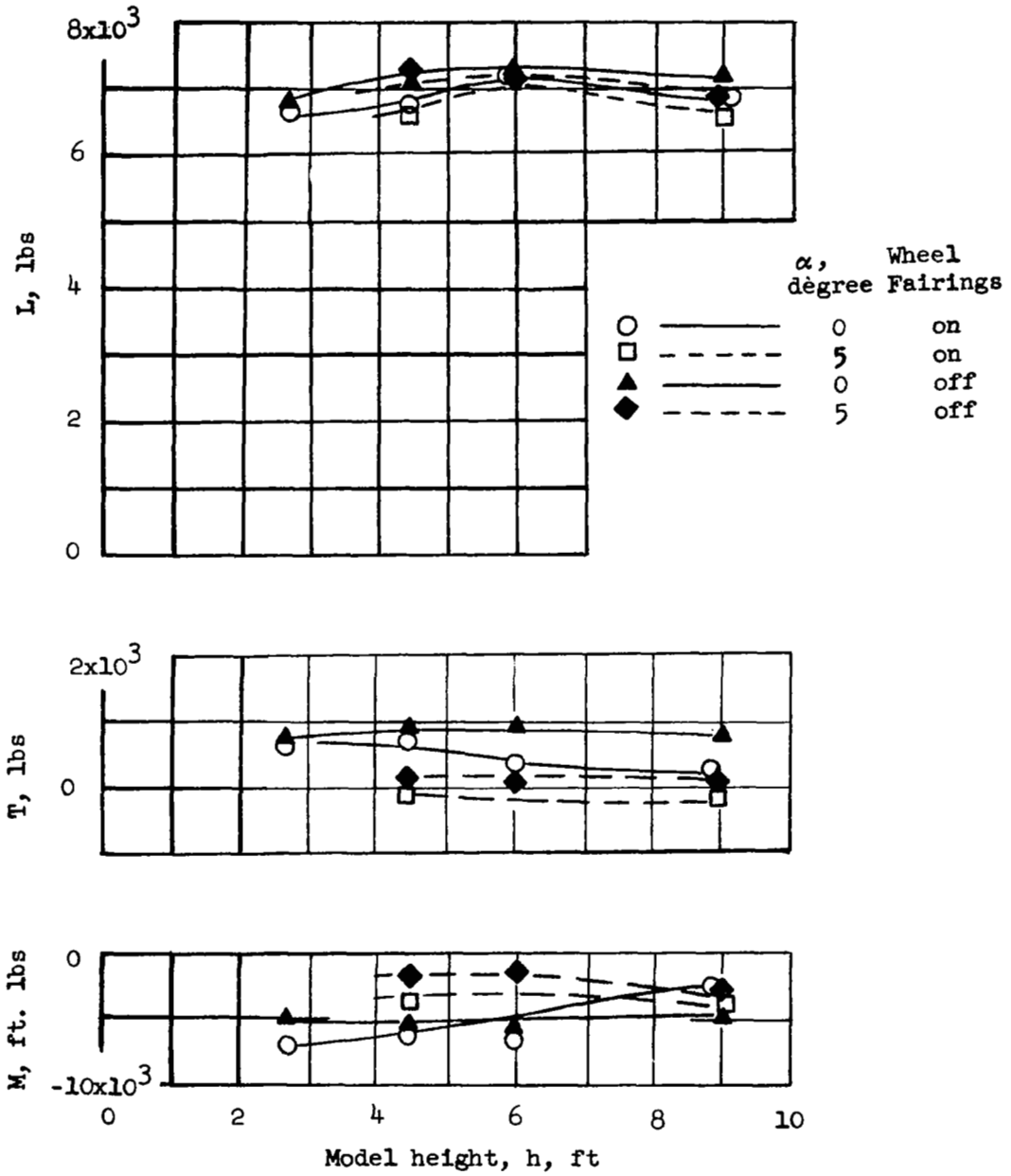

(a) $\beta_v = 0°$

Figure 16. Effect of Ground Distance With and Without Wheel Fairings, Six Fans at 3600 rpm, L/C Power Off

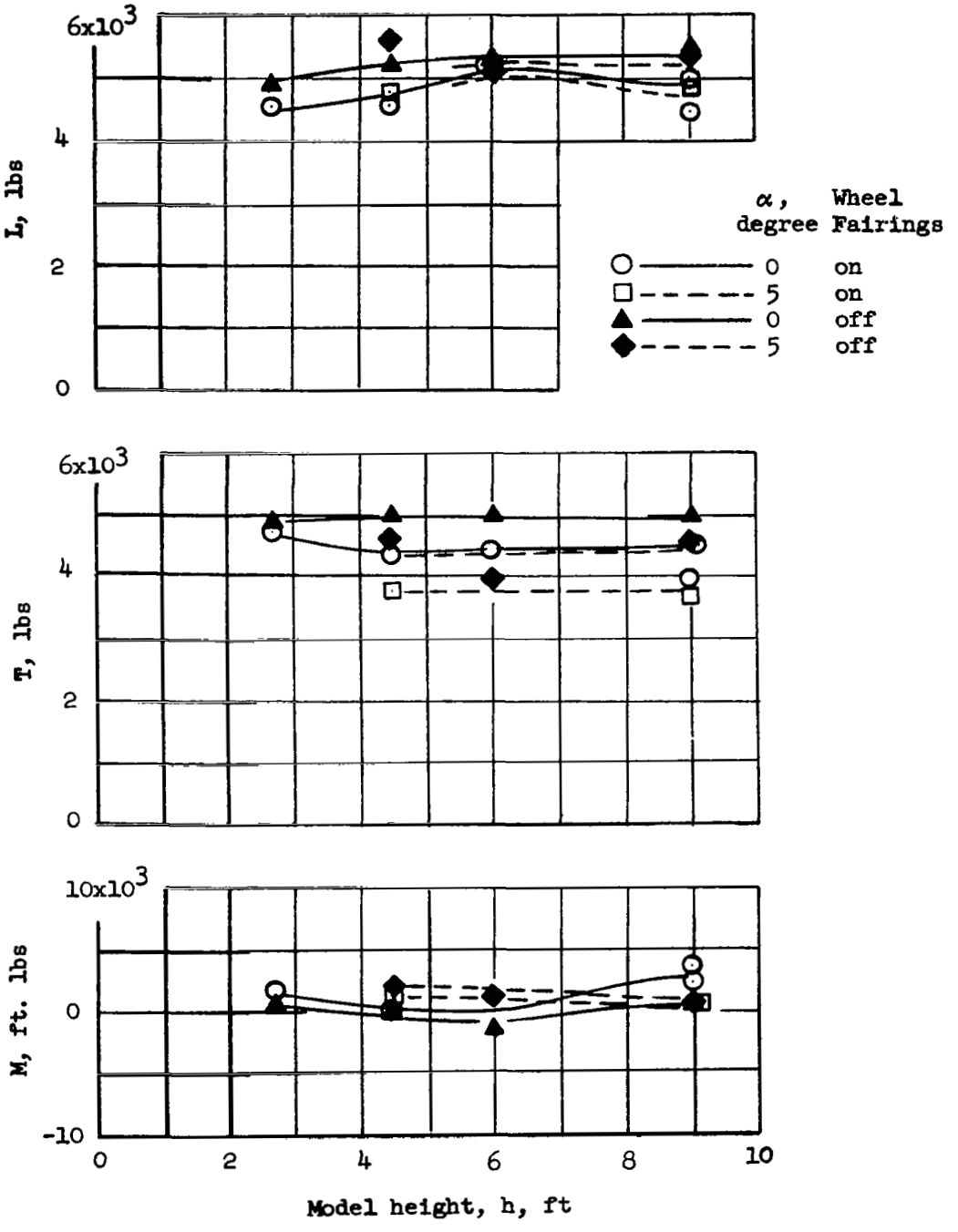

(b) $\beta_v = 30°$

Figure 16. Effect of Ground Distance With and Without Wheel Fairings, Six Fans at 3600 rpm, L/C Power Off (Concluded)

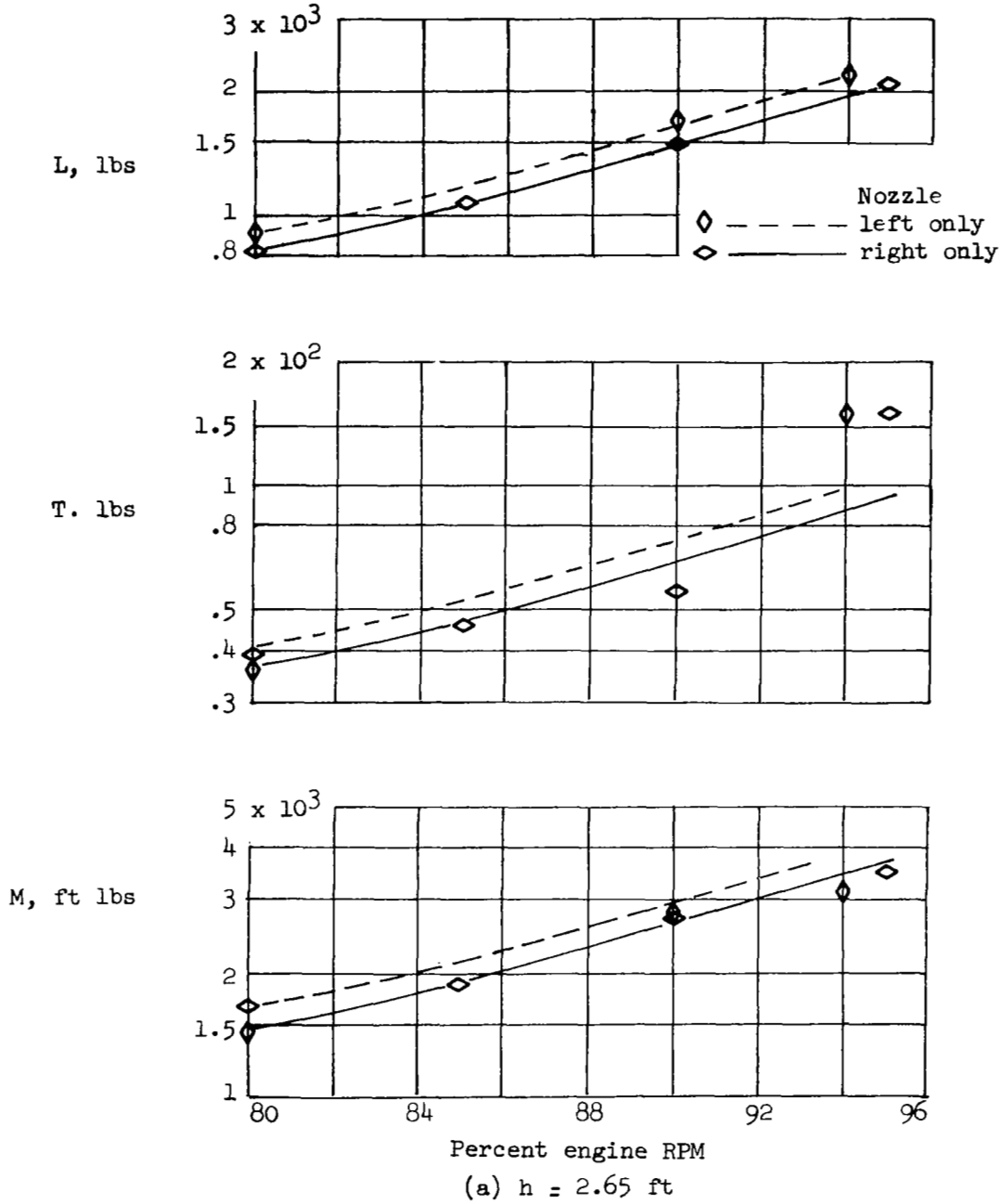

(a) h = 2.65 ft

Figure 17. Comparison of Left and Right L/C Nozzles Versus % Engine RPM, Fan Power Off, $\delta_N = 0°, \alpha = 0°$, Wheel Fairings On

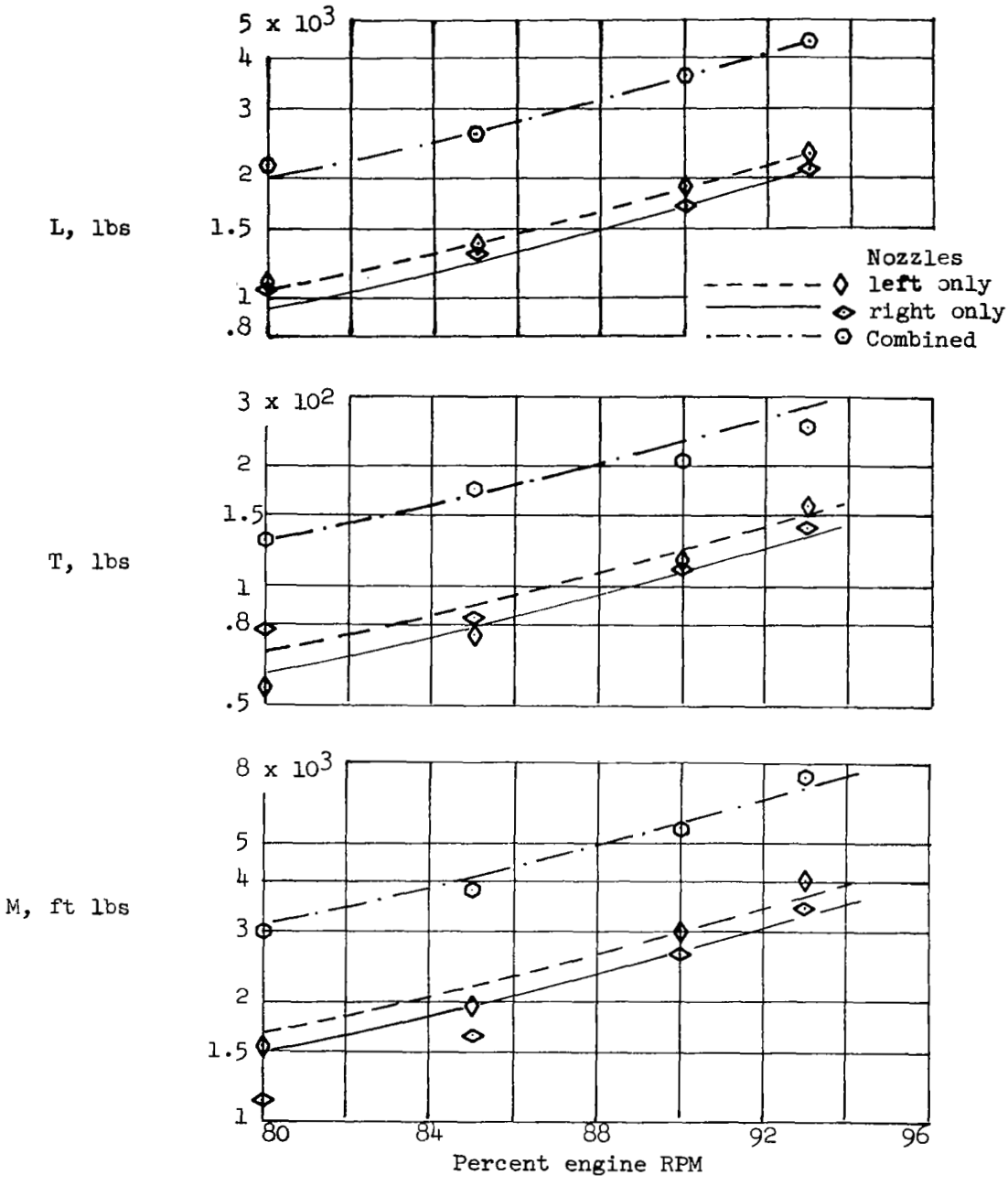

(b) h = 9 ft

Figure 17. Comparison of Left and Right L/C Nozzles Versus % Engine RPM, Fan Power Off, $\delta_N = 0°$, $\alpha = 0°$, Wheel Fairings On (Concluded)

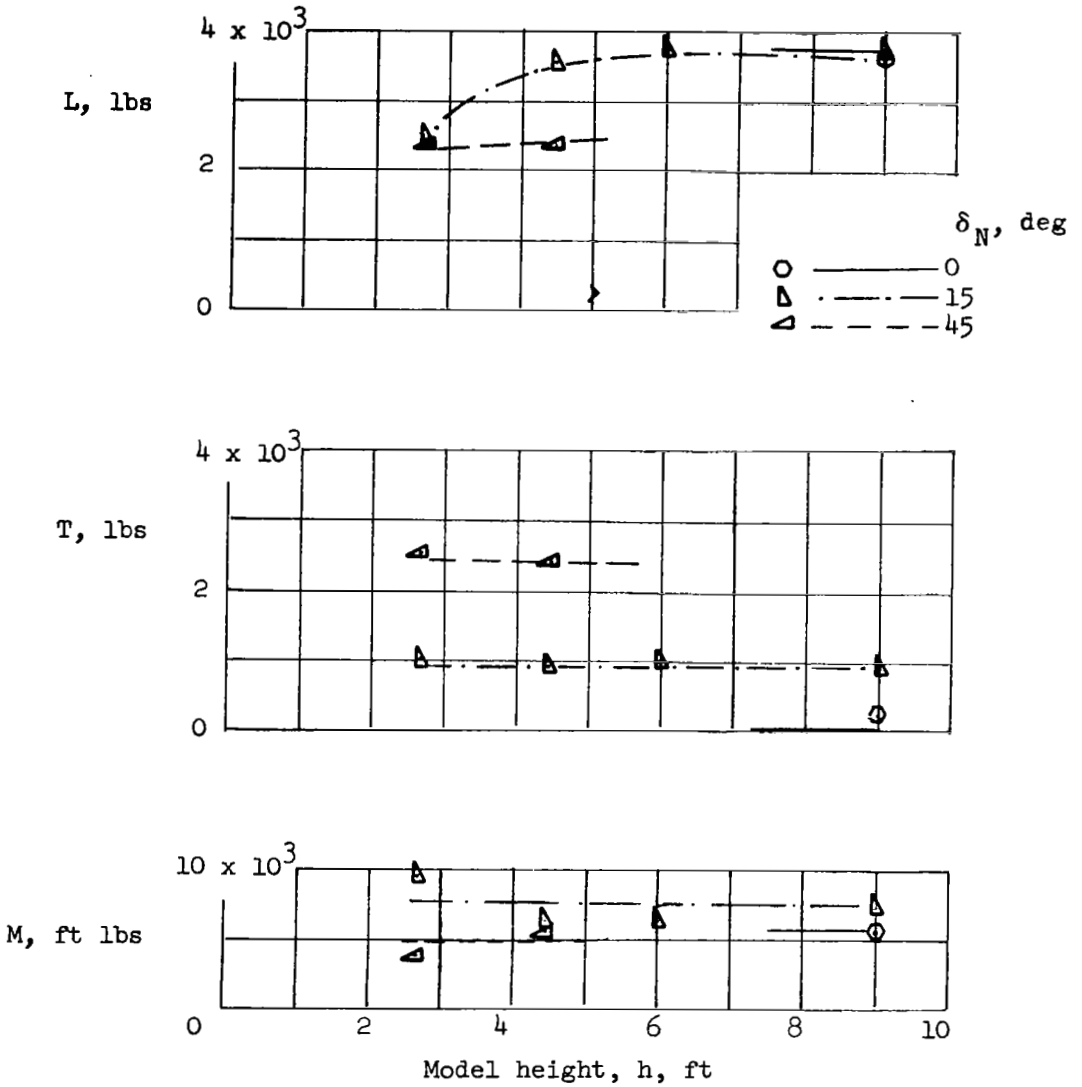

Figure 18. Effect of Model Height With L/C Nozzles Only, 90% RPM, Fan Power Off, Wheel Fairings On

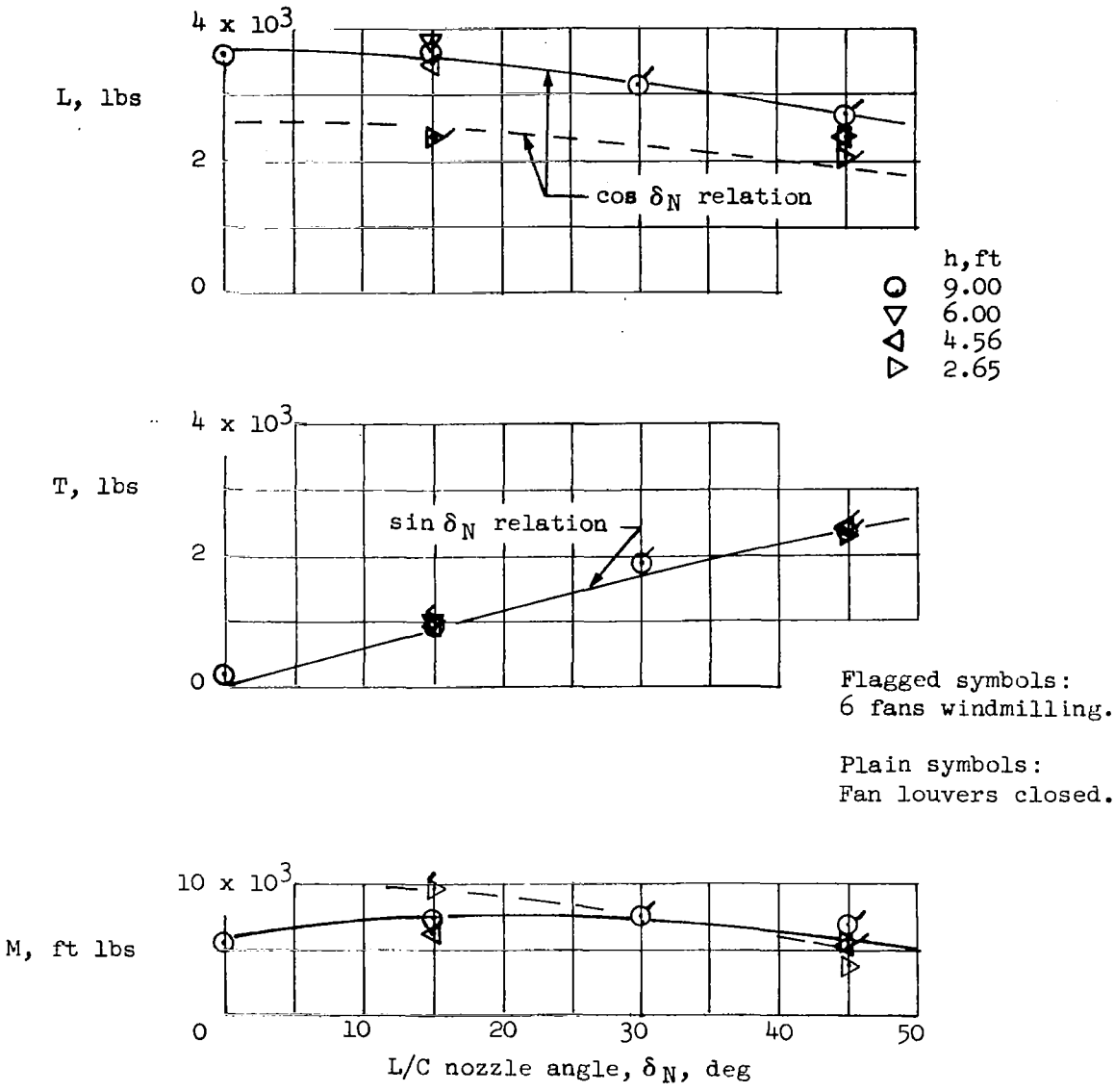

(a) 90% RPM

Figure 19. Effect of L/C Nozzle Rotation, Fan Power Off, Wheel Fairings On, $\alpha = 0°$

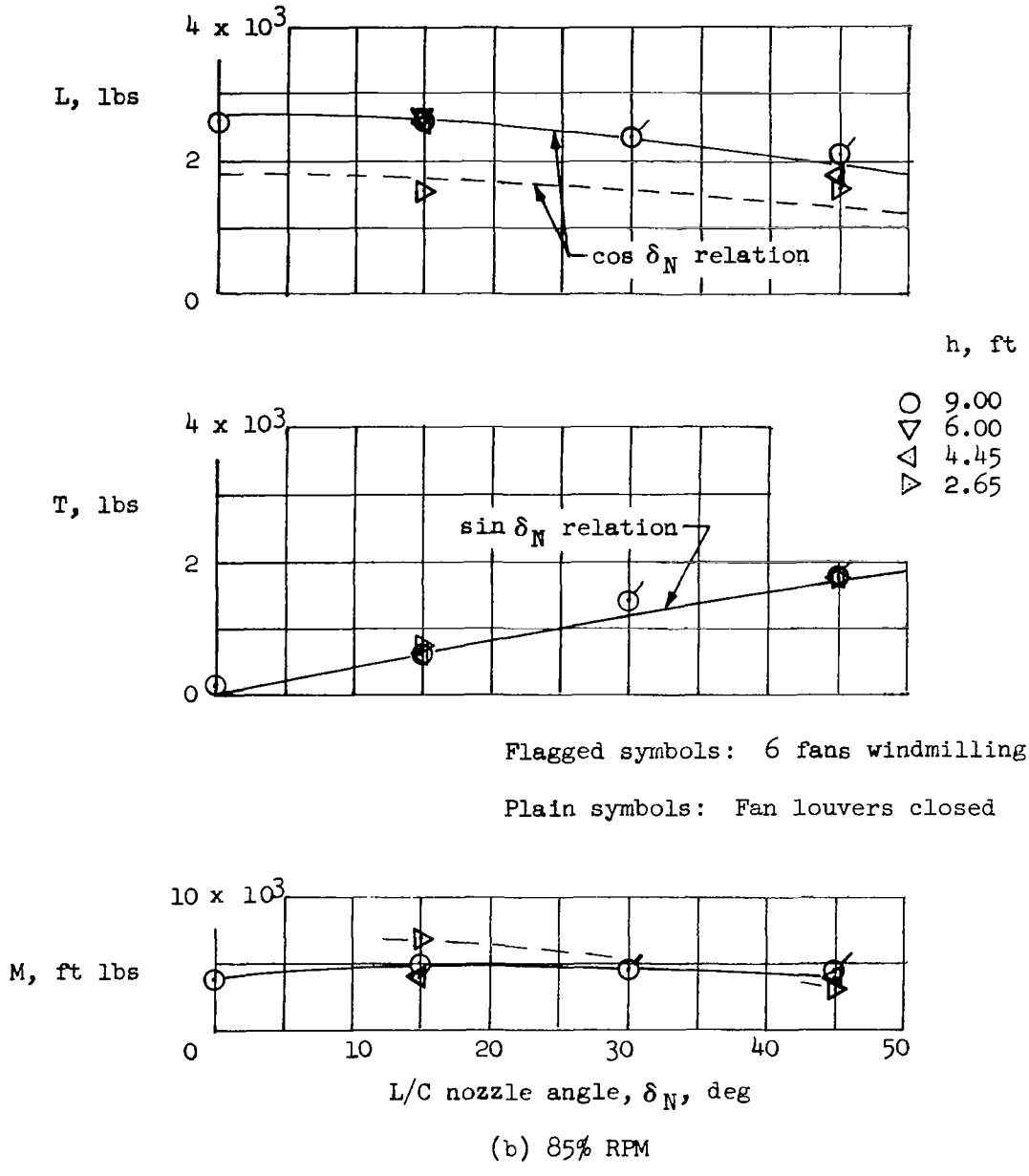

(b) 85% RPM

Figure 19. Effect of L/C Nozzle Rotation, Fan Power Off, Wheel Fairings On, $\alpha = 0°$ (Concluded)

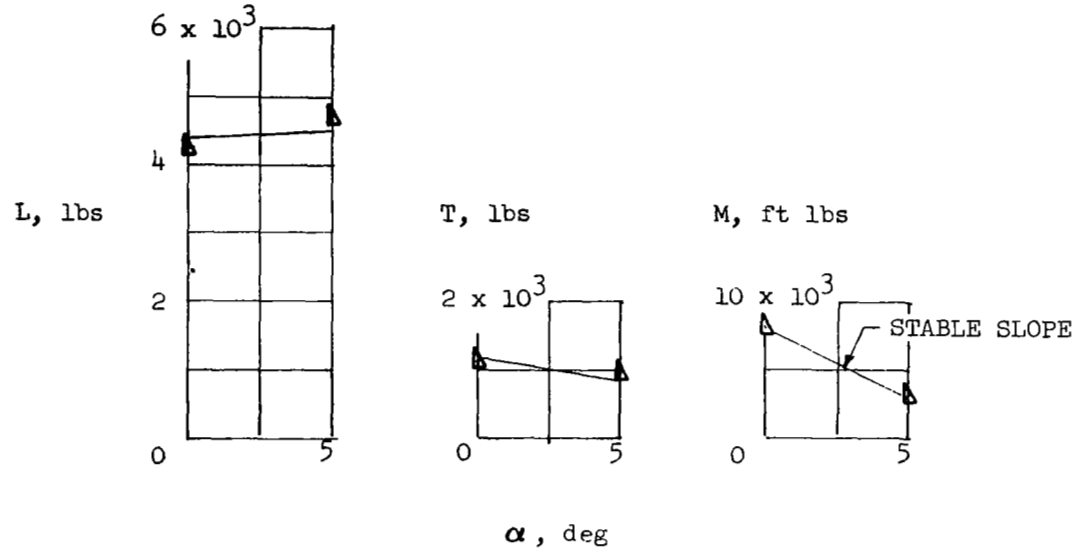

Figure 20. Effect of Angle of Attack, L/C Nozzles at δ_N = 15°, 93% RPM, Fan Power Off, Louvers Closed, Wheel Fairing On, h = 9.0'

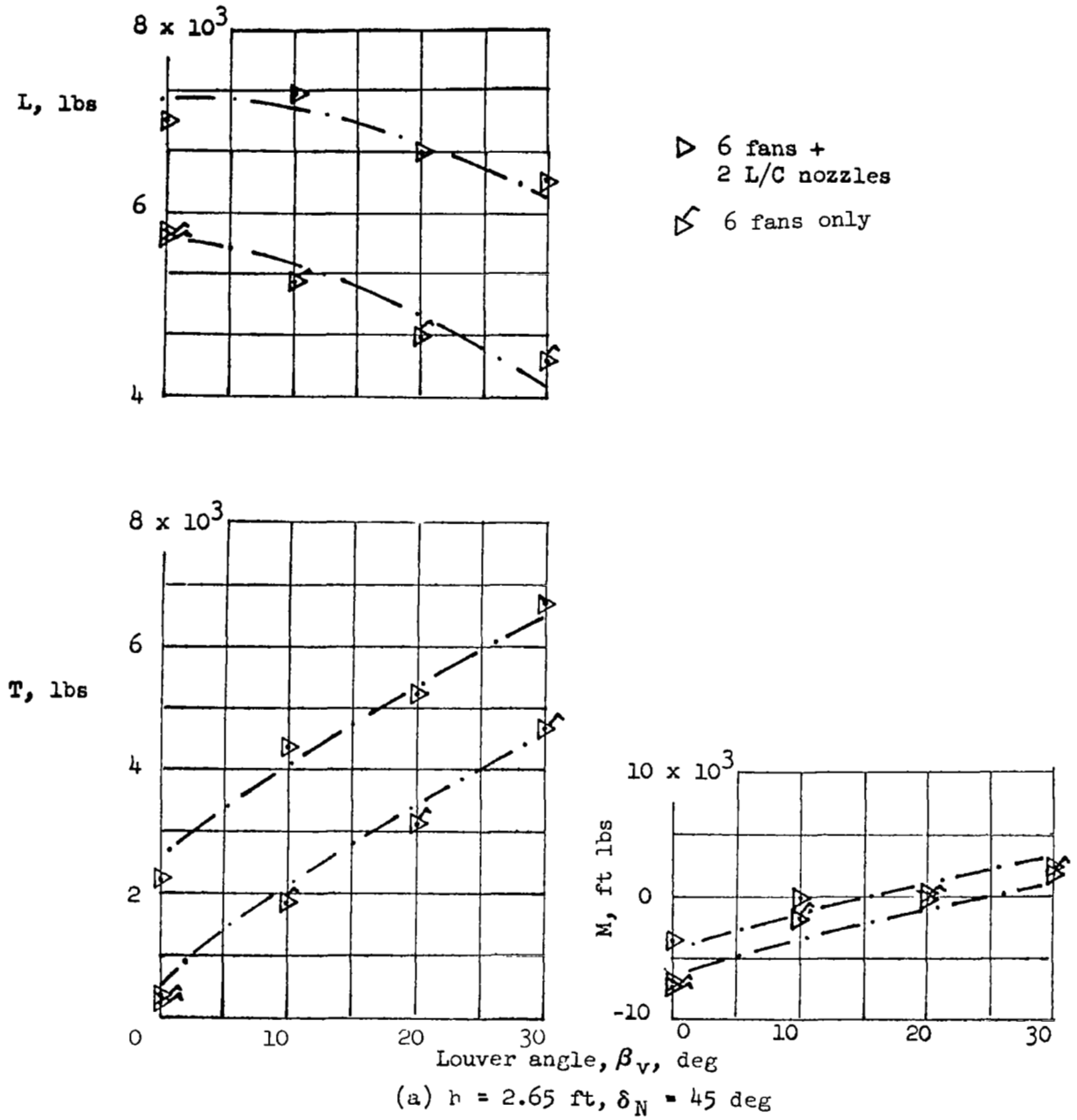

(a) h = 2.65 ft, δ_N = 45 deg

Figure 21. Comparison With and Without L/C Nozzle Operation, Fans at 3600 RPM, 90% L/C Engine RPM, Wheel Fairings On, α = 0

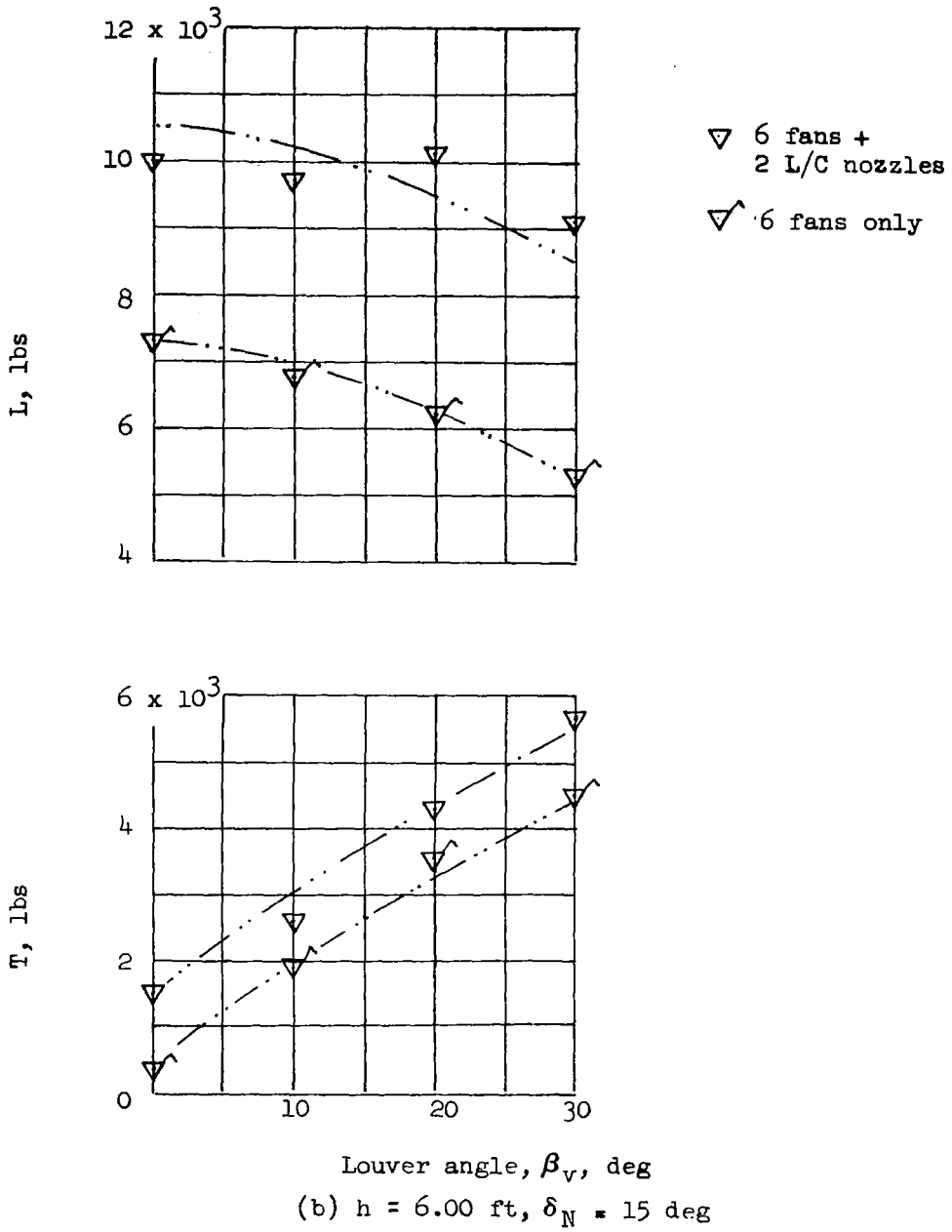

(b) h = 6.00 ft, δ_N = 15 deg

Figure 21. Comparison With and Without L/C Nozzle Operation, Fans at 3600 RPM, 90% L/C Engine RPM, Wheel Fairings on, α = 0 (Continued)

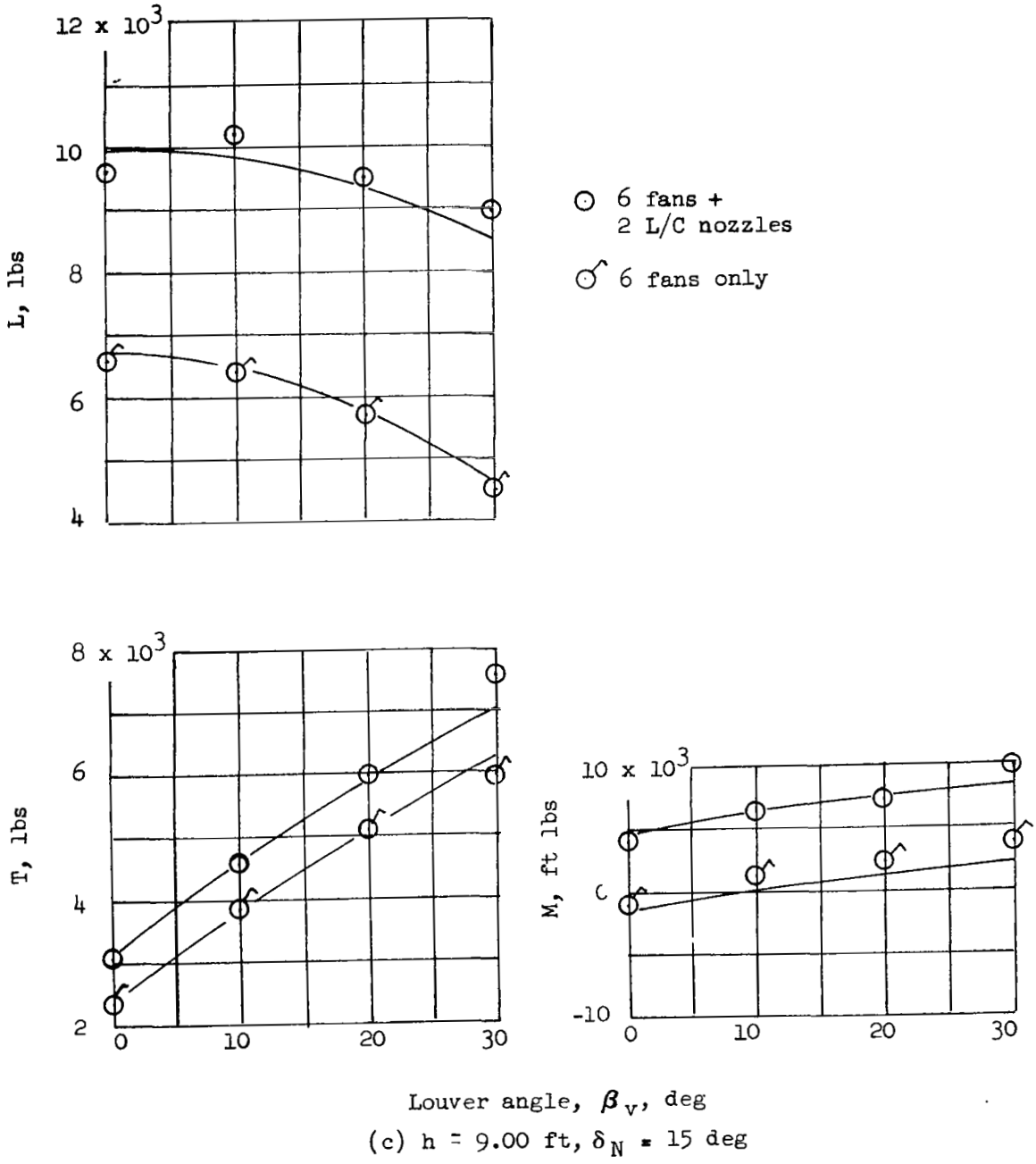

(c) h = 9.00 ft, δ_N = 15 deg

Figure 21. Comparison With and Without L/C Nozzle Operation, Fans at 3600 RPM, 90% L/C Engine RPM, Wheel Fairings on, α = 0 (Concluded)

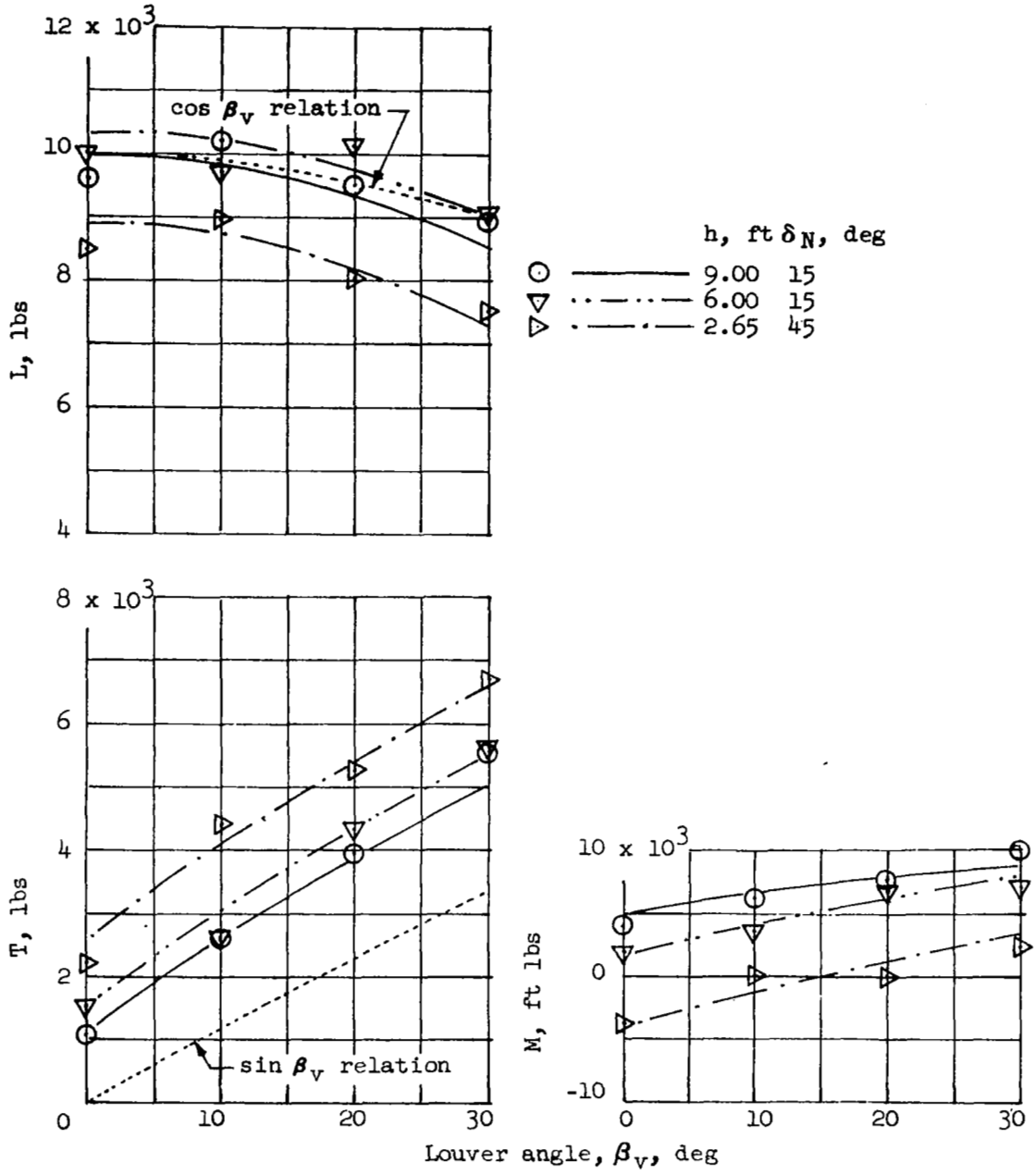

Figure 22. Effect of Fan Louver Angle, Fans at 36 RPM, 90% L/C Engine RPM, $\delta_N = 0°$, Wheel Fairings On, $\alpha = 0$

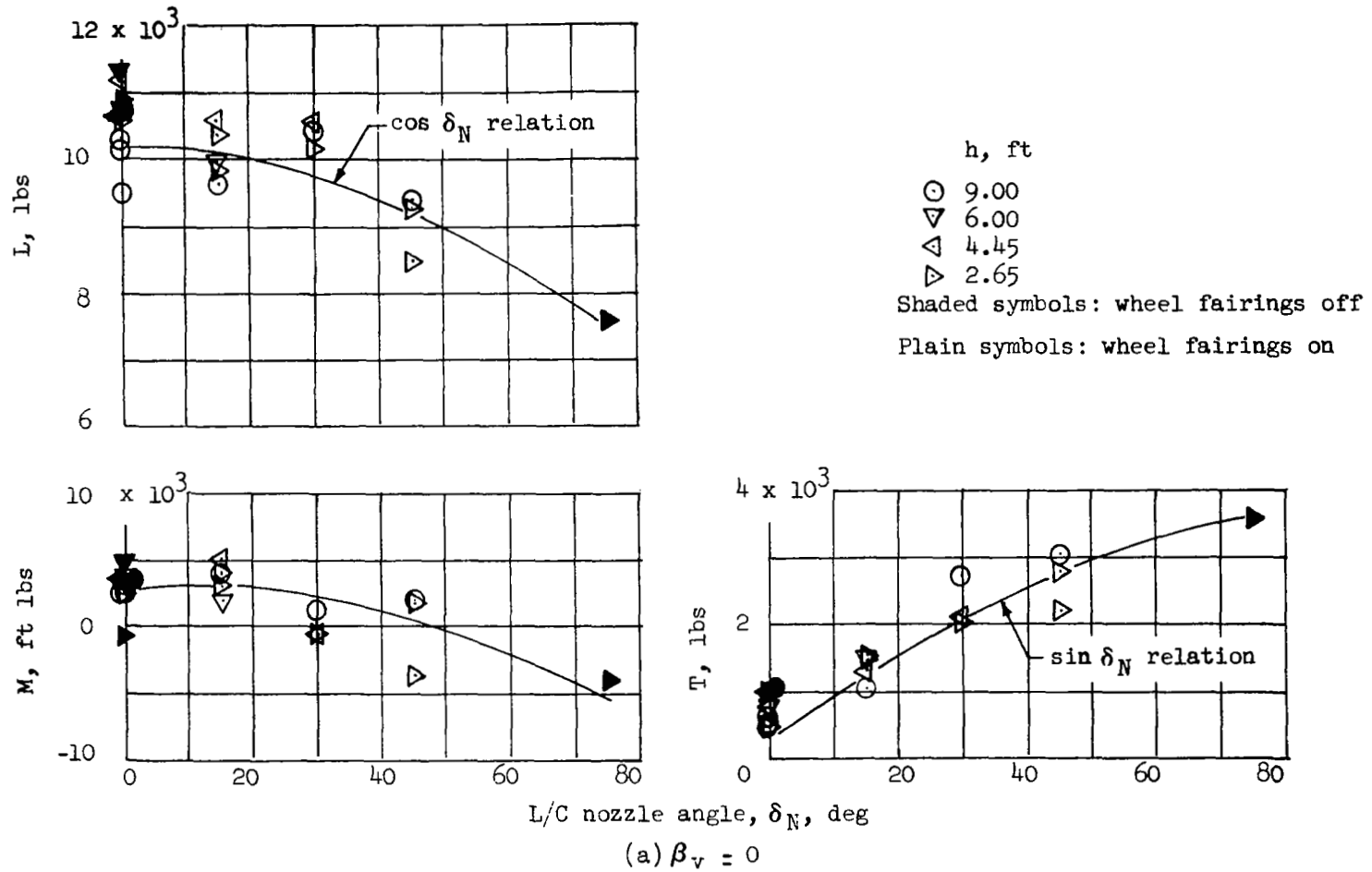

Figure 23. Effect of L/C Nozzle Rotation, Fans at 3600 RPM, L/C Nozzles 90% Power, $\alpha = 0$

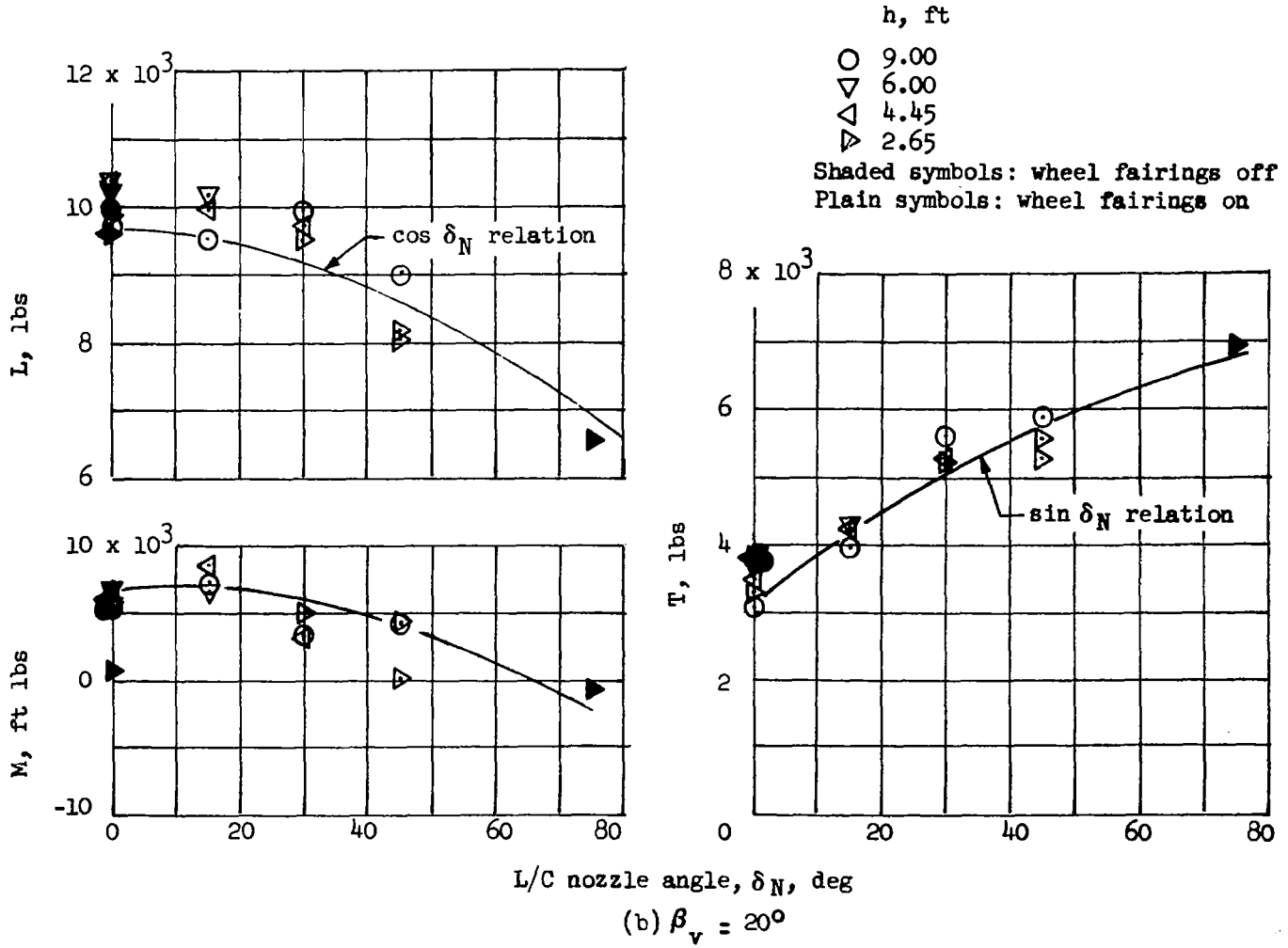

(b) $\beta_v = 20^o$

Figure 23. Effect of L/C Nozzle Rotation, Fans at 3600 RPM, L/C Nozzles 90% Power, $\alpha = 0$ (Continued)

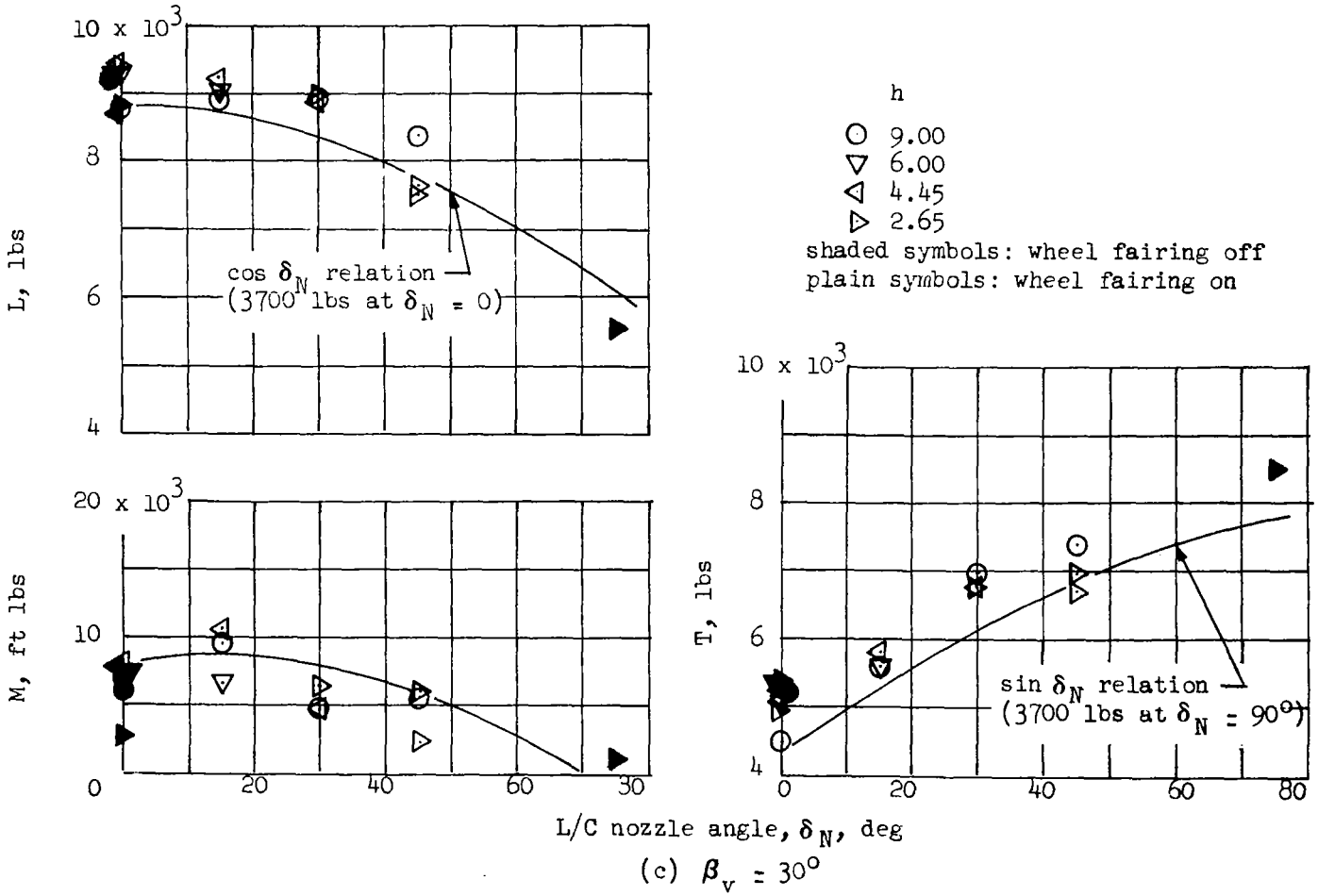

Figure 23. Effect of L/C Nozzle Rotation, Fans at 3600 RPM, L/C Nozzles 90% Power, α = 0 (Concluded)

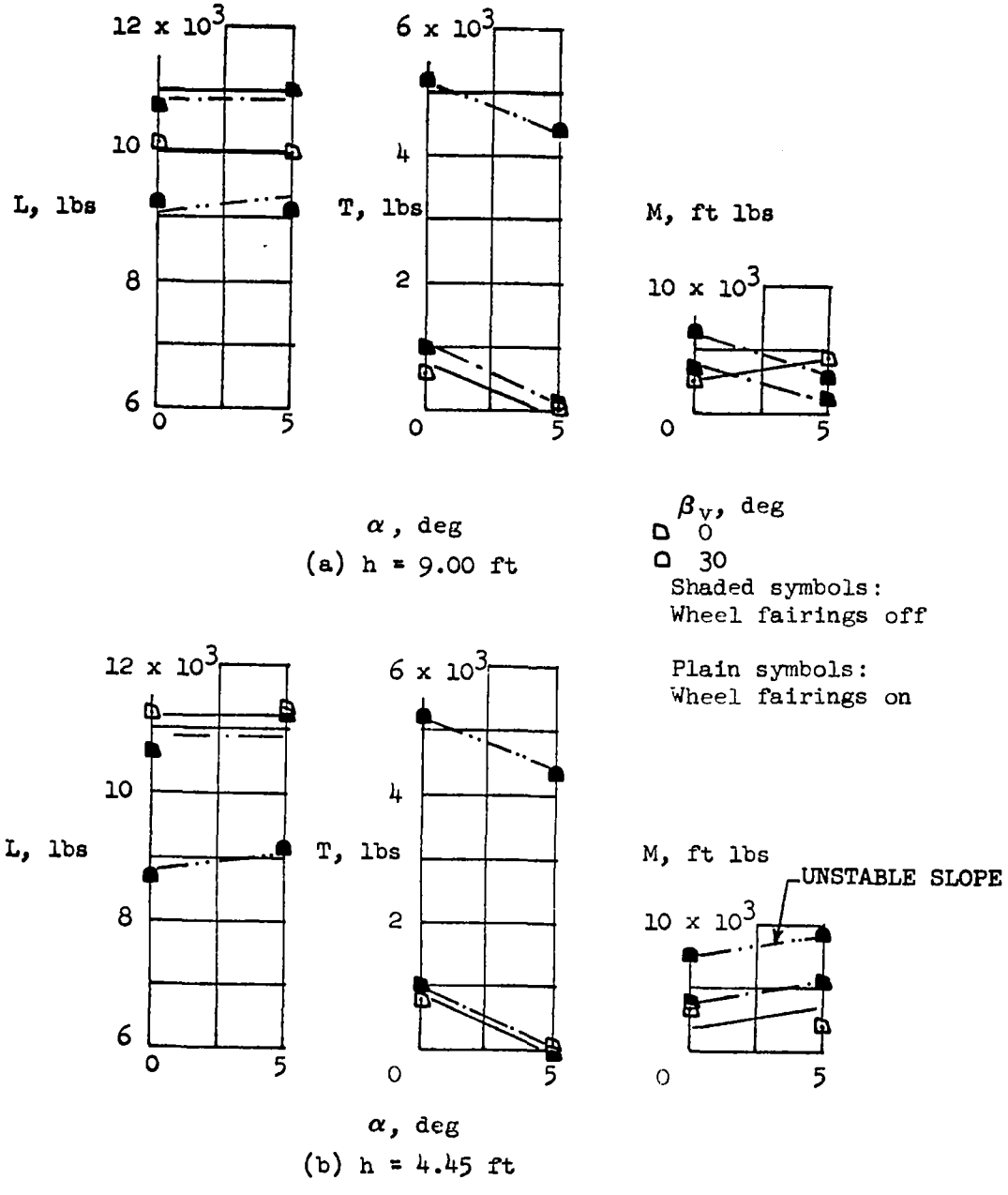

Figure 24. Effect of Angle of Attack, Fans at 3600 RPM, L/C Nozzles 90% Power, $\delta_N = 0°$

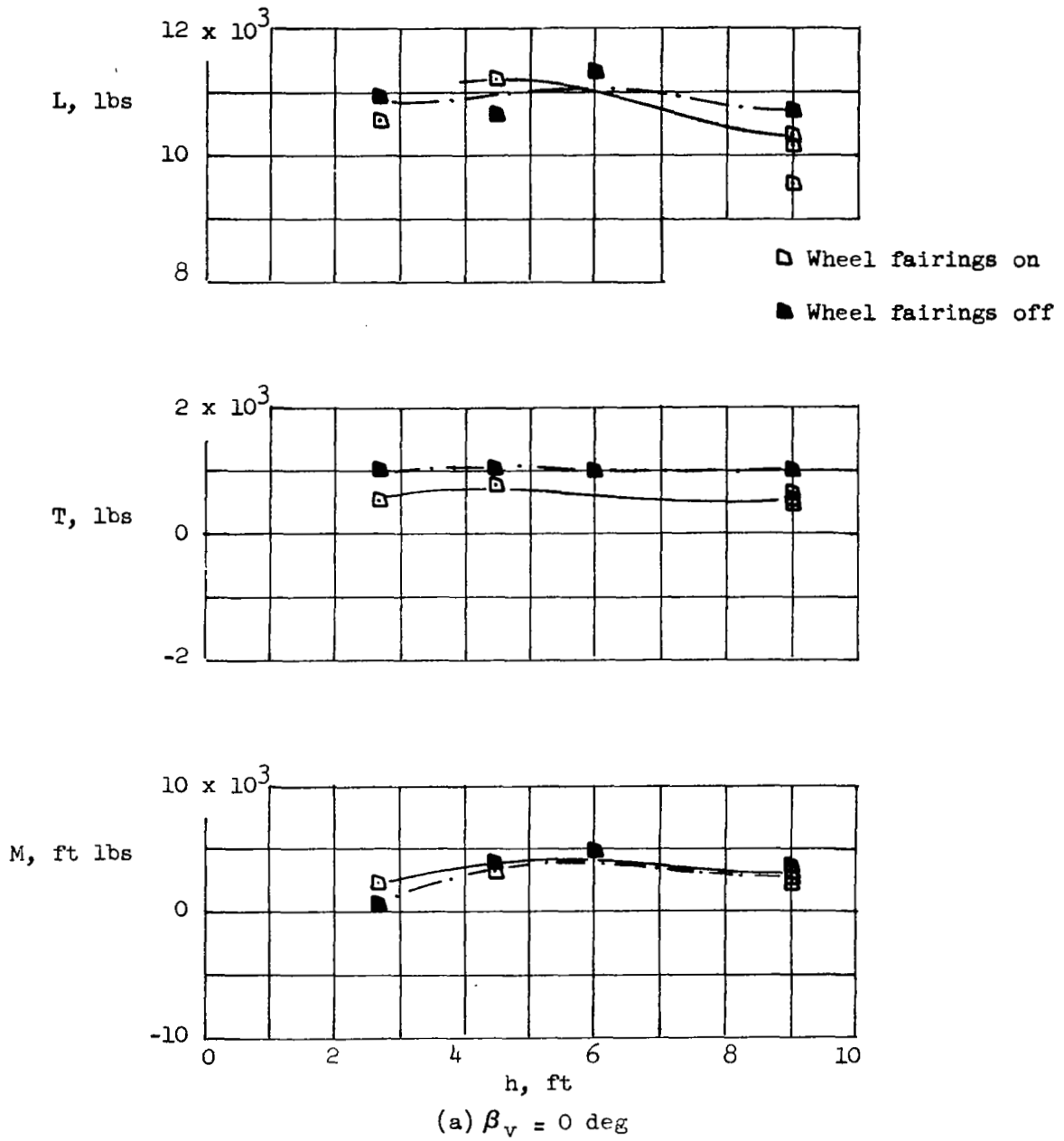

(a) β_V = 0 deg

Figure 25. Effect of Model Height, Fans at 3600 RPM, L/C Nozzles 90% Power, δ_N = 0°, α = 0

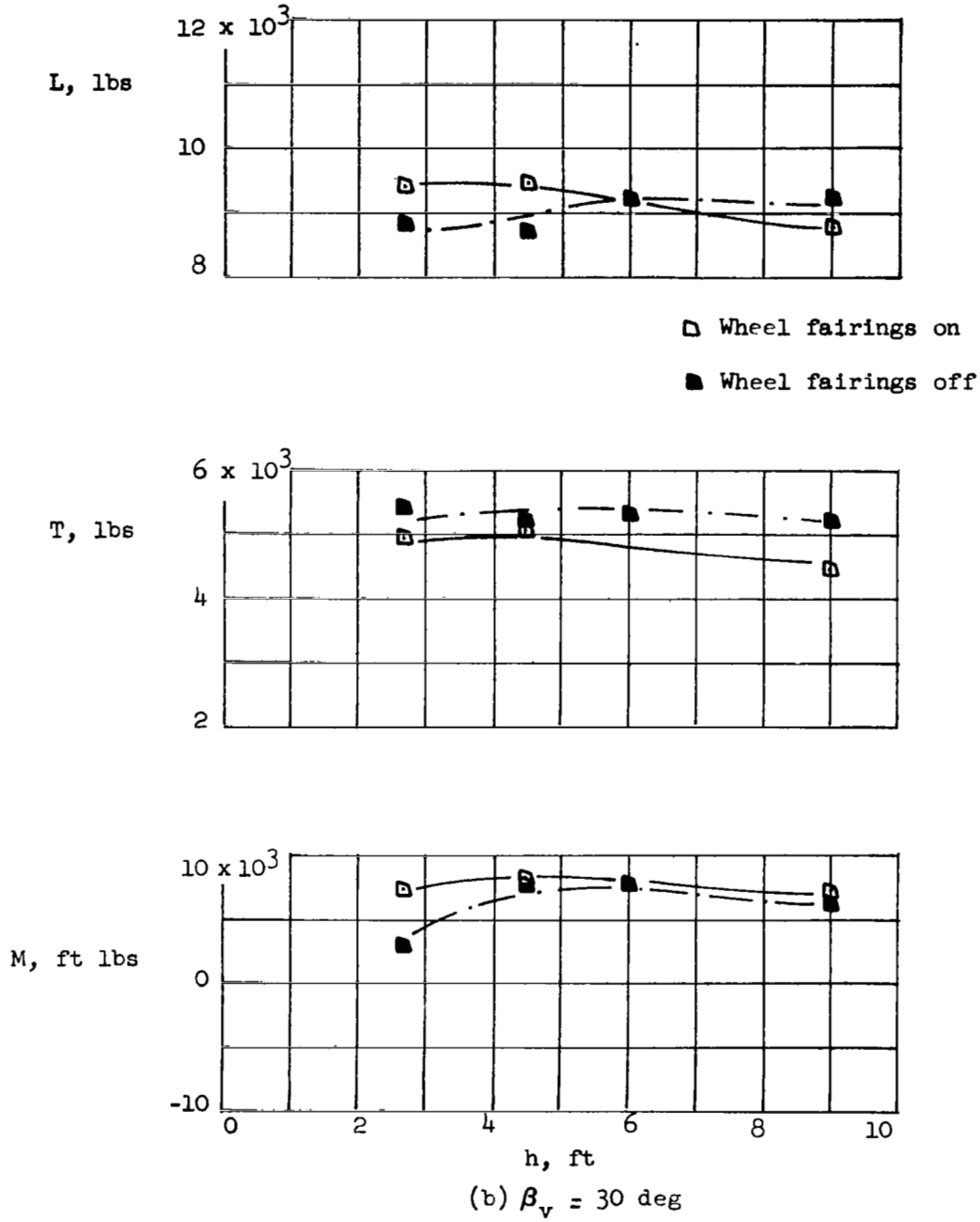

(b) β_V = 30 deg

Figure 25. Effect of Model Height, Fans at 3600 RPM, L/C Nozzles 90% Power, $\delta_N = 0°, \alpha = 0$ (Concluded)

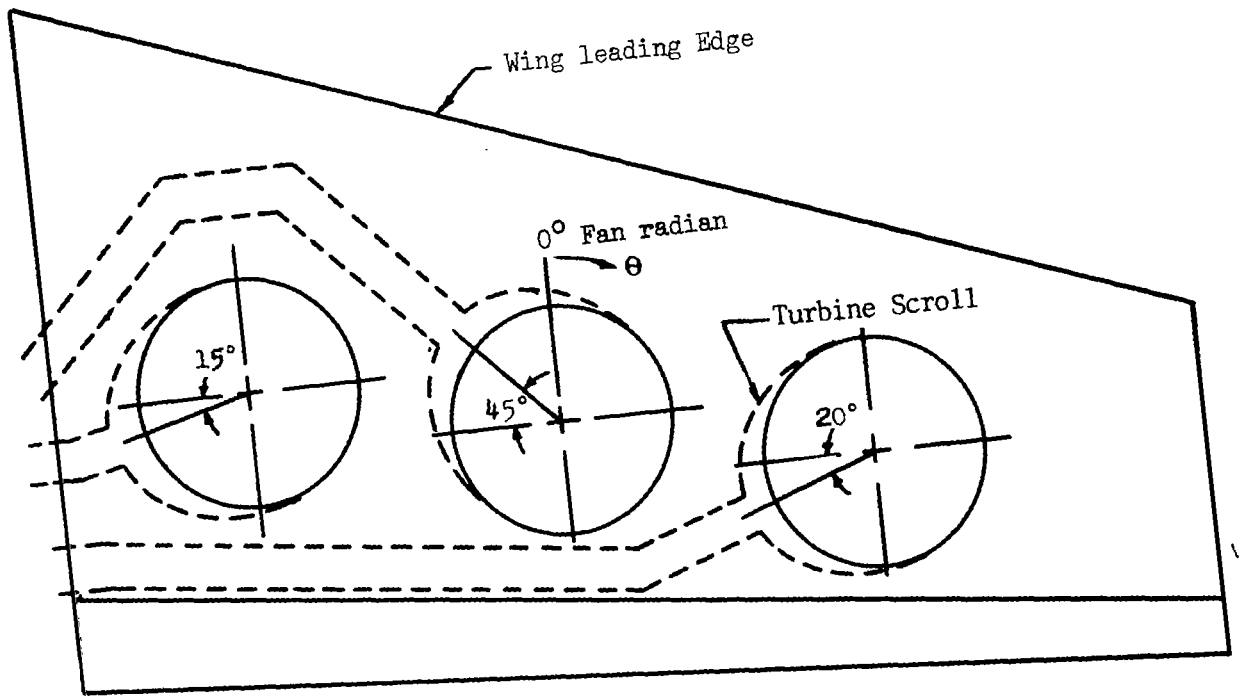

Figure 26. Schematic Diagram of Right-Hand Wing Panel Showing Fan Perimeter Areas Covered By Turbine Scrolls

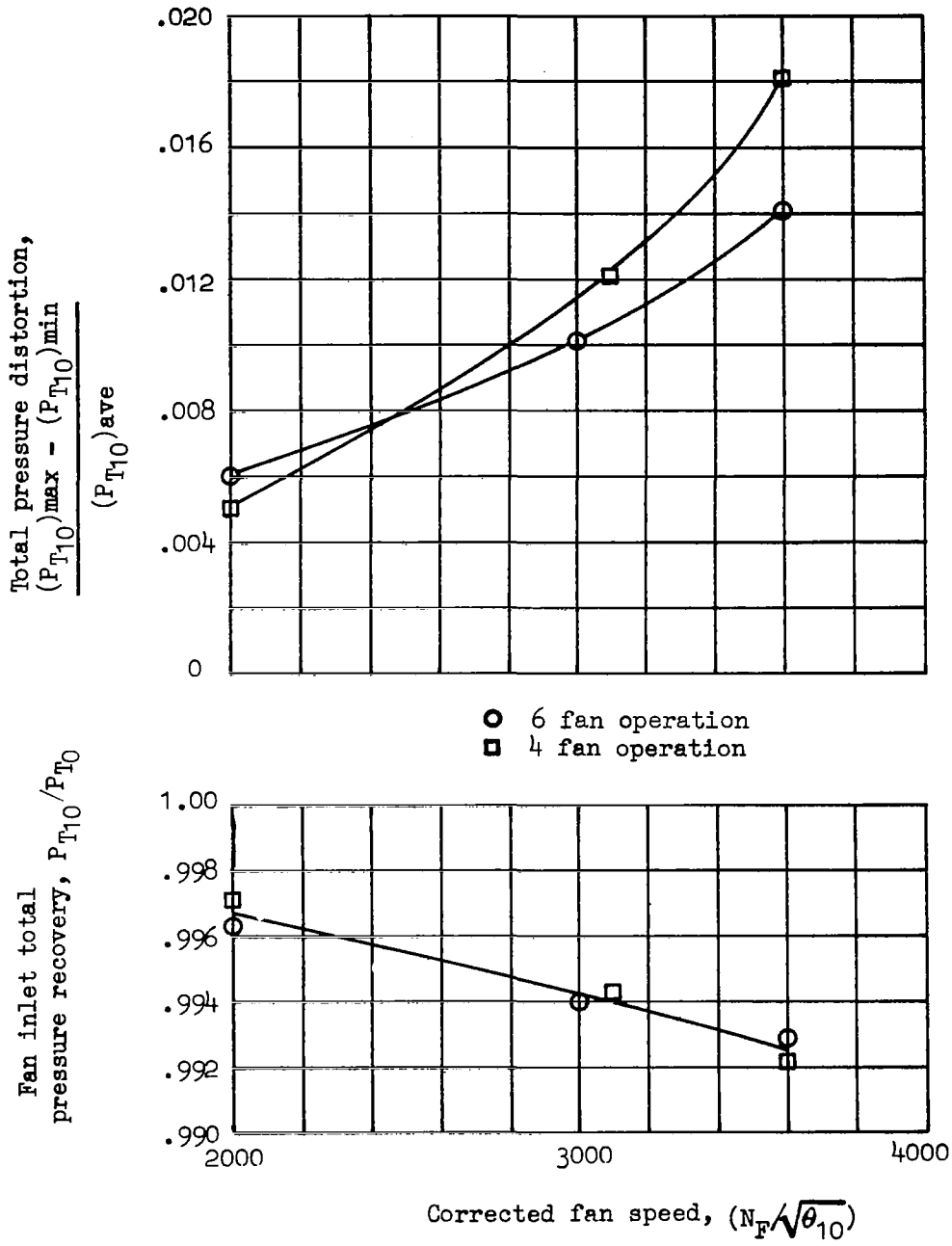

Figure 27. Fan Bellmouth Inlet Performance, Right-Hand Center Fan, Ground Height = 2.65 Ft, L/C Engines Off, β_V = 0°

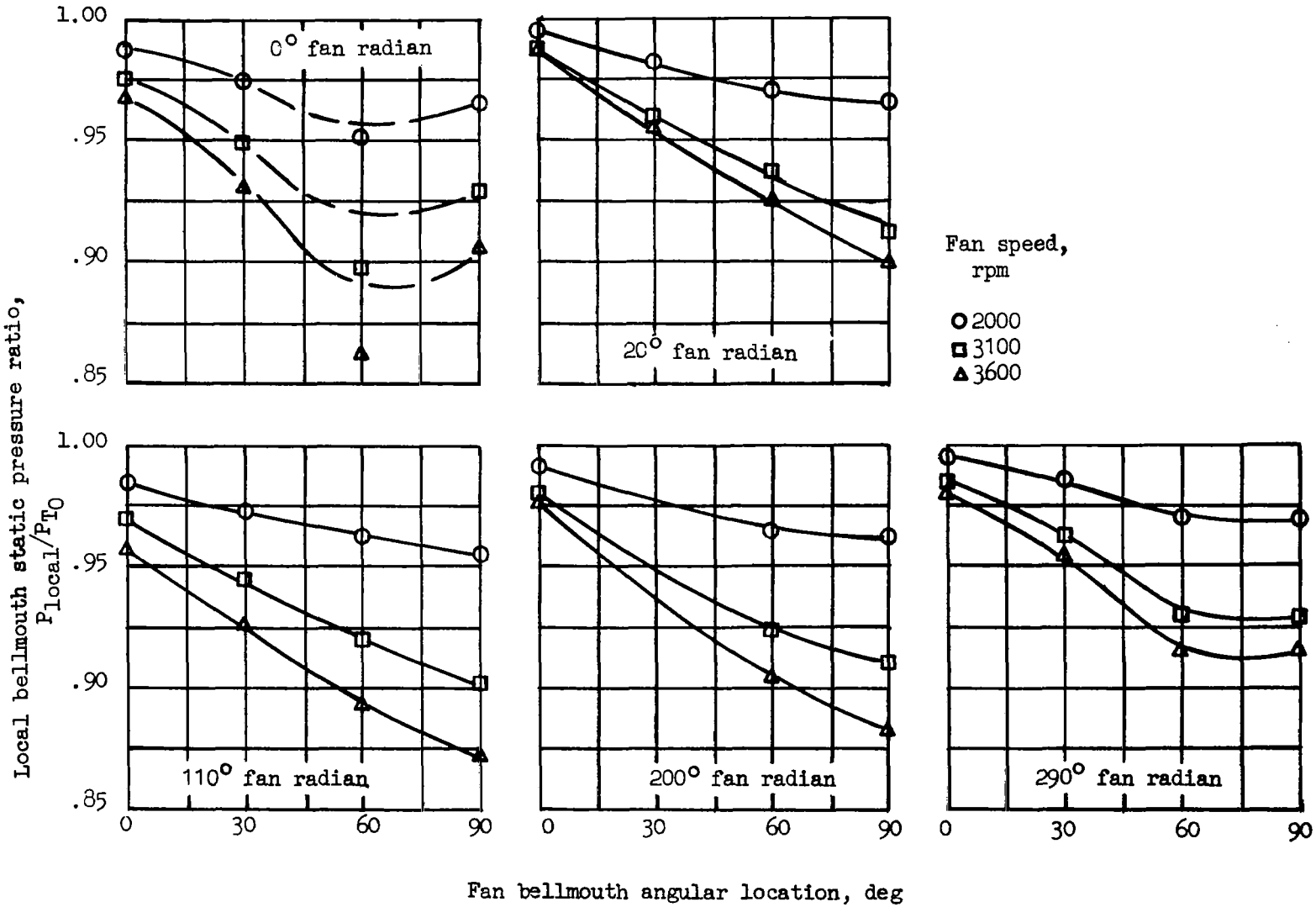

Figure 28. Fan Bellmouth Static Pressure Distributions; Right-Hand Center Fan, Four-Fan Operation, Ground Height = 2.65 Ft, L/C Engines Off, β_V = 0°

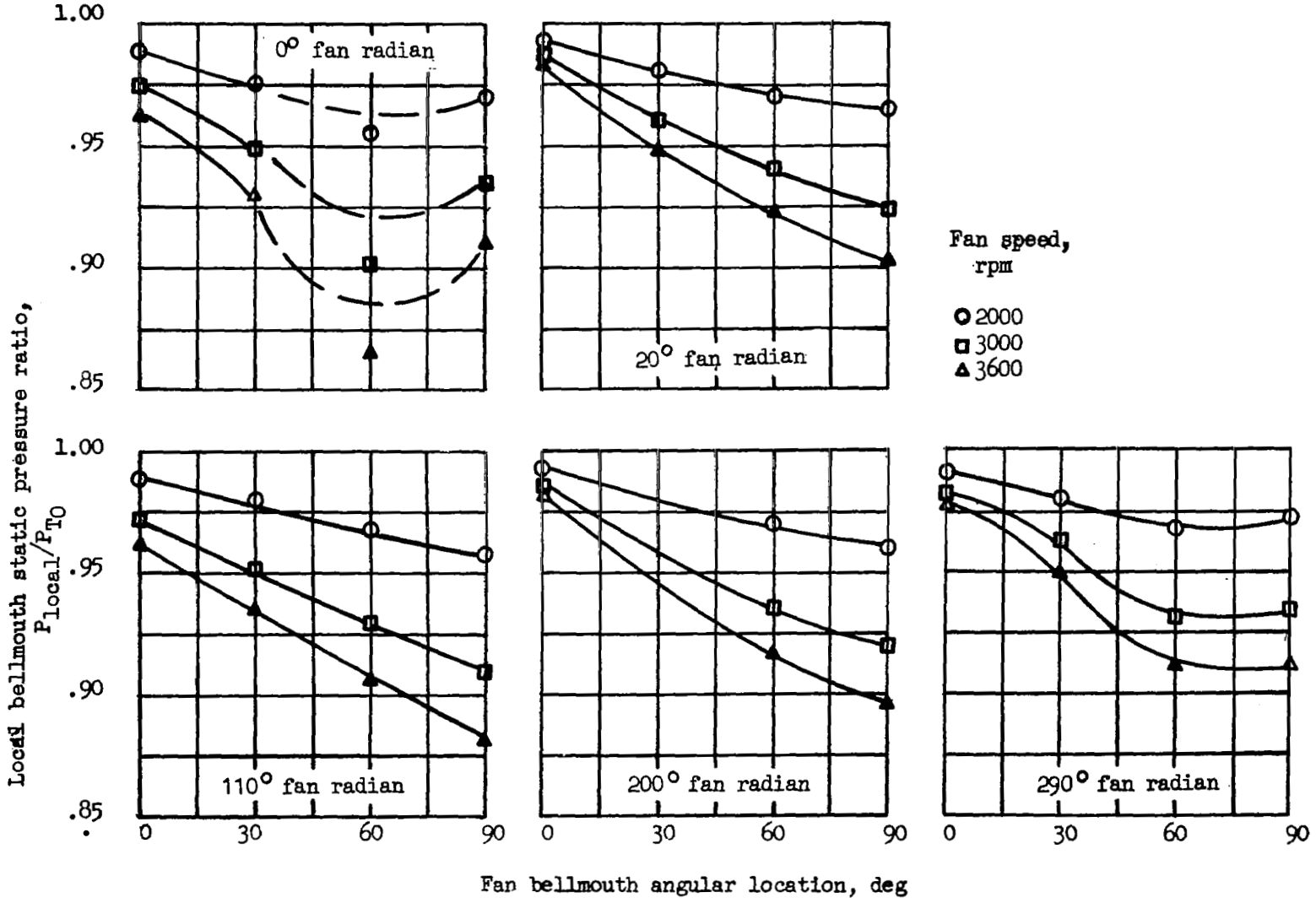

Figure 29. Fan Bellmouth Static Pressure Distributions; Right-Hand Center Fan, Six-Fan Operation, Ground Height = 2.65 Ft; L/C Engines Off, $\beta_V = 0°$

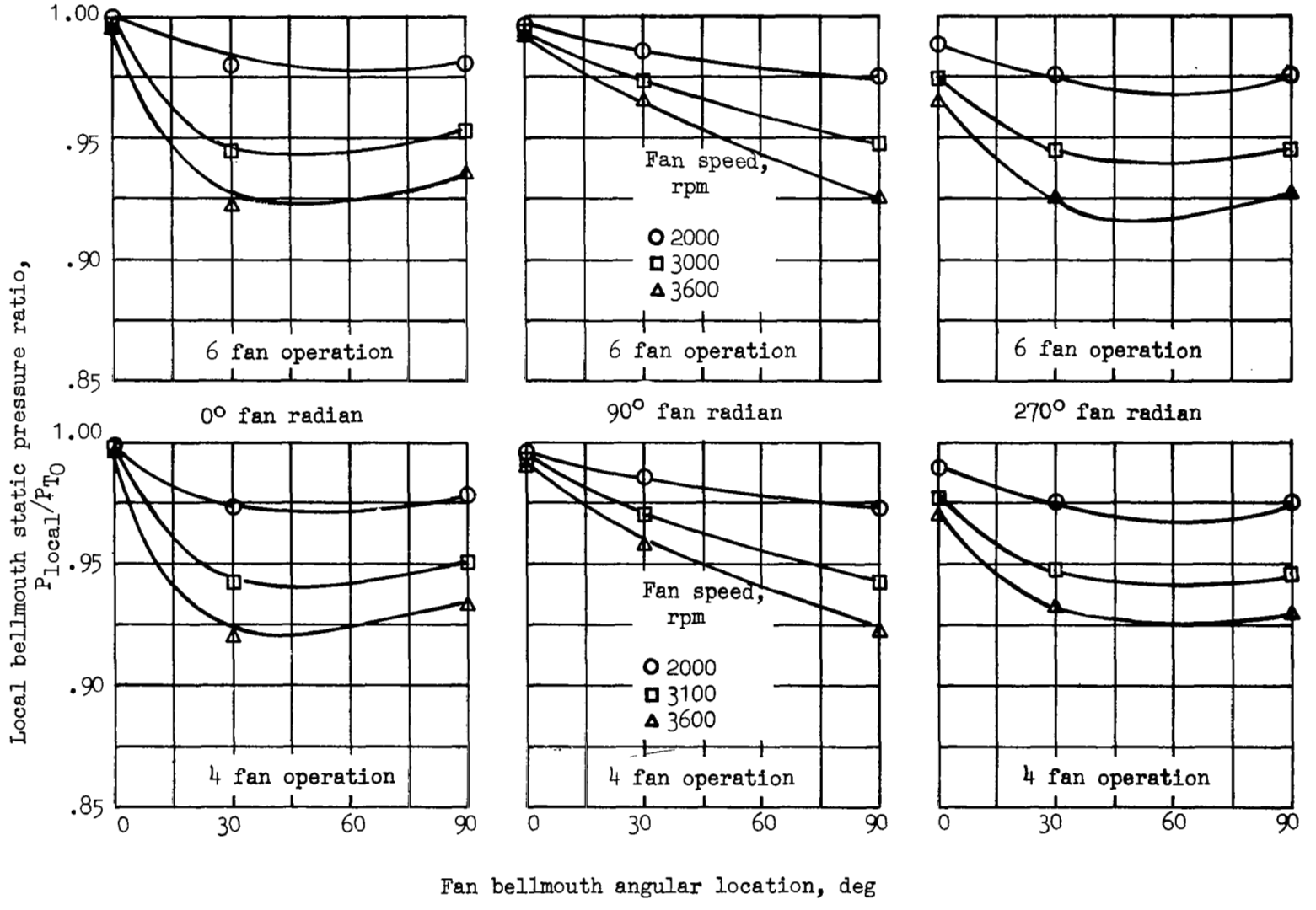

Figure 30. Fan Bellmouth Static Pressure Distributions; Right-Hand Inboard Fan, Ground Height = 2.65 Ft, L/C Engines Off, β_V = 0°

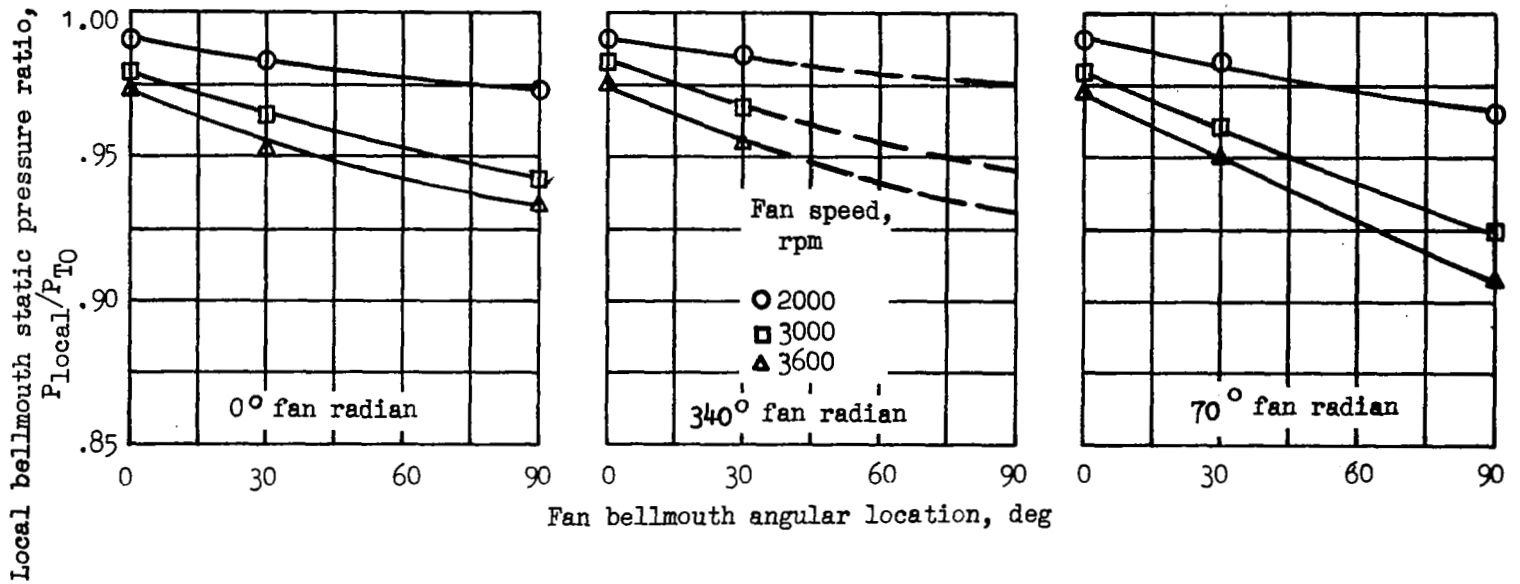

Figure 31. Fan Bellmouth Static Pressure Distributions; Right-Hand Outboard Fan, Six-Fan Operation, Ground Height = 2.65 Ft, L/C Engines Off, β_V = 0°

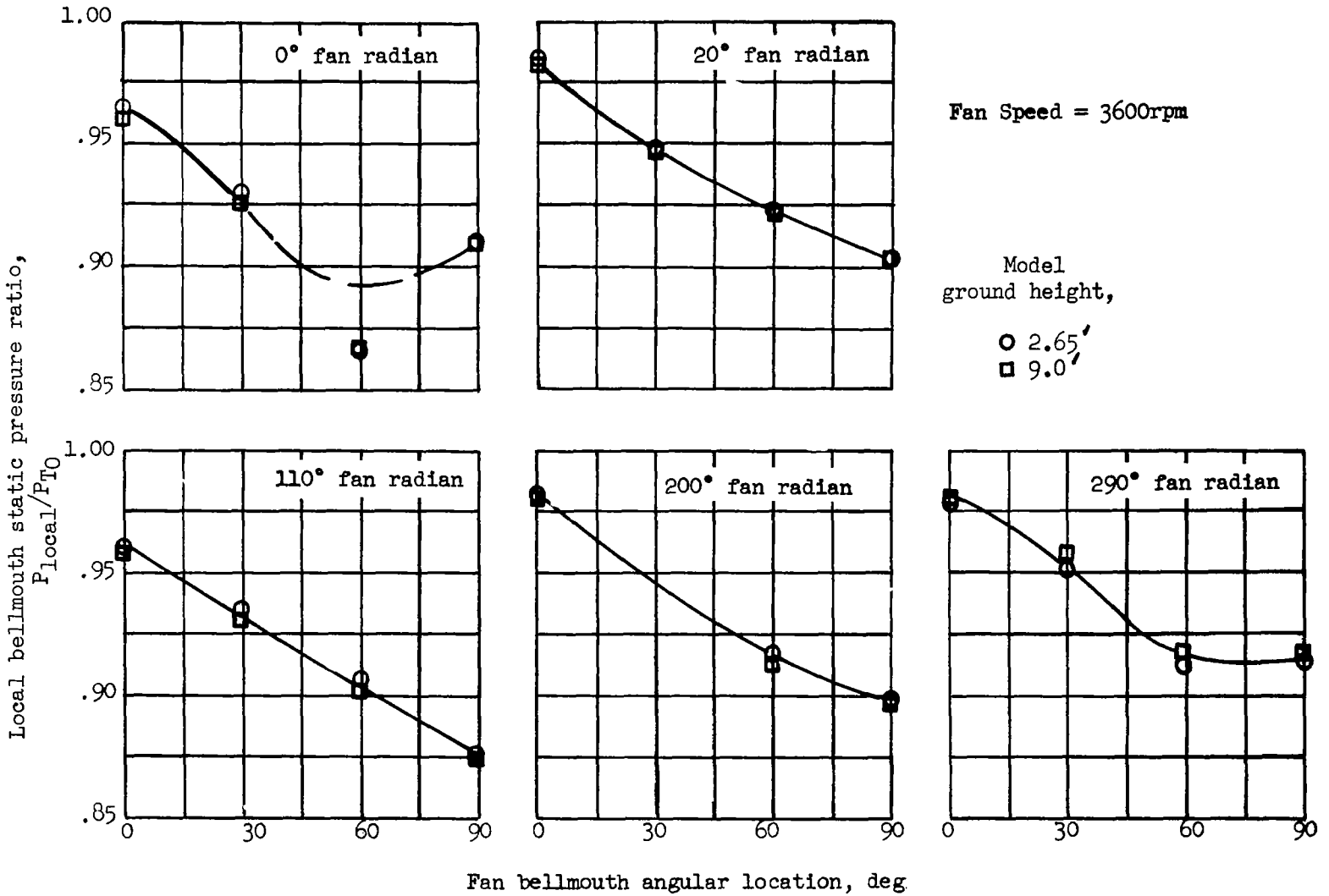

Figure 32. Effect of Ground Height on Fan Bellmouth Static Pressure Distributions; Right-Hand Center Fan, Six-Fan Operation, L/C Engines Off, β_V = 0°

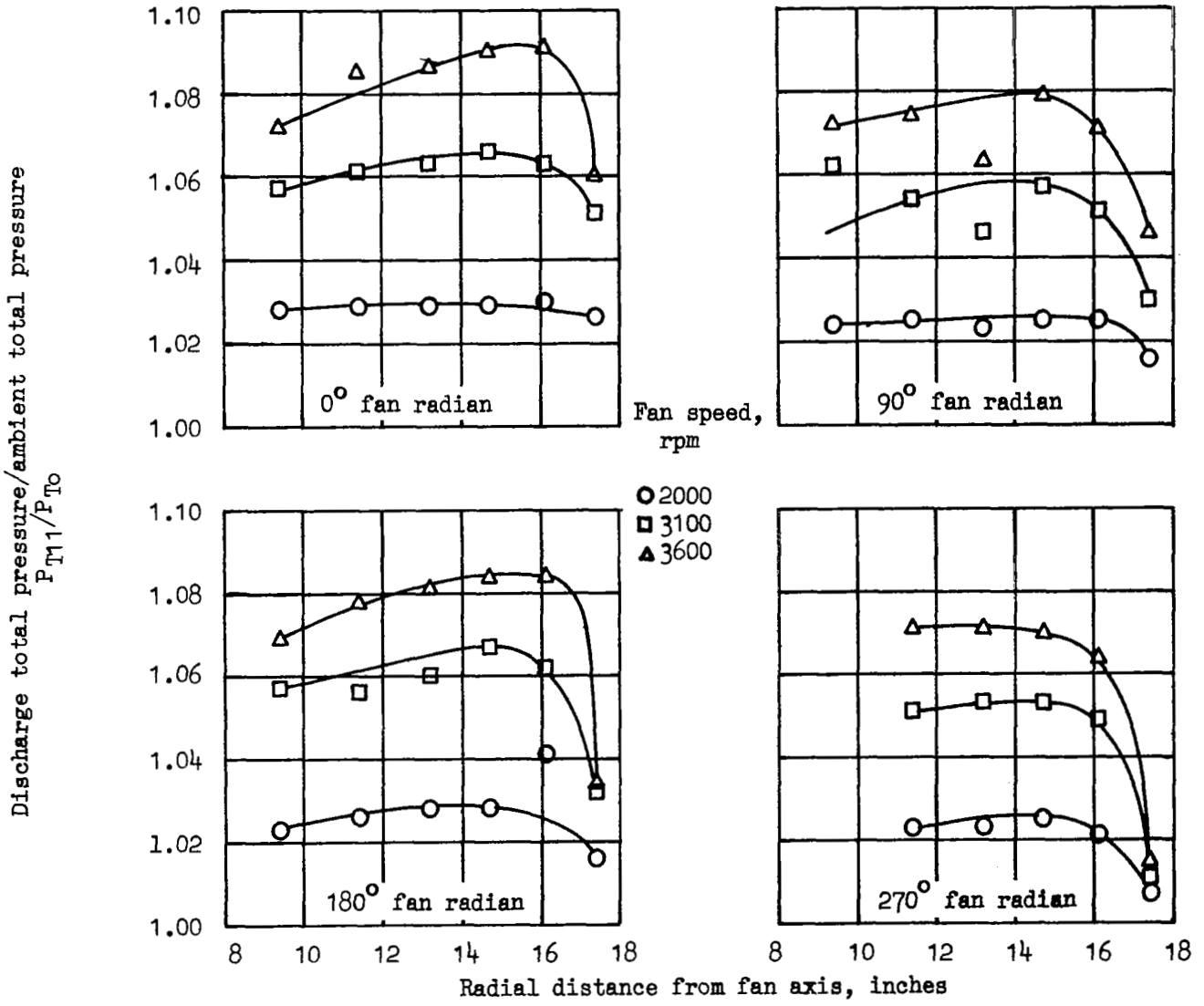

Figure 33. Fan Discharge Total Pressure Distribution; Right-Hand Center Fan, Four-Fan Operation, Ground Height = 2.65 Ft, L/C Engines Off, $\beta_V = 0$

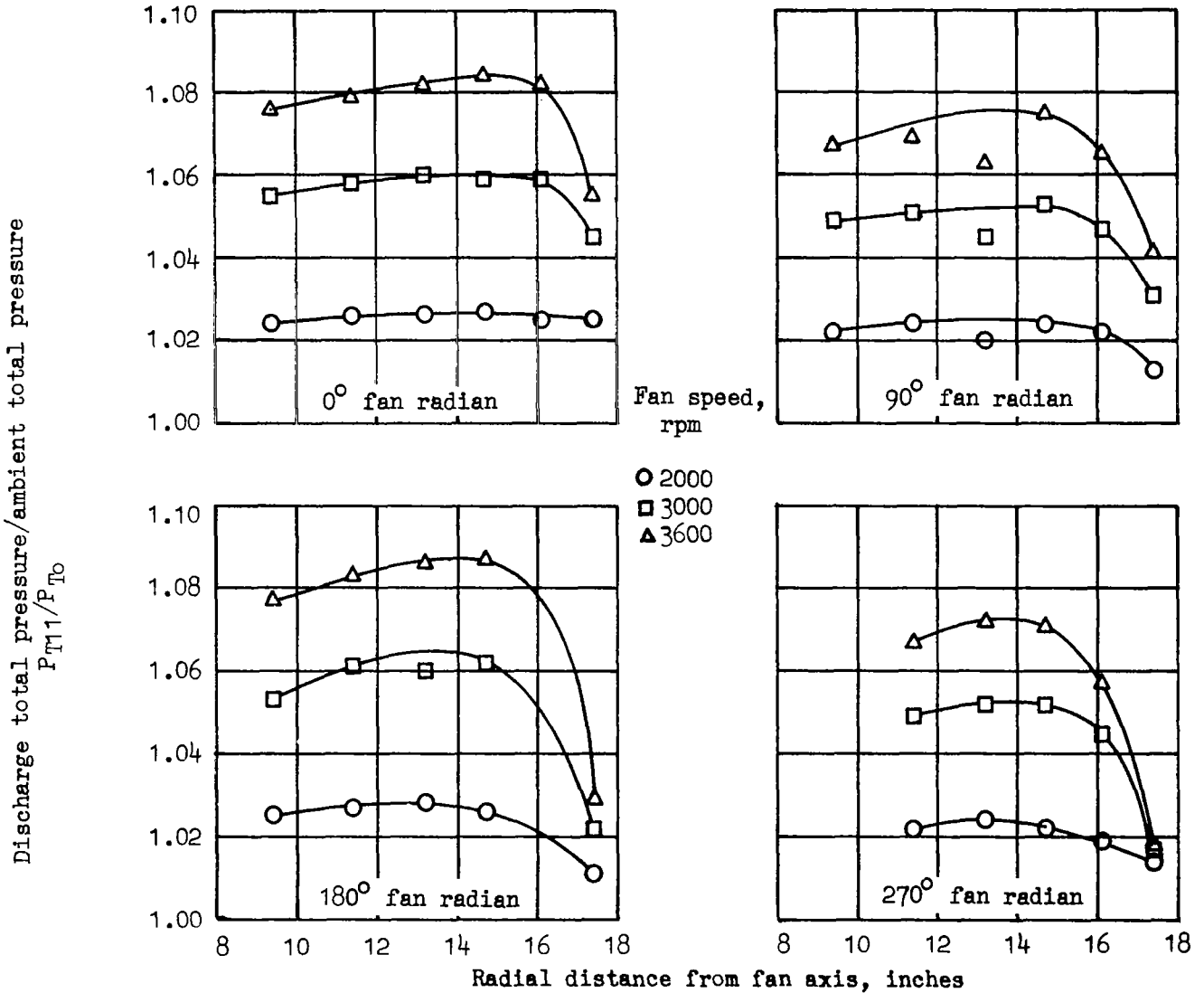

Figure 34. Fan Discharge Total Pressure Distribution; Right-Hand Center Fan, Six-Fan Operation, Ground Height = 2.65 Ft, L/C Engines Off, β_V = 0

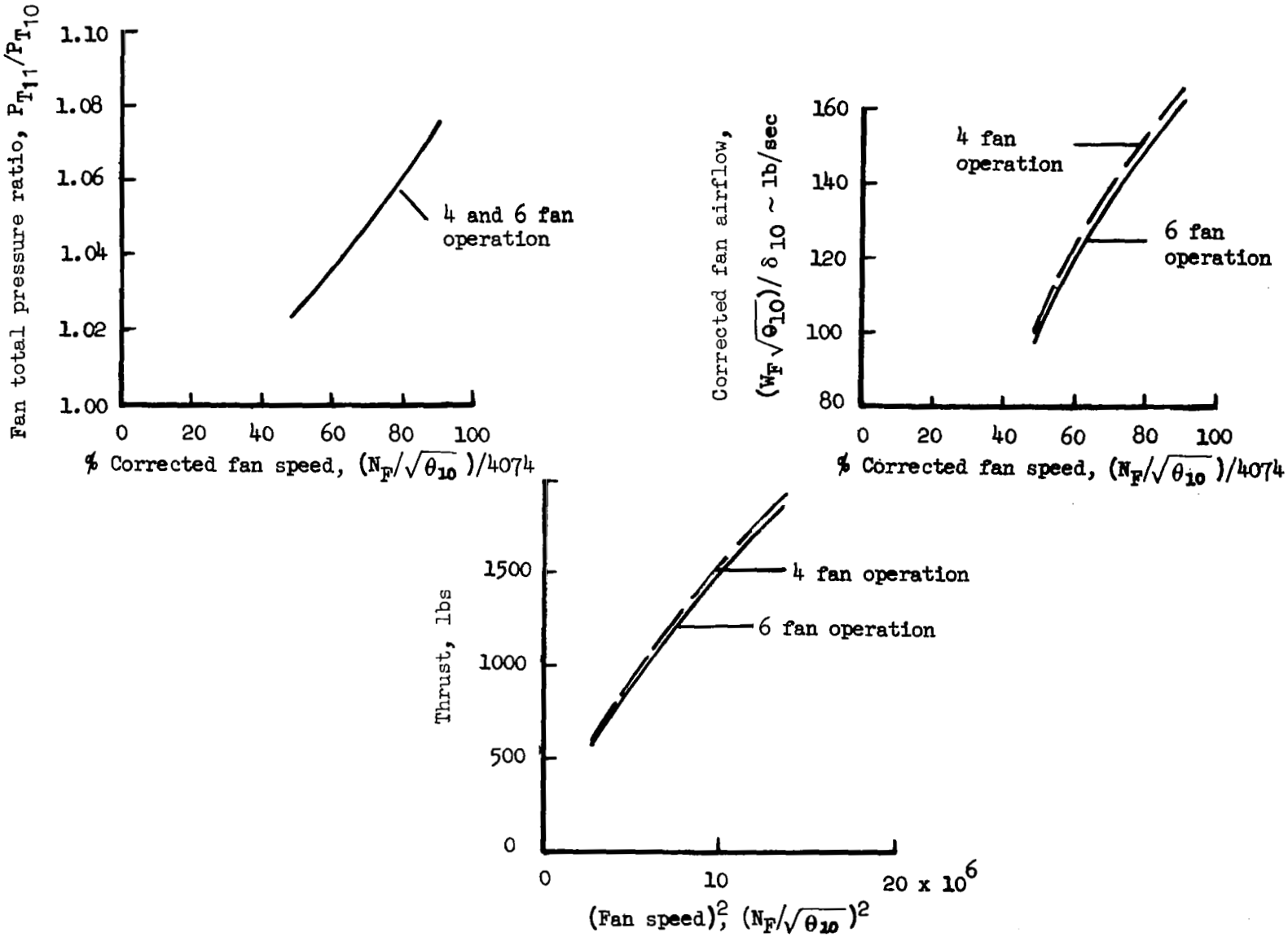

Figure 35. Fan Performance Characteristics, Right-Hand Center Fan, L/C Engines Off, Ground Height = 2.65 Feet, β_V = 0°

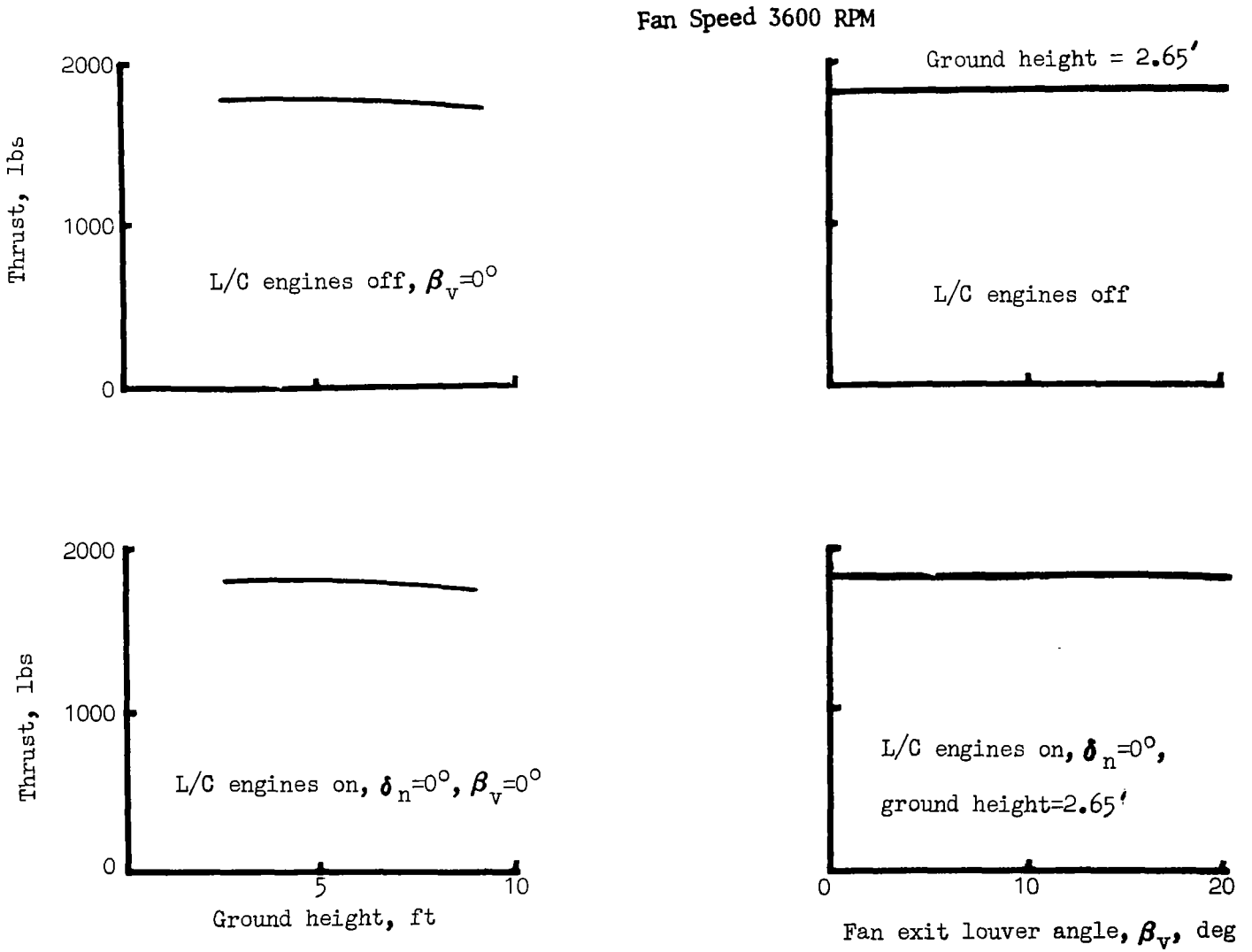

Figure 36. Variation of Right-Hand Center Fan Thrust With Model Ground Height and Fan Exit Louver Angle, Six-Fan Operation

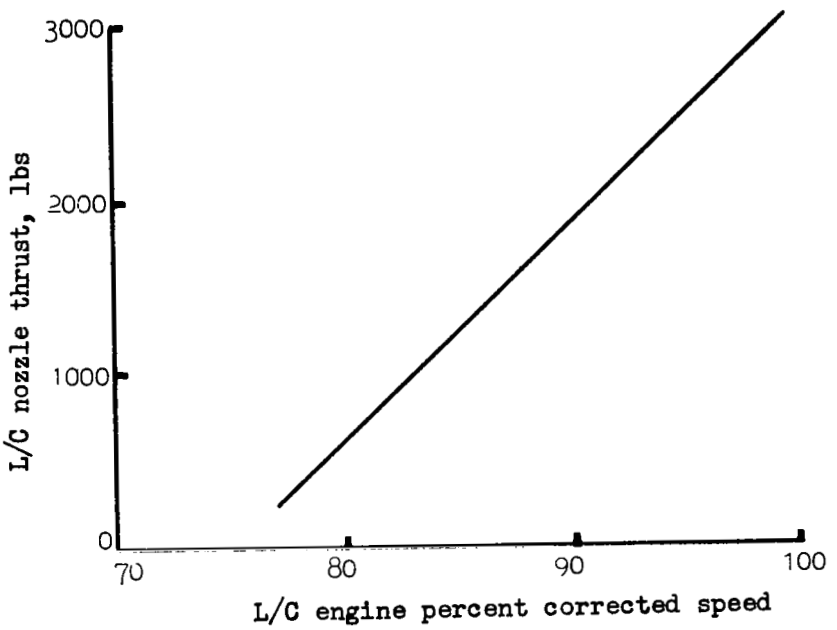

Figure 37. Right-Hand L/C Engine Thrust

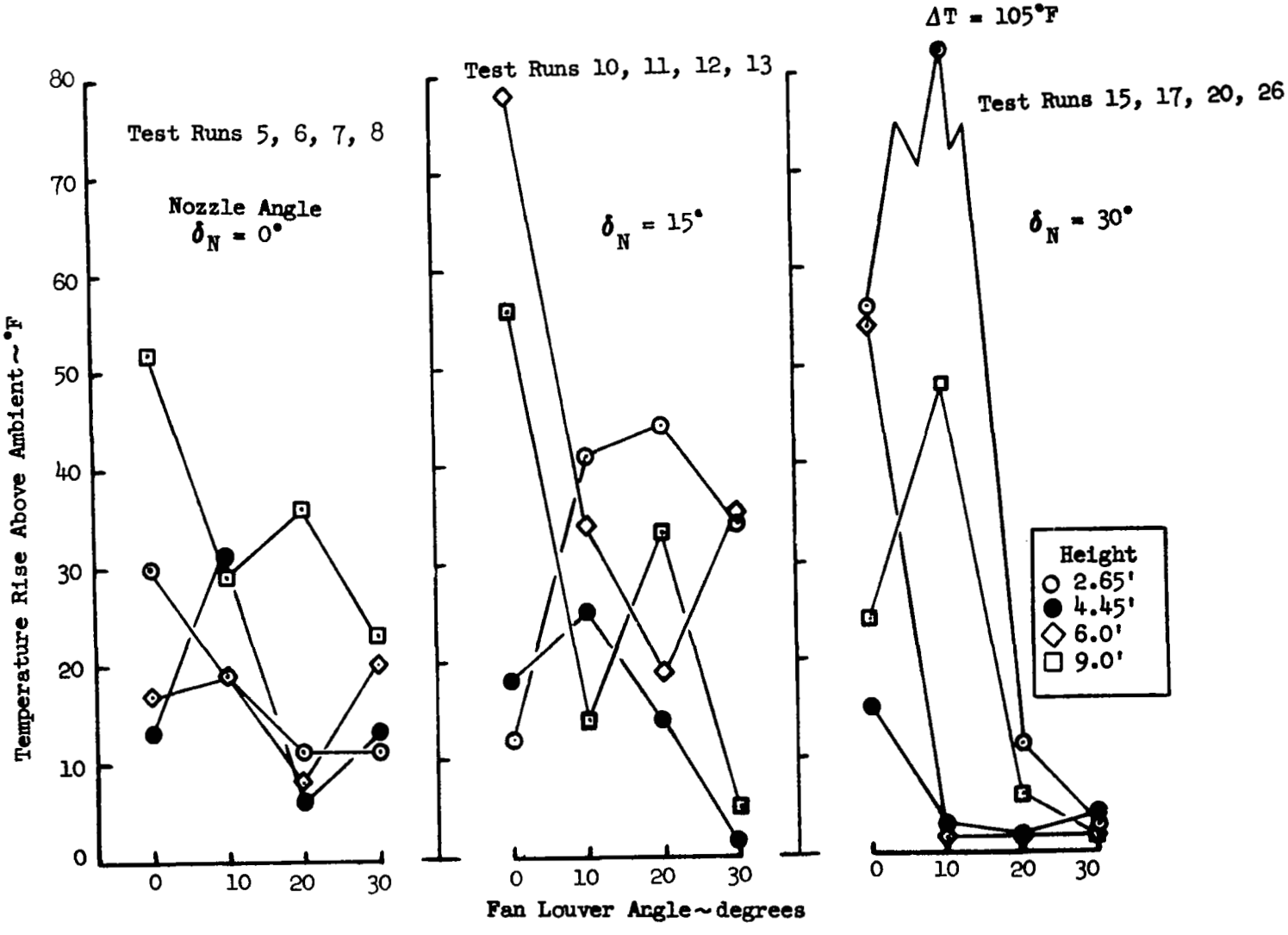

Figure 38. L/C Engine Inlet Temperature Rise Summary – All Engines Operating

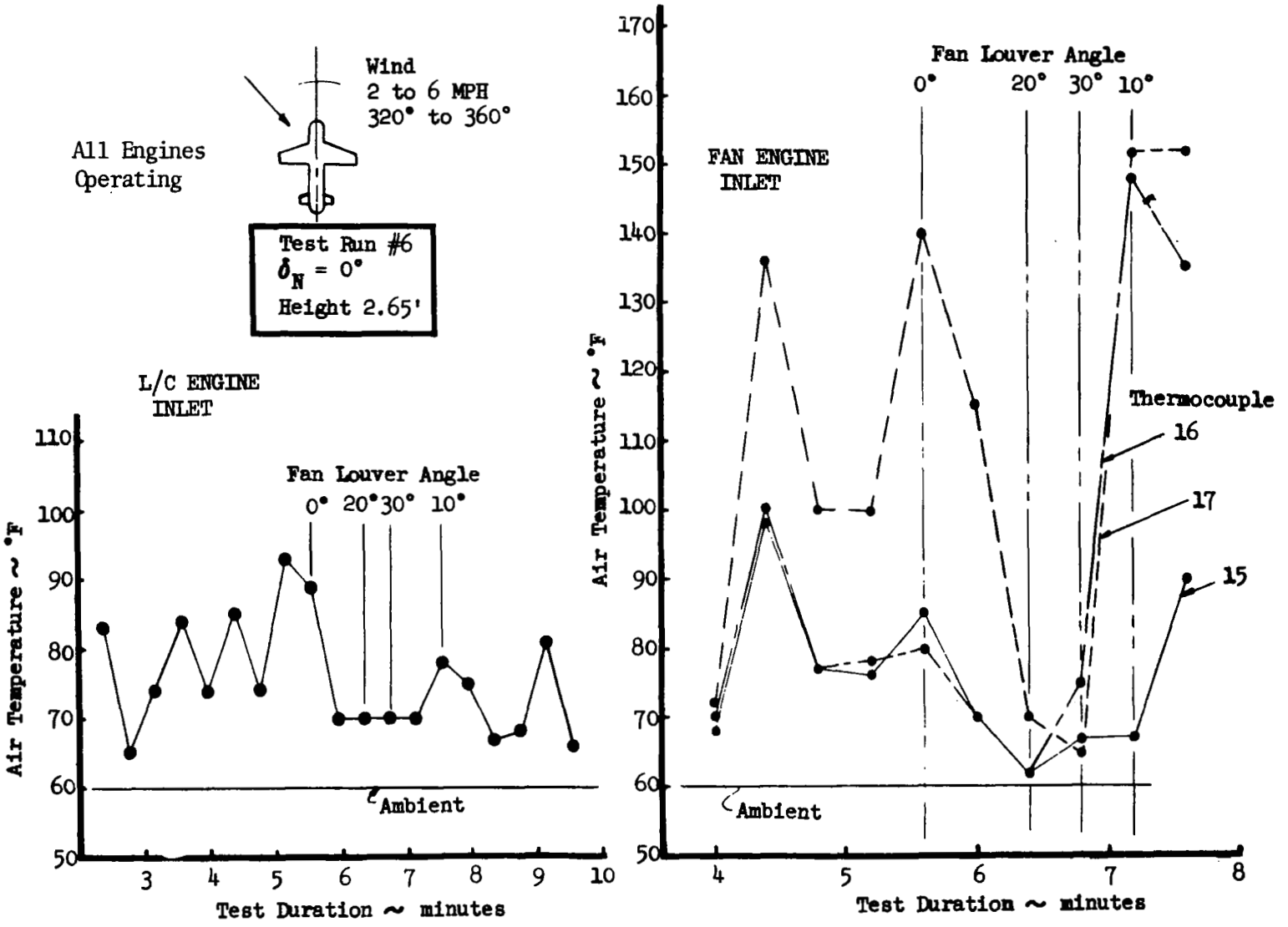

Figure 39. Engine Inlet Air Temperature Versus Time, δ_N = 0°, h = 2.65 Ft

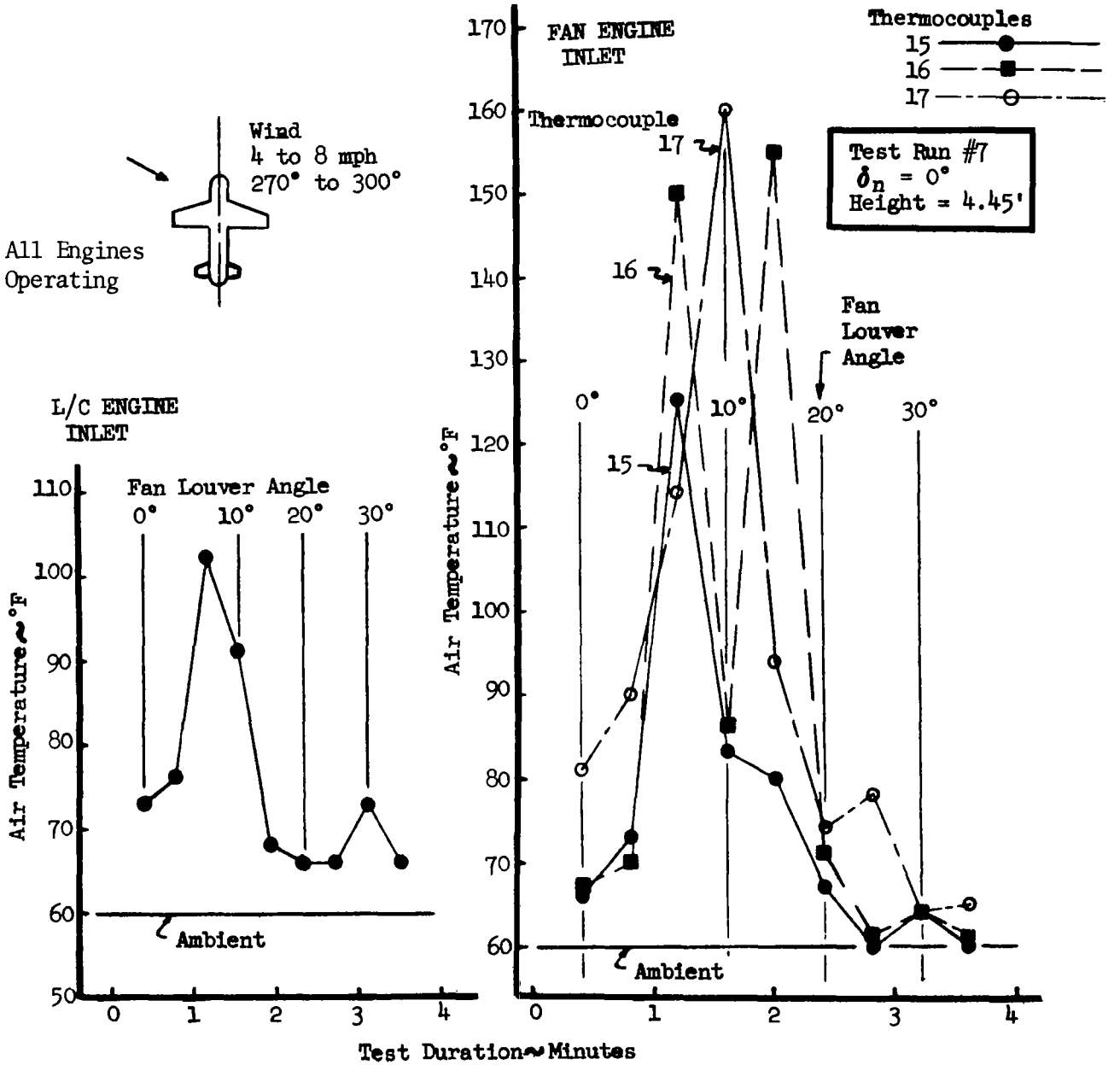

Figure 40. Engine Inlet Air Temperature Versus Time, δ_N = 0°, h = 4.45 Feet

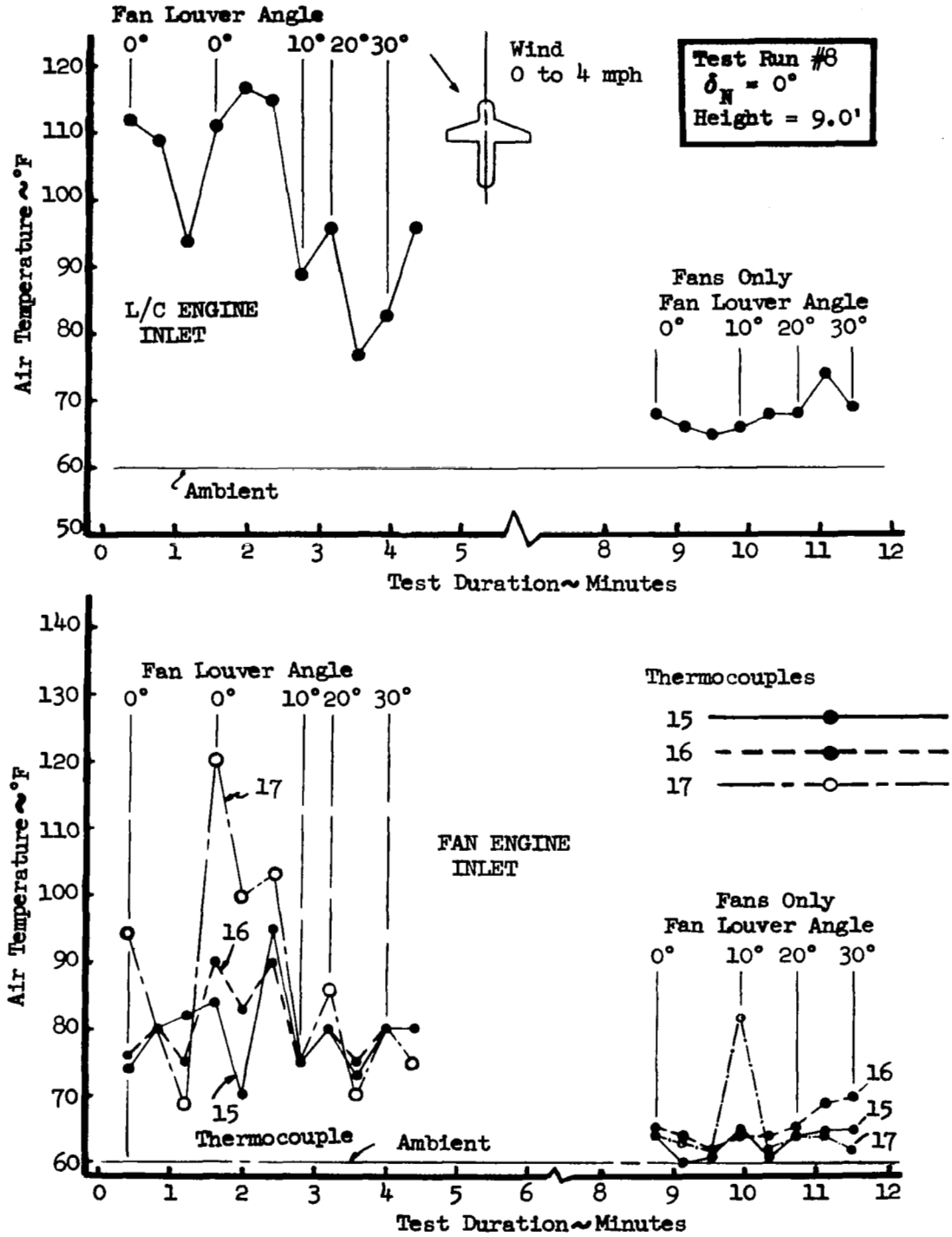

Figure 41. Engine Inlet Air Temperature Versus Time, δ_N = 0°, h = 9.0 Ft

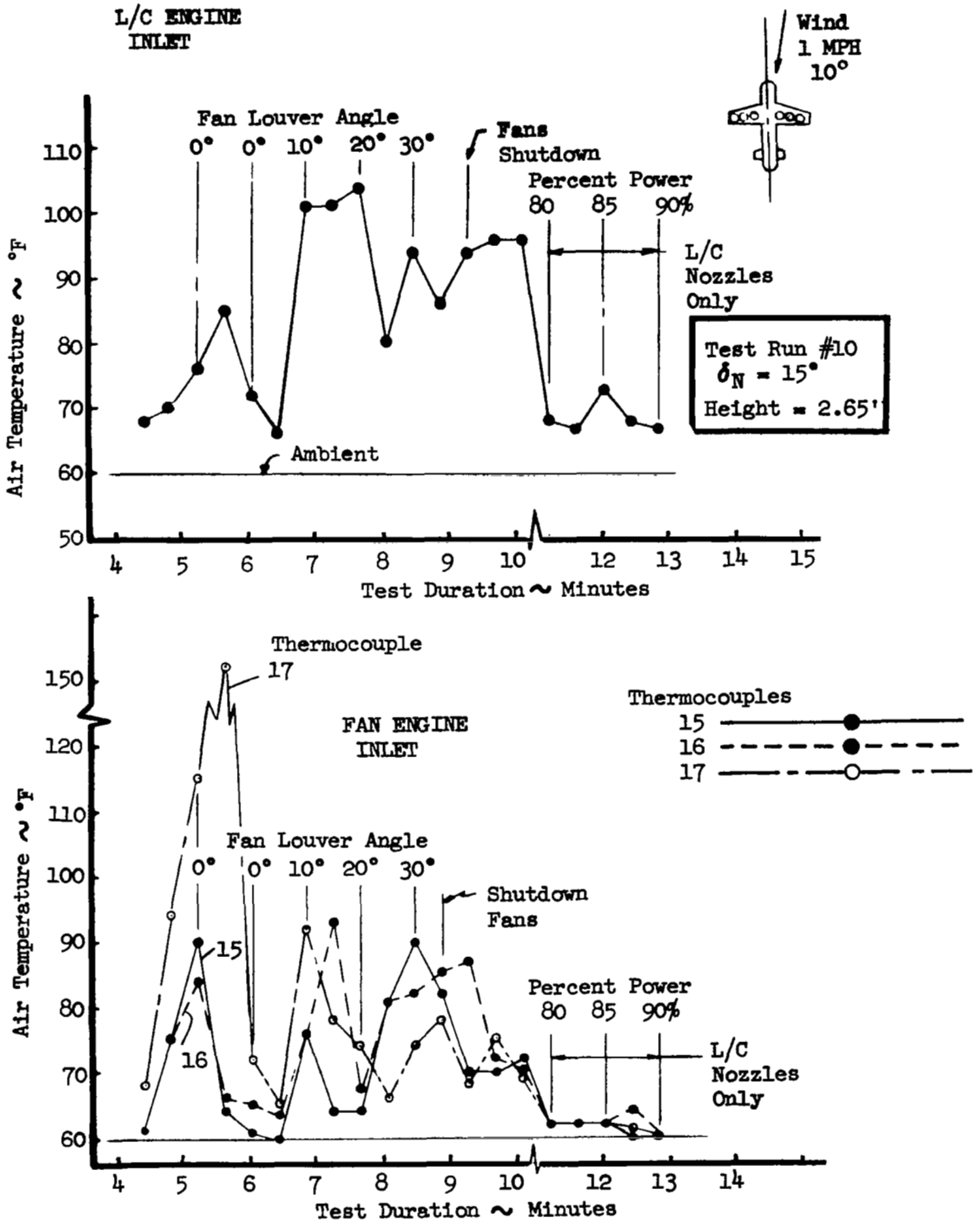

Figure 42. Engine Inlet Air Temperature Versus Time δ_N = 15°, h = 2.65 Ft.

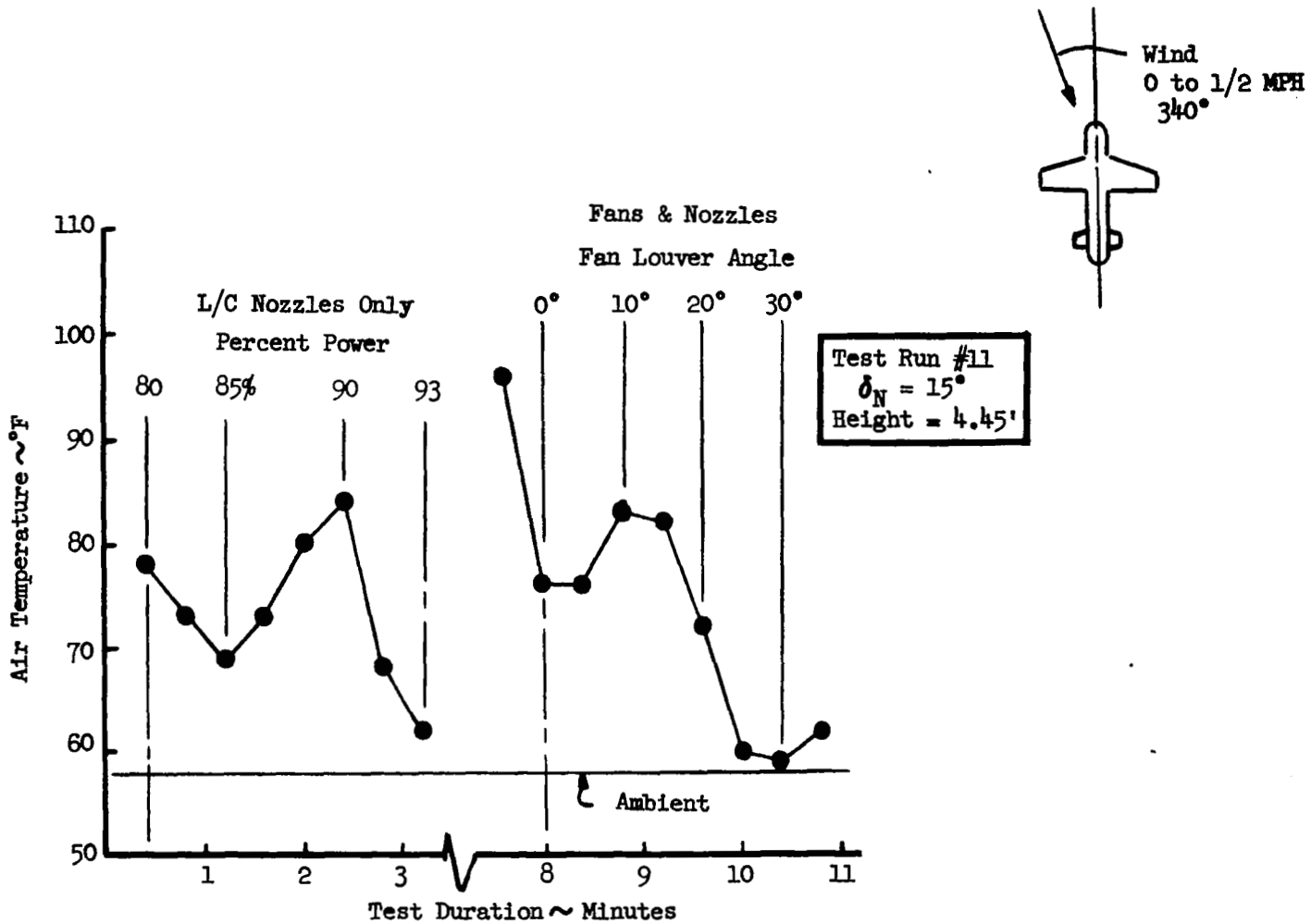

Figure 43. L/C Engine Inlet Air Temperature Versus Time, δ_N = 15°, h = 4.45 Ft.

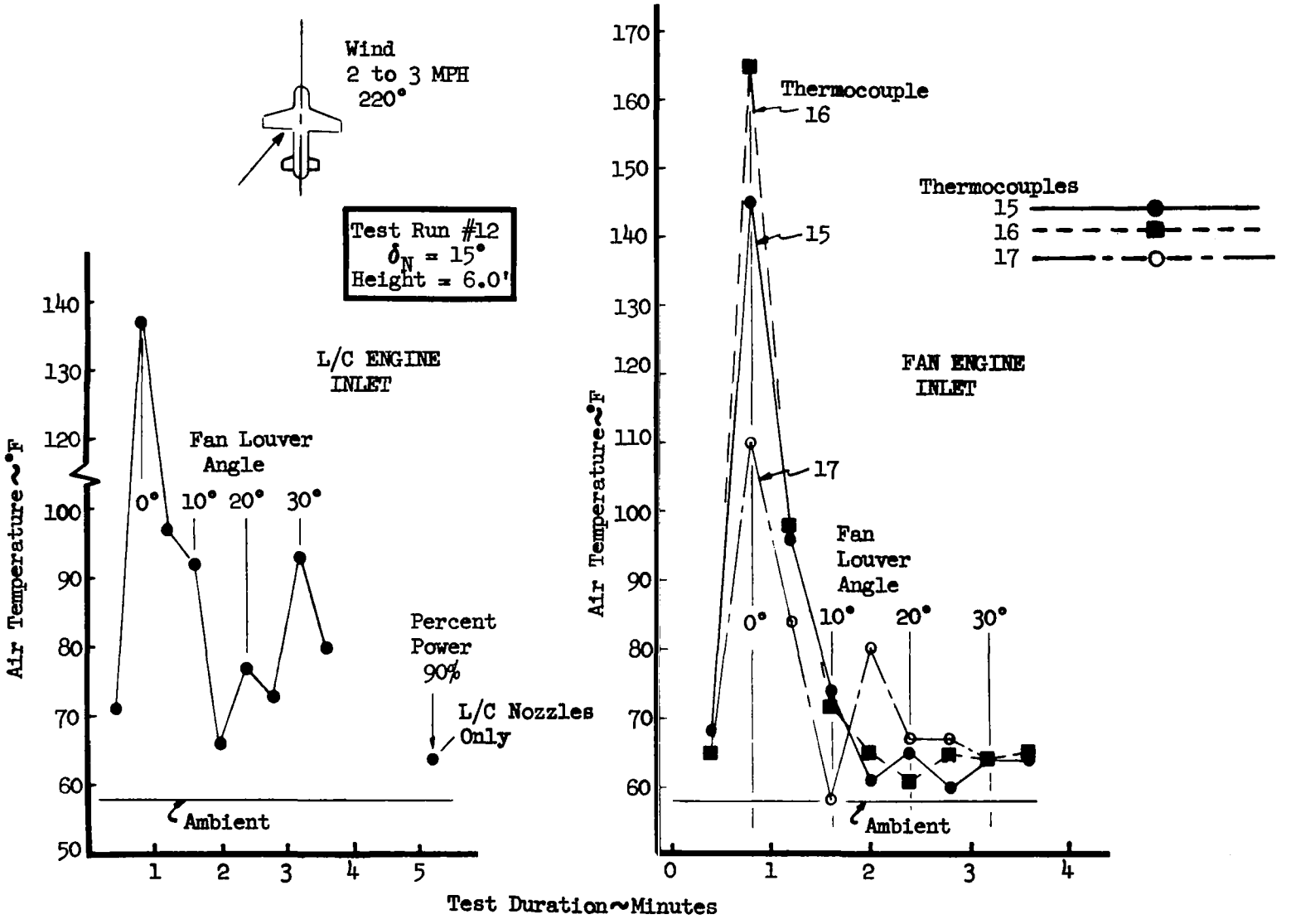

Figure 44. Engine Inlet Air Temperature Versus Time, δ_N = 15°, h = 6.0 Ft.

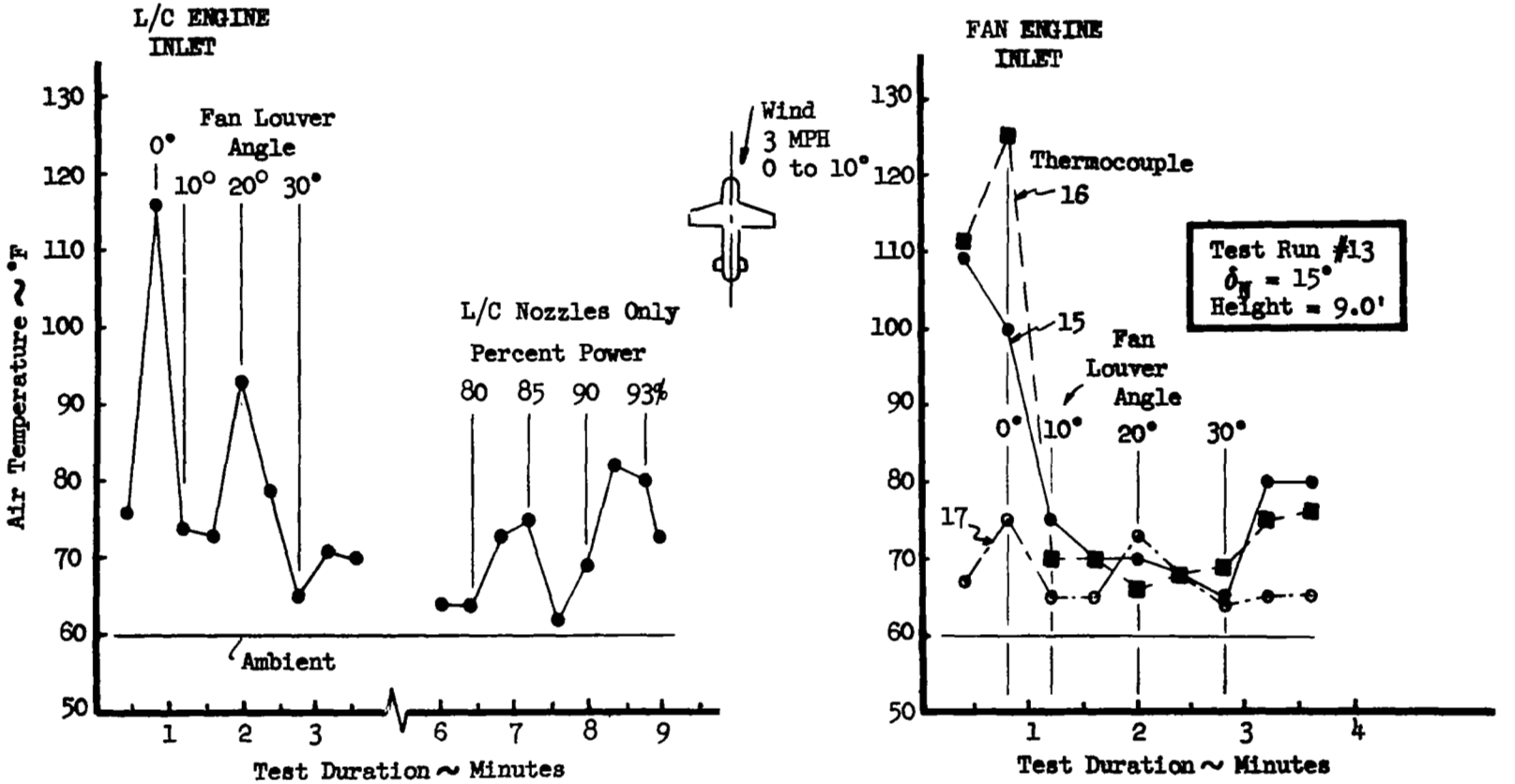

Figure 45. Engine Inlet Air Temperature Versus Time, δ_N = 15°, h = 9.0 Ft.

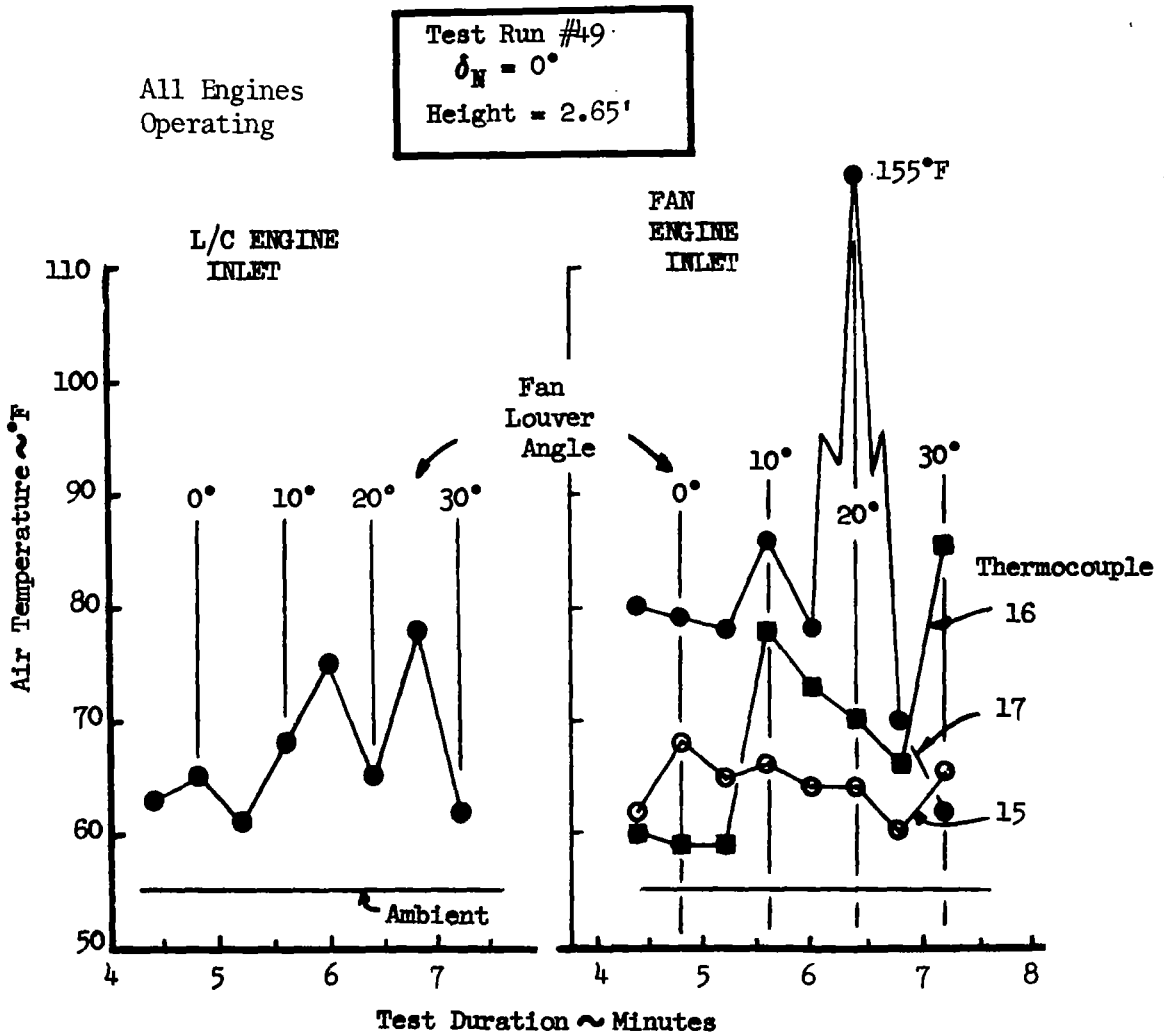

Figure 46. Engine Inlet Air Temperature Versus Time, δ_N = 0°, h = 2.65 Ft With Wheel Fairings and Wheels Removed

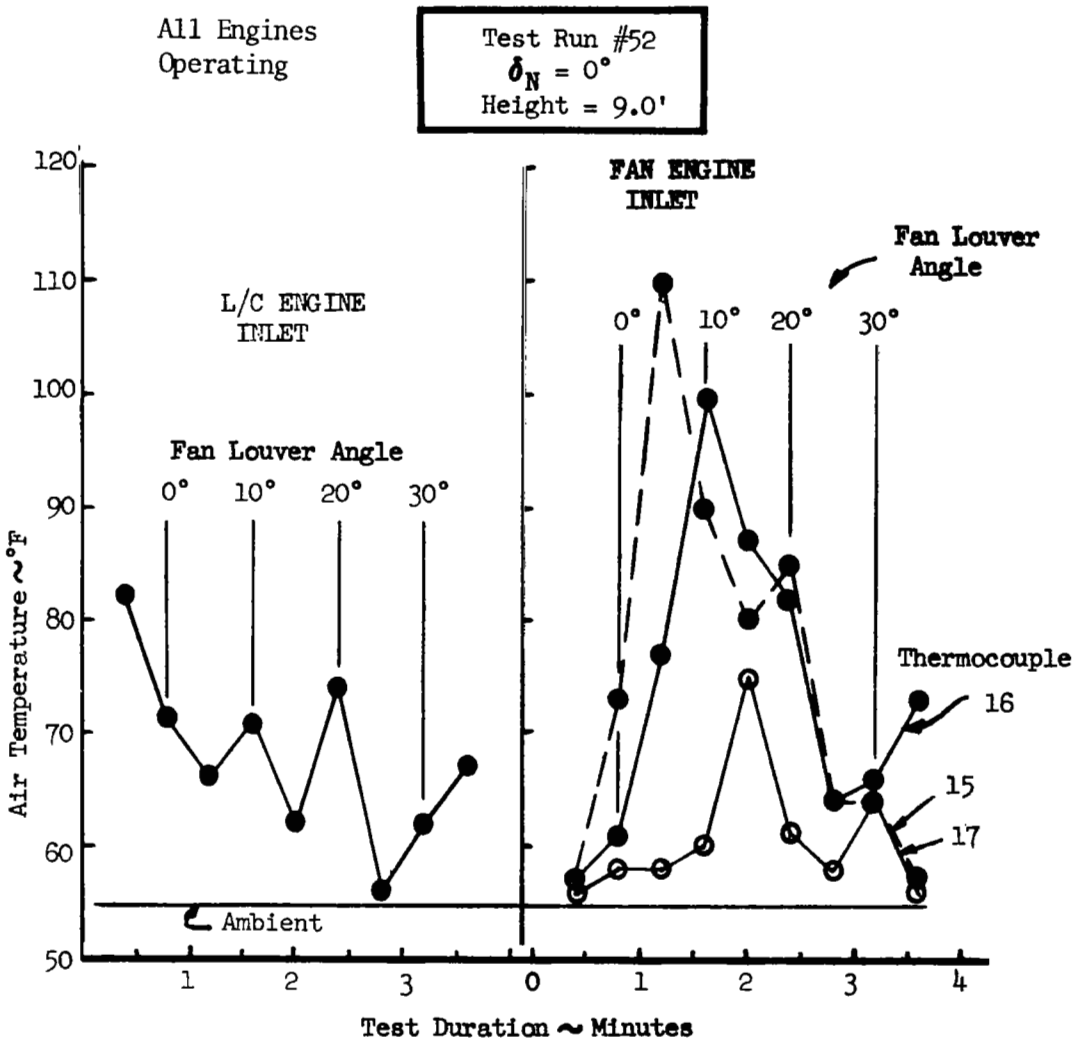

Figure 47. Engine Inlet Air Temperature Versus Time, δ_N = 0°, h = 9.0 Ft With Wheel Fairings and Wheels Removed

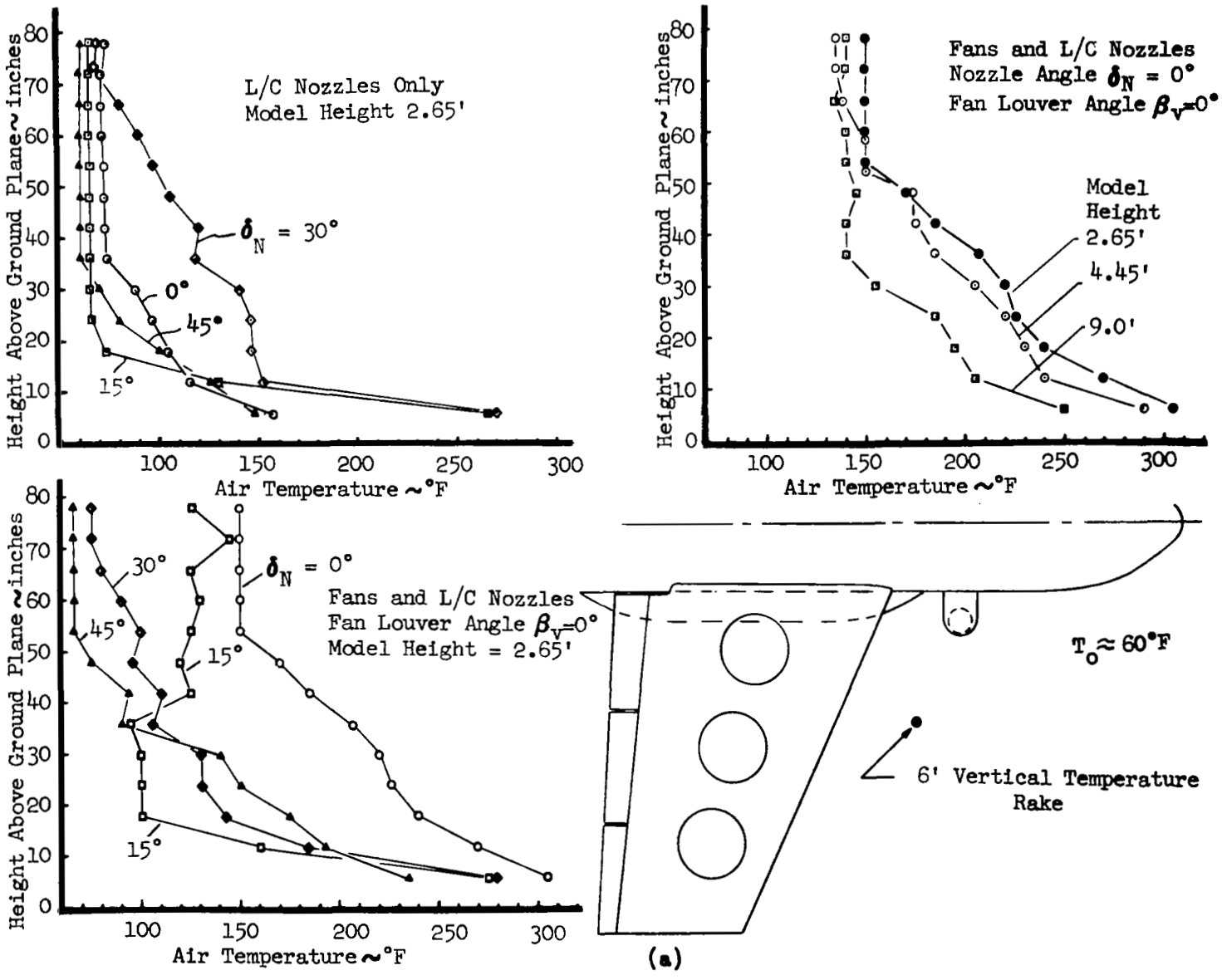

Figure 48. Six Foot Vertical Rake Temperatures

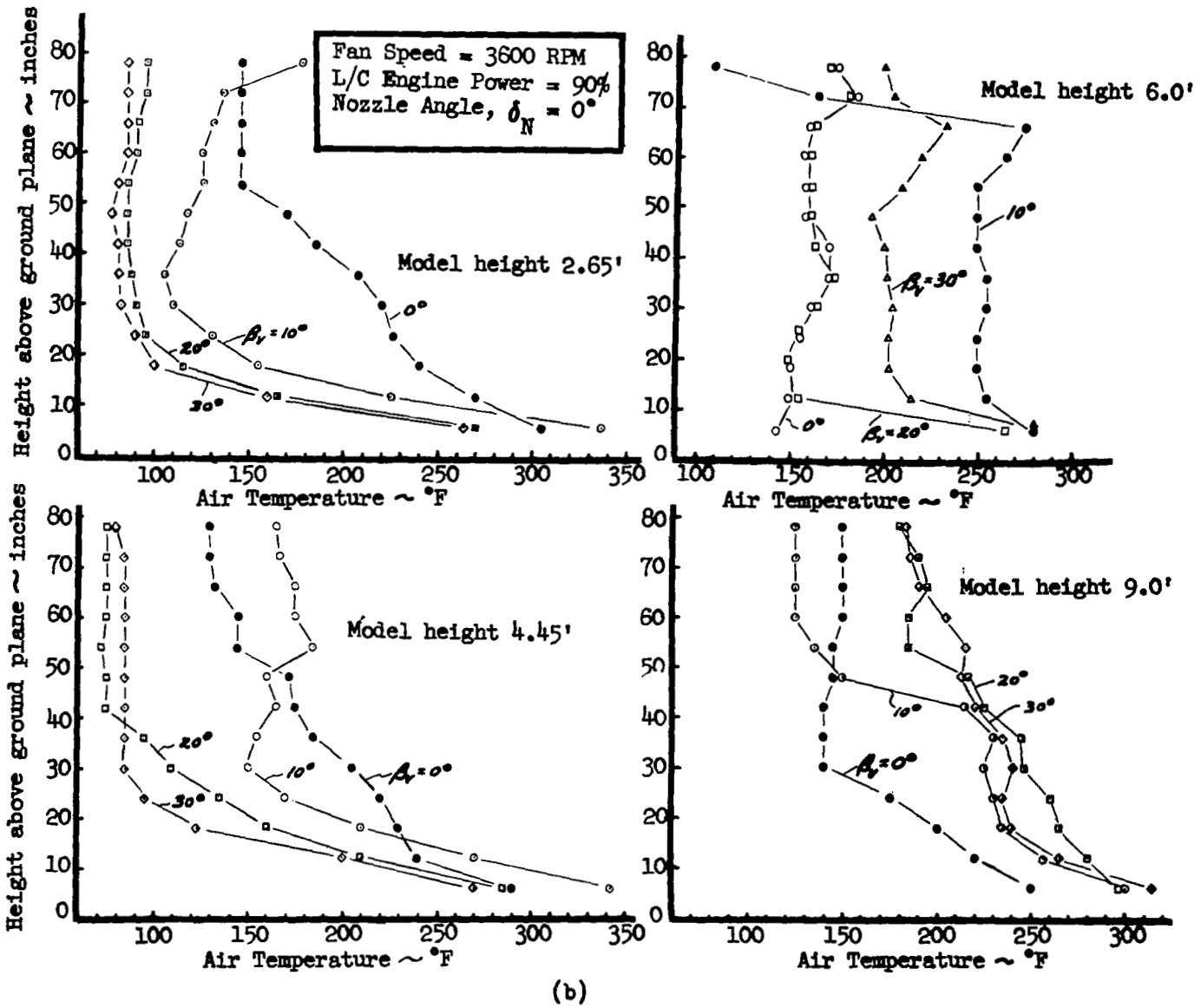

Figure 48. Six Foot Vertical Rake Temperatures - Concluded

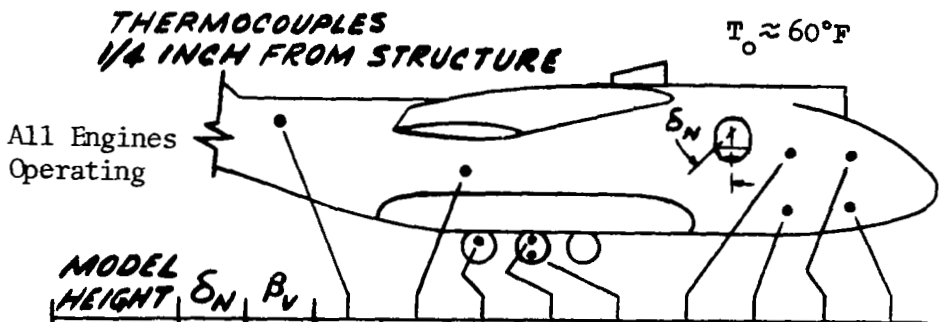

MODEL HEIGHT	δ_N	β_v									
2.65'	0°	0°	110	376	230	256	250	106	111	77	121
		10°	130	445	243	303	336	108	108	92	140
		20°	150	385	240	243	237	98	95	80	125
		30°	120	400	245	245	240	100	96	85	120
4.45'	0°	0°	100	345	225	140	126	106	115	90	157
		10°	125	440	250	270	315	125	125	125	172
		20°	140	375	224	235	226	113	111	84	135
		30°	135	410	230	210	235	120	120	90	120
6.0'	0°	0°	120	319	233	140	130	98	100	81	100
		10°	95	394	230	244	252	100	100	78	100
		20°	180	414	230	195	222	107	110	96	145
		30°	130	390	225	257	317	105	99	75	100
9.0'	0°	0°	95	375	280	140	140	140	145	150	160
		10°	100	400	200	200	260	115	120	95	120
		20°	125	365	195	200	255	120	135	100	120
		30°	160	405	215	185	215	119	113	90	110
2.65'	15°	0°	120	355	264	215	136	97	100	94	95
		10°	145	434	260	300	270	100	96	80	95
		20°	135	406	255	295	260	104	103	100	101
		30°	160	370	272	240	270	110	112	101	114
2.65'	30°	0°	125	385	247	185	136	135	195	125	200
		10°	140	380	240	330	300	135	145	182	176
		20°	140	345	270	250	248	110	157	87	155
		30°	145	342	258	210	250	82	125	70	95
2.65'	45°	0°	145	390	230	190	230	120	135	80	103
		10°	135	350	200	264	200	97	126	65	88
		20°	155	310	205	220	205	97	94	60	70
		30°	140	340	217	211	216	100	95	61	78

Figure 49. Near-structure Air Temperature

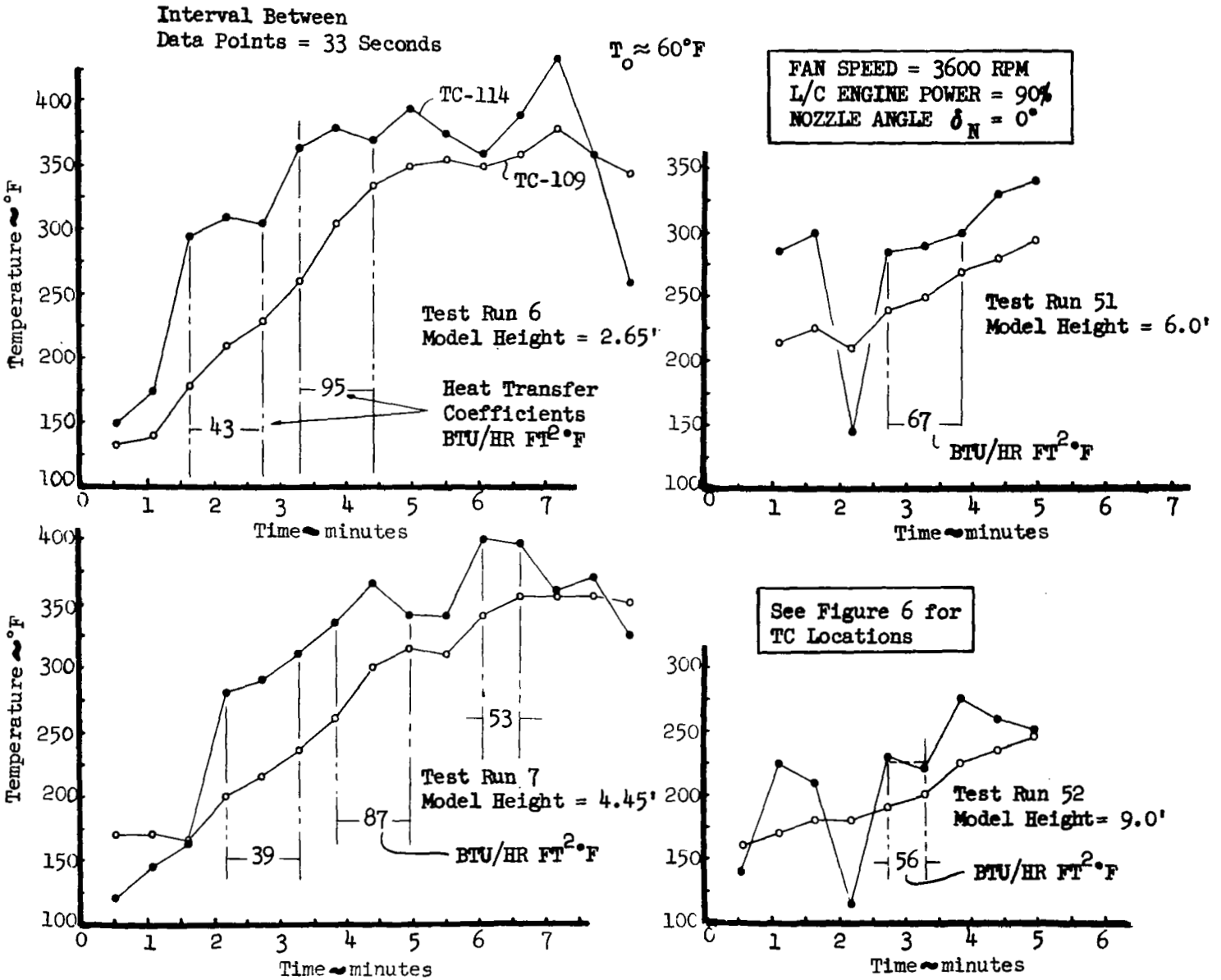

Figure 50. Ground Surface Heating Conditions

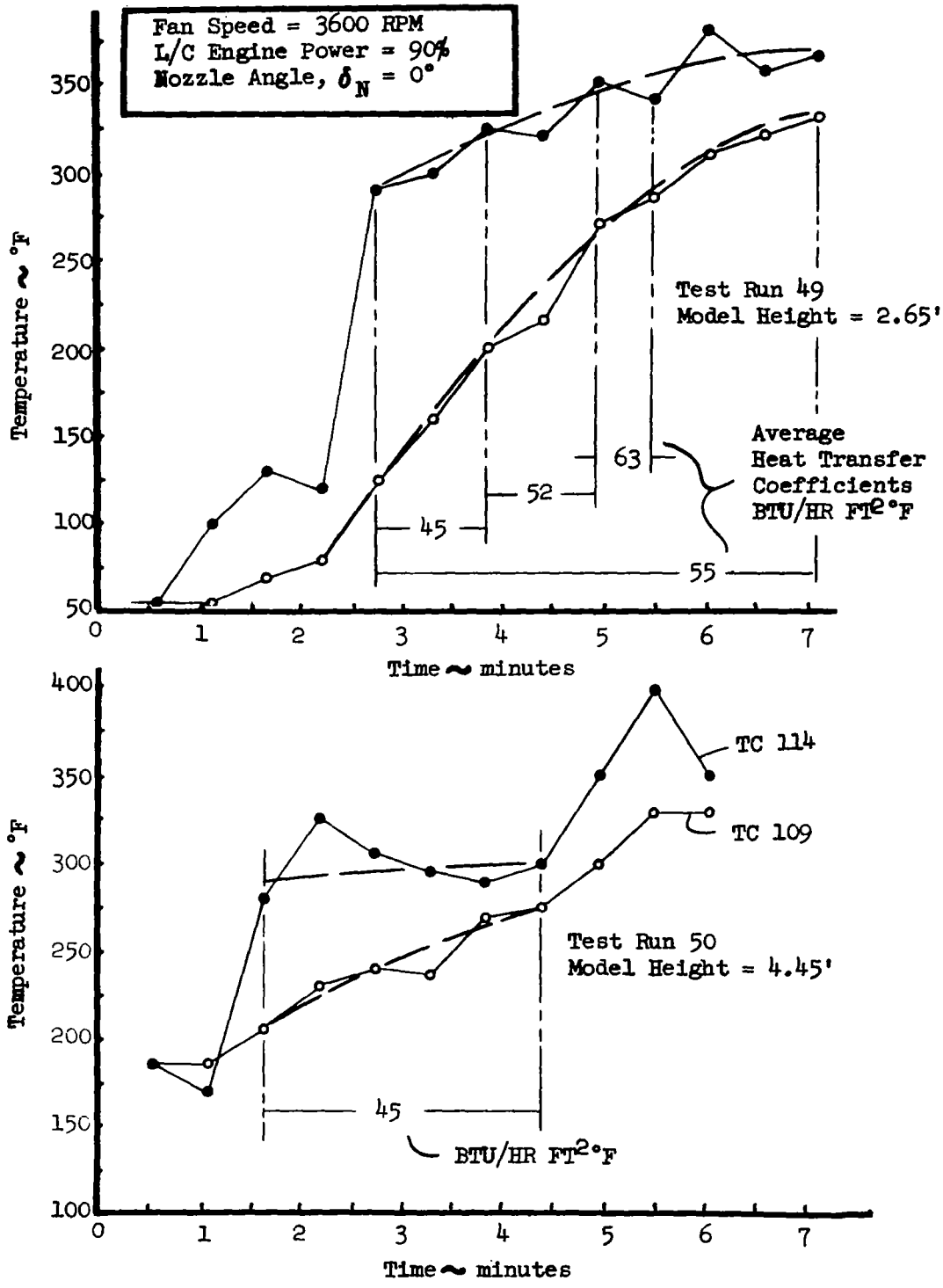

Figure 50. Ground Surface Heating Conditions - Concluded

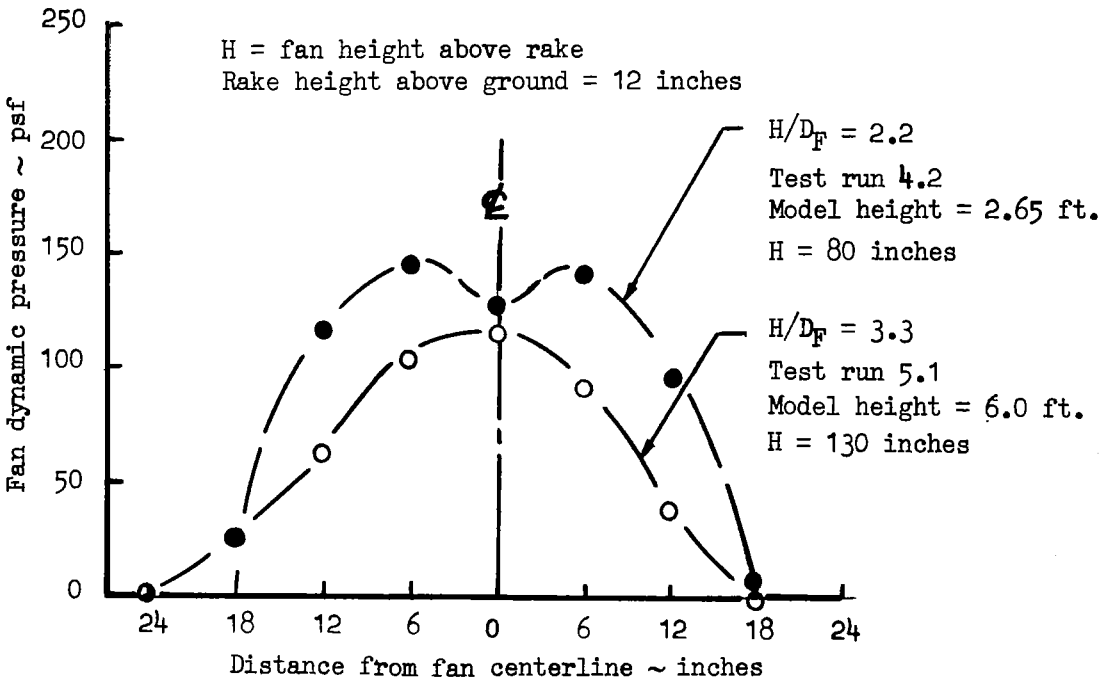

Figure 51. Fan Dynamic Pressures at Two Heights

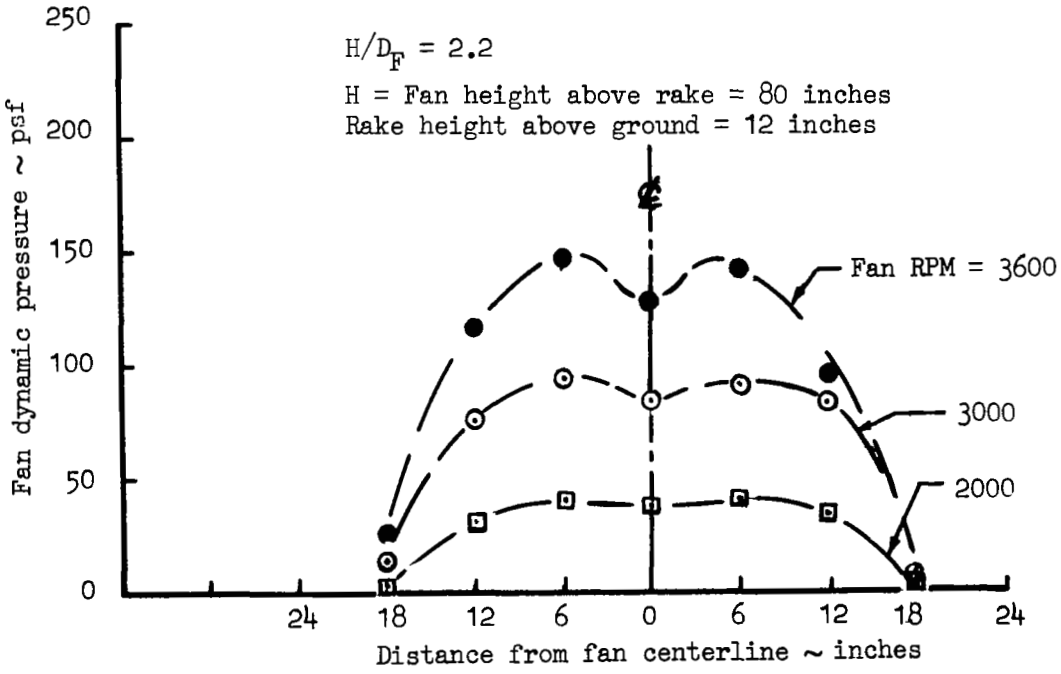

Figure 52. Fan Dynamic Pressures Near Ground

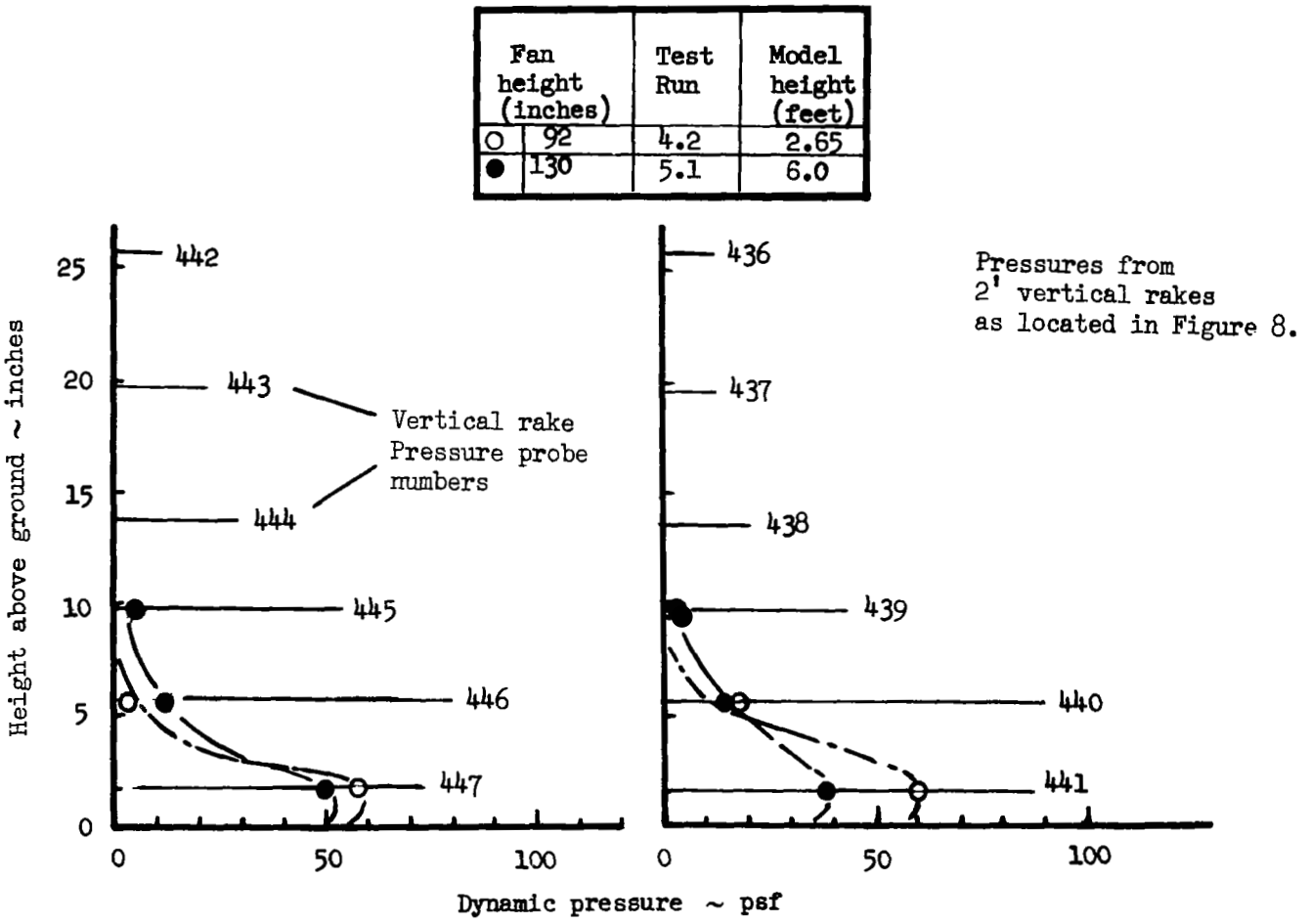

Figure 53. Ground Jet Pressure Profile from Lift Fan

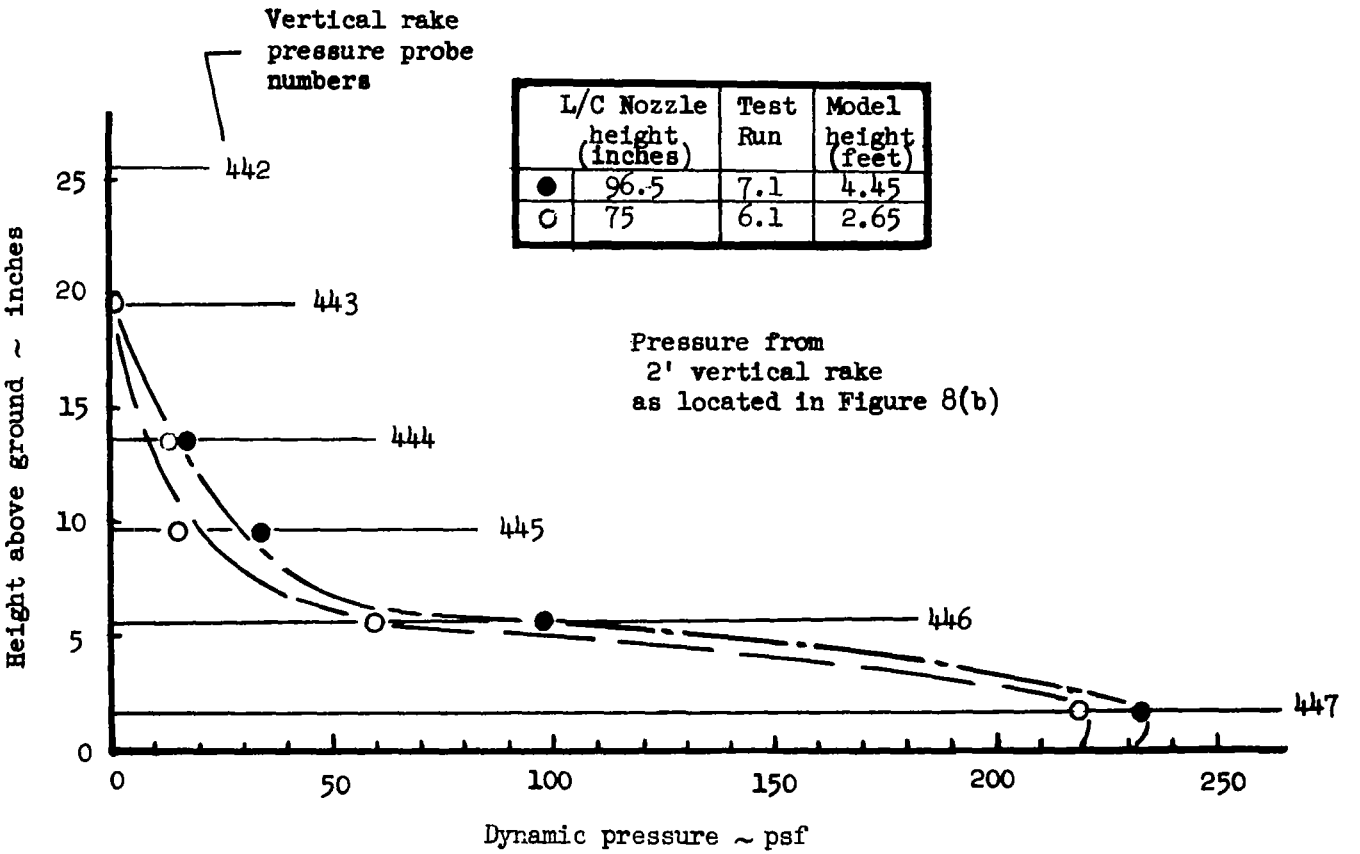

Figure 54. Ground Jet Pressure Profiles From L/C Nozzle

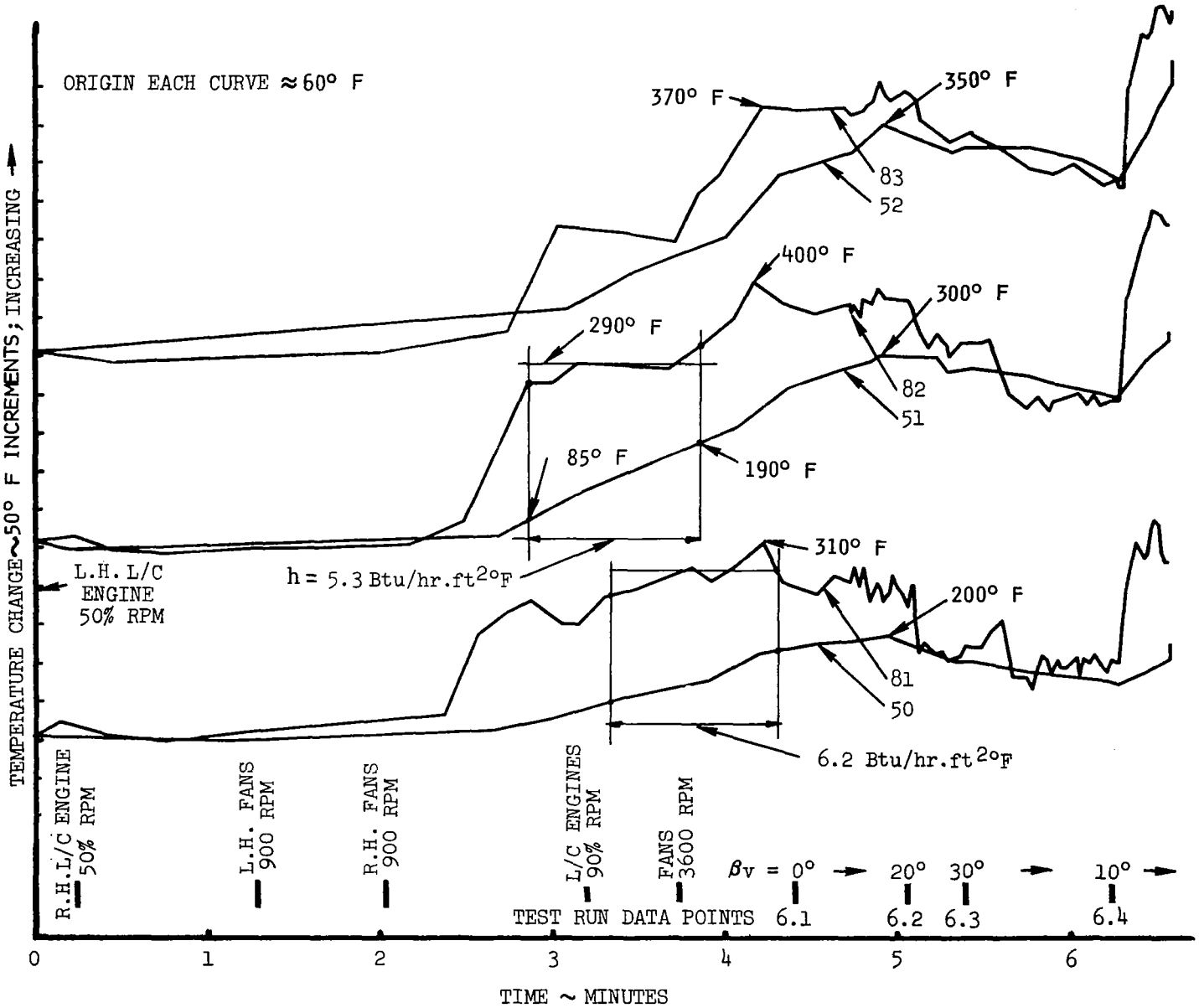

Figure 55. - Side of Fuselage Air and Structure Temperature Traces; $\delta_N = 0°$, h = 2.65 Ft.

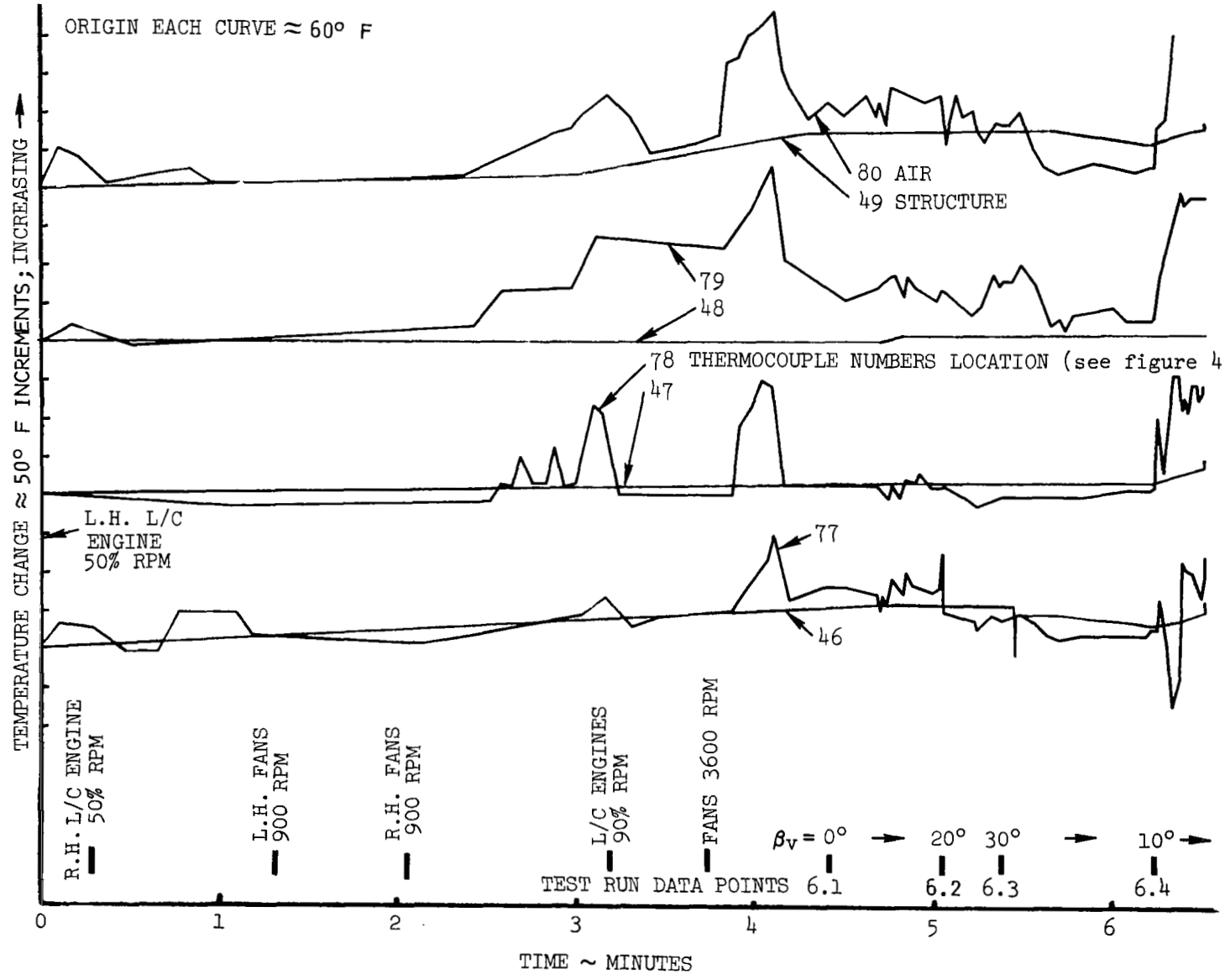

Figure 55. - Side of Fuselage Air and Structure Temperature Traces; δ_N = 0°, h = 2.65 Ft - Concluded

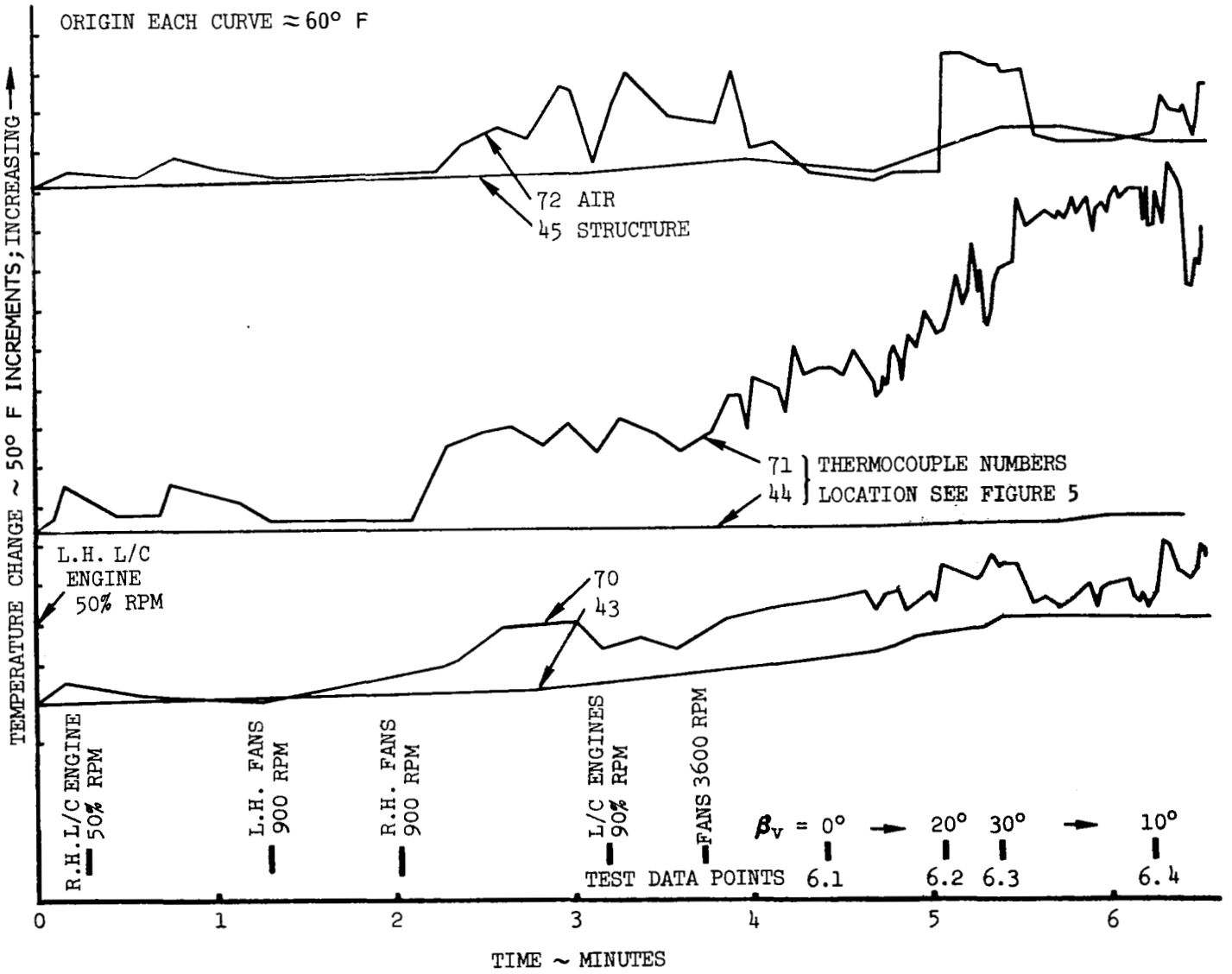

Figure 56. - Under Wing Air and Structure Temperature Traces; δ_N = 0°, h = 2.65 Ft

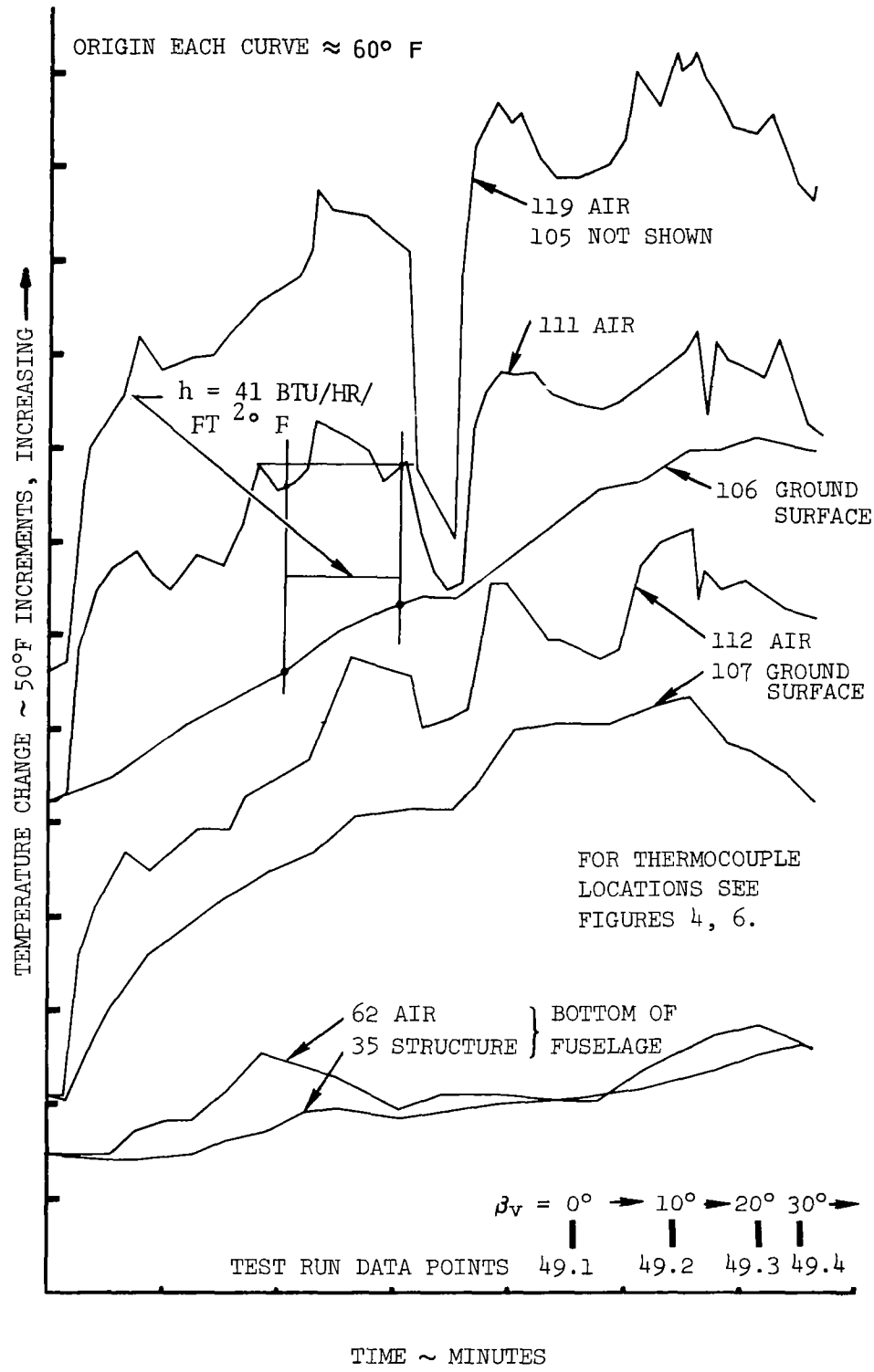

Figure 57. - Air, Structure, and Ground Surface Temperature Traces; $\delta_N = 0°$, h = 2.65 Ft

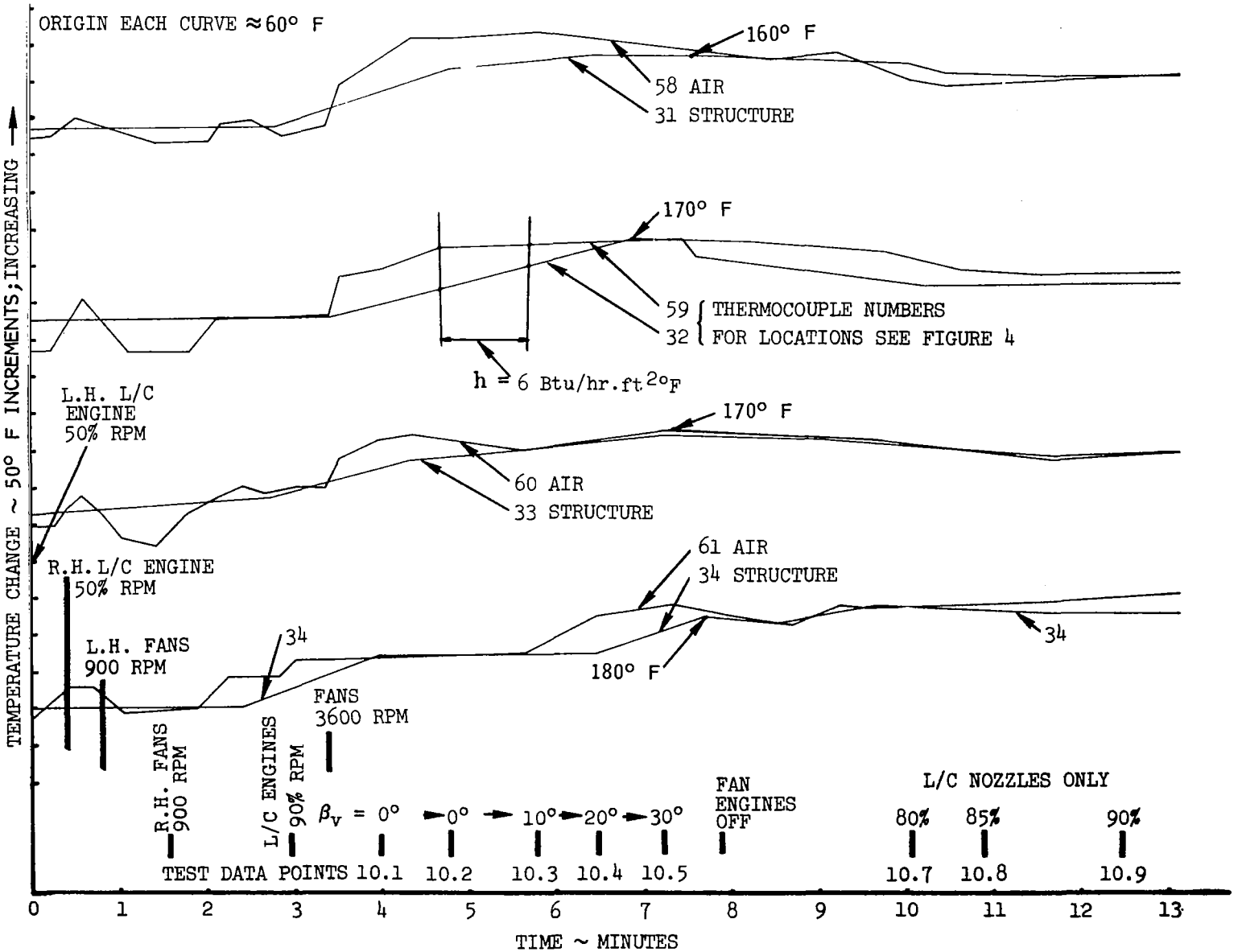

Figure 58. - Bottom of Fuselage Air and Structure Temperature Traces;
δ_N = 15°, h = 2.65 Ft

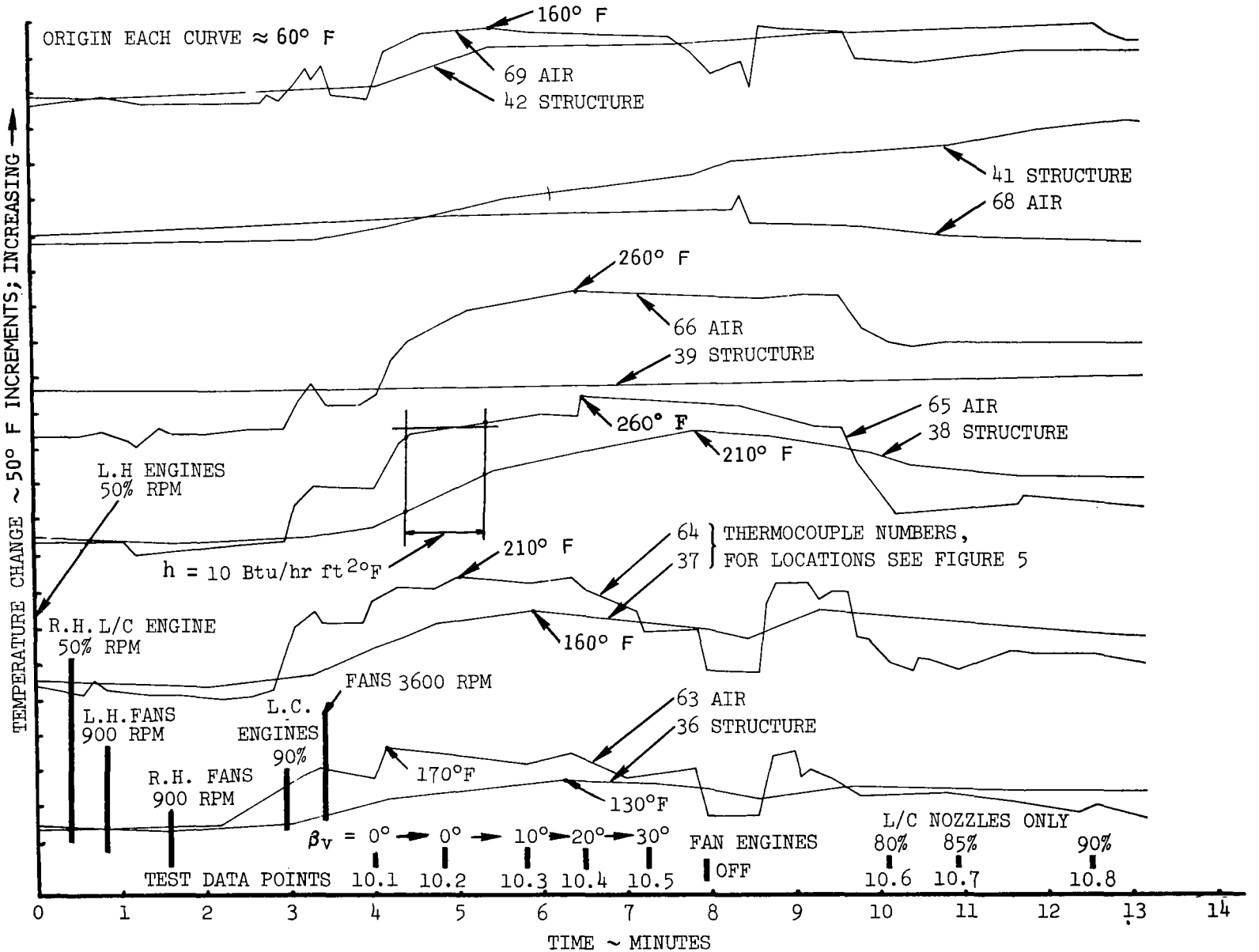

Figure 59. - Under Wing Air and Structure Temperature Traces; δ_N = 15°, h = 2.65 Ft

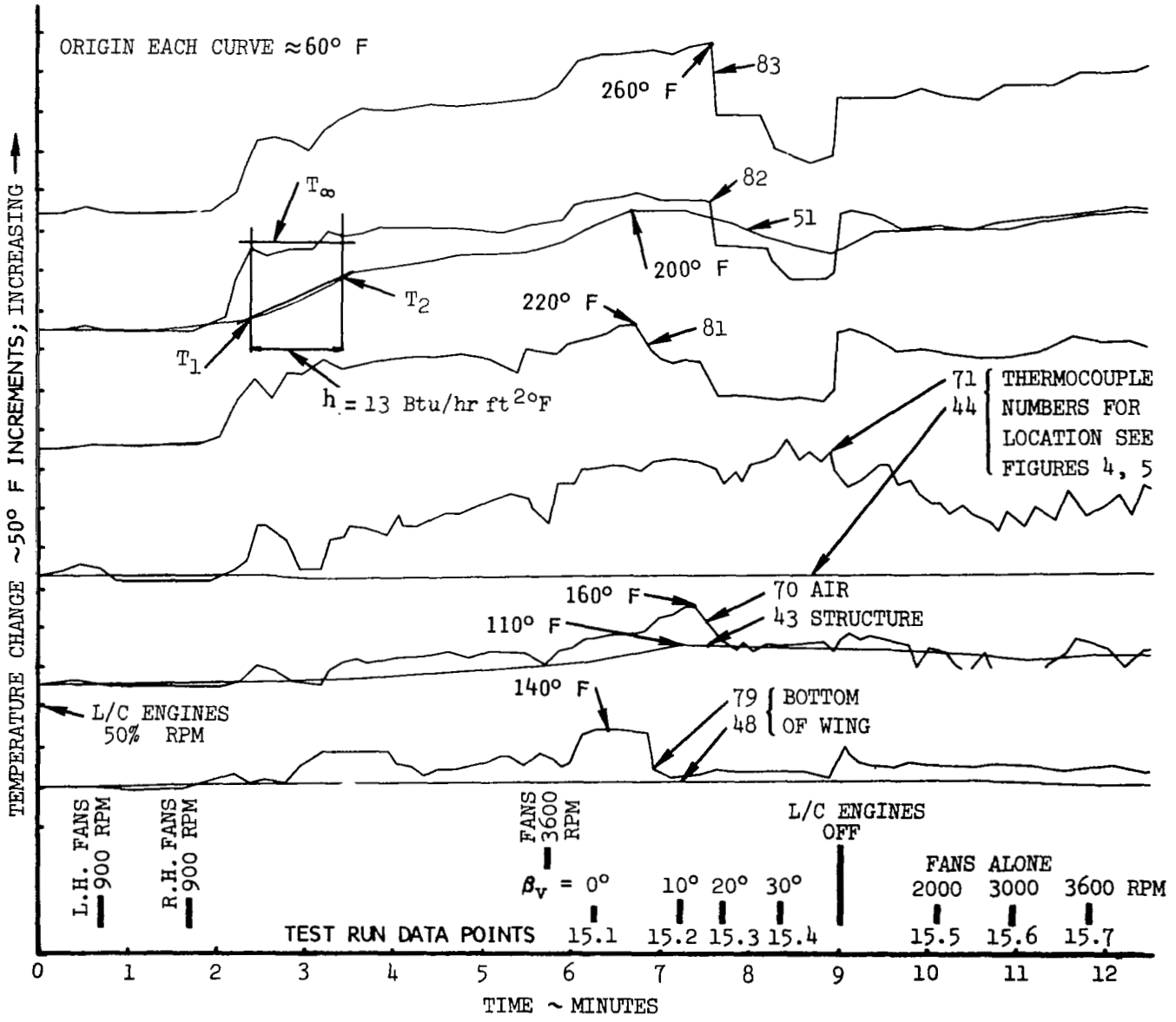

Figure 60. - Structure and Near-Structure Temperature Traces; δ_N = 30°, h = 4.45 Ft

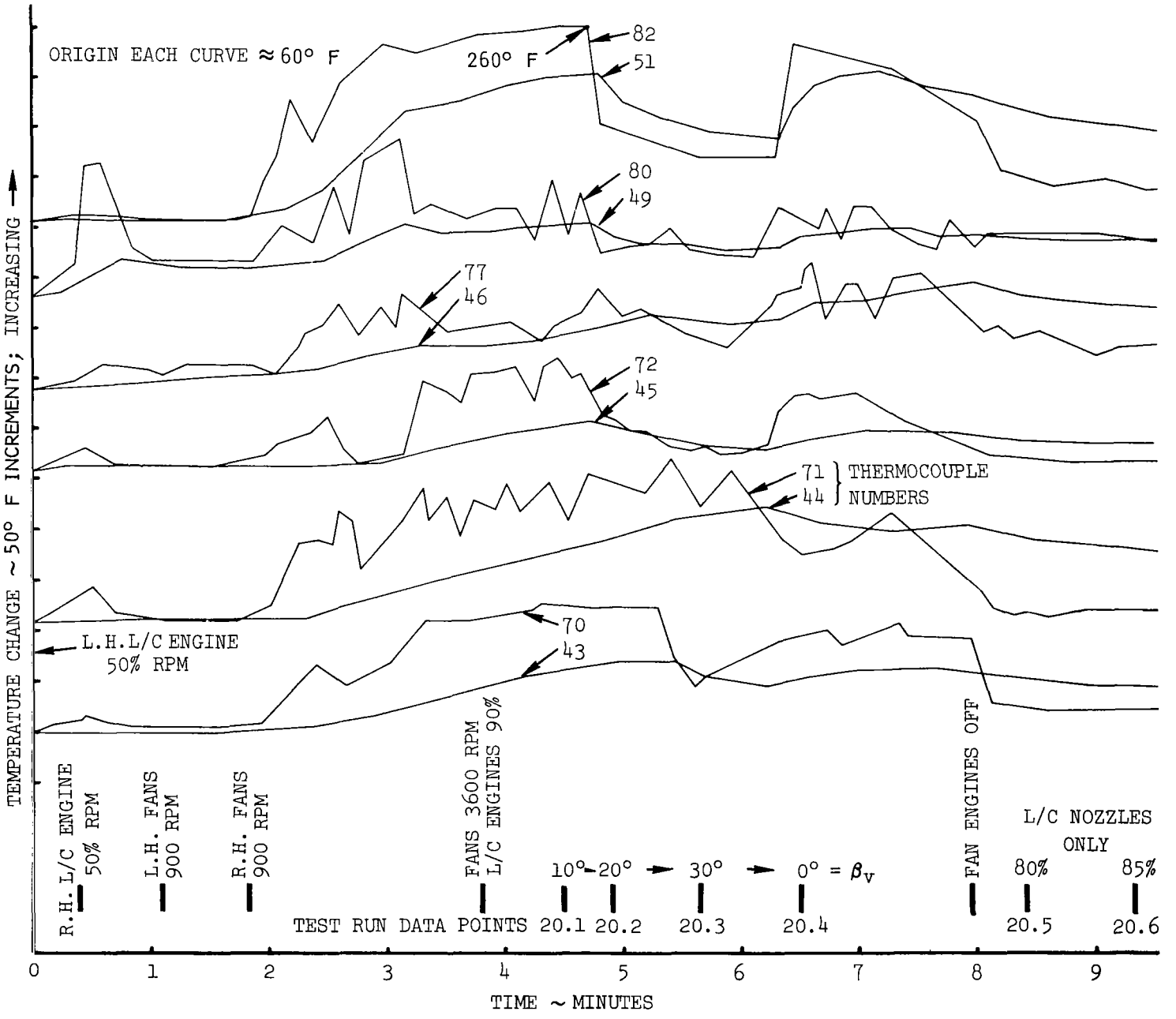

Figure 61. - Wing and Fuselage Air and Structure Temperature Traces; δ_N = 30°, h = 2.65 Ft

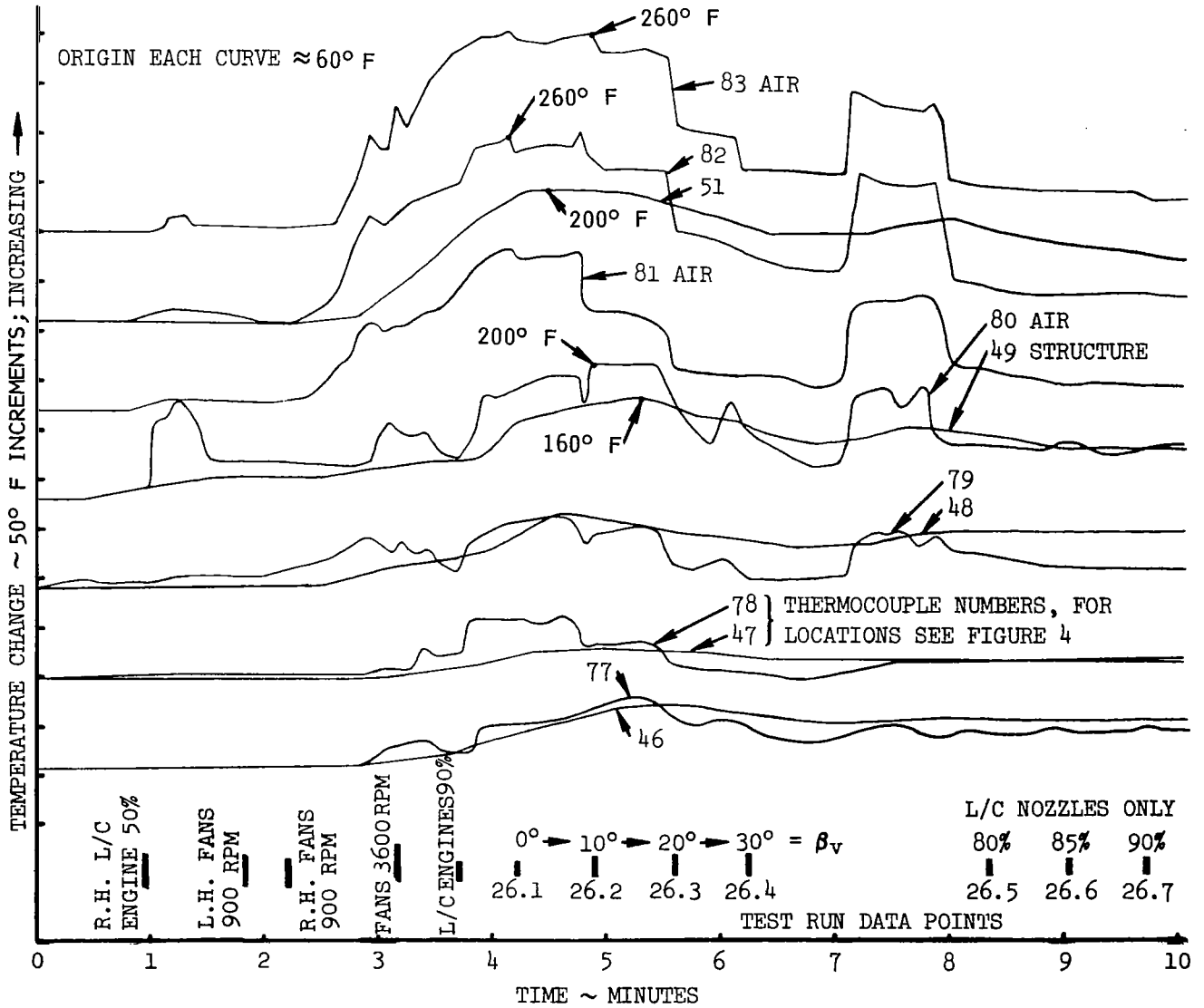

Figure 62. - Side of Fuselage Air and Structure Temperature Traces; δ_N = 30°, h = 9.0 Ft

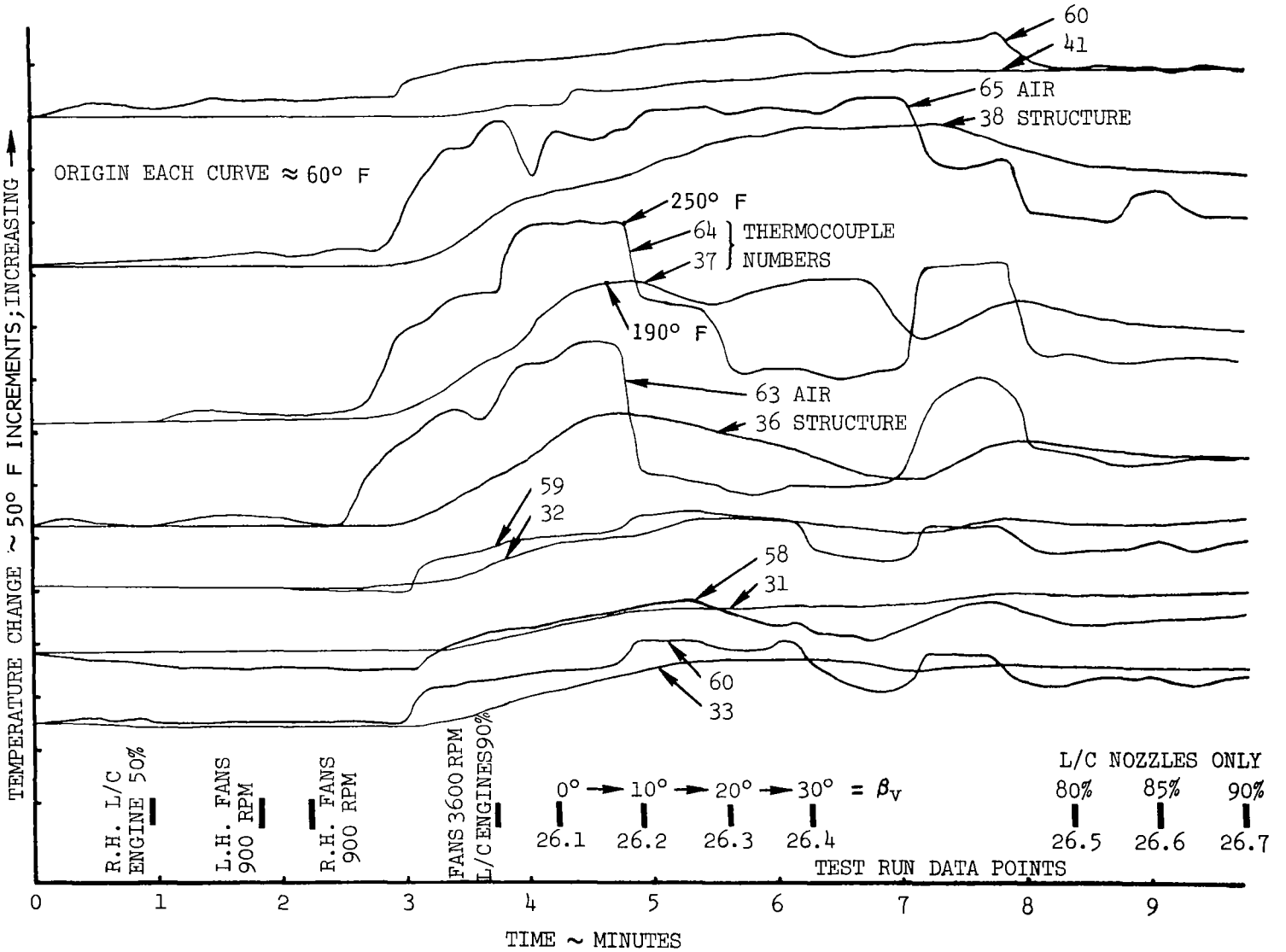

Figure 63. - Wing and Bottom of Fuselage Air and Structure Temperature Traces; $\delta_N = 30°$, h = 9.0 Ft

TABLE I. - LIST OF TEST RUNS

TEST RUN	CONFIGURATION	FAN RPM	β_V (DEGREES)	L/C POWER	δ_H	MODEL HEIGHT	α	VARIABLE	WIND VEL (MPH)	WIND DIR.
1.1 & 1.2	6 Fans	3600	0	0	0°	2.65'	0°			
1.3-1.6	3 R.H. Fans	2000.3000,3500,3800	↓	↓	↓	↓	↓	RPM	↓	↓
1.7-1.10	3 L.H. Fans	↓						↓		
1.11-1.13	6 Fans	2000,3000,3500								
1.14-1.16	↓	3600	10,20,30					β_V		
1.17-1.20		3000	0,10.20,30					↓		
1.21-1.24		2000	↓	↓						
2.1-2.3	L.H. L/C Calib.	0	90	80,90,94%	0°			L/C Pwr	8-12	355°
3.1-3.4	R.H. L/C Calib.	0	↓	80,85,90,95%	↓			↓	8-12	355°
4.1-4.2	6 Fans + L/C	3600	0	1500#/side					1/2-2	300°
5.1-5.6	↓	↓	0,20,30,10	↓		6.0		β_V	1/2	10°
6.1-6.4			↓			2.65		β_V	2-6	340°
7.1-7.4			0,10,20,30			4.45		↓	4-8	270°
8.1-8.6		↓	↓	↓		9.0			0-4	270°
8.7-8.12	6 Fans	3600		0		↓			0-4	270°
9.1-9.4		↓	↓	↓	↓	6.0	↓	↓	0-2	350°
10.1-10.5	6 Fans + L/C	3600	0,10,20,30	1500#/side	15°	2.65			1	10°
10.6-10.8	L/C Calib.	0	0	80,85, & 90%		↓		L/C Pwr	1	10°
11.1-11.4	↓	↓	90°	80.85,90,93%		4.45		↓	0-1/2	340°
11.5-11.8	L/C + 6 Fans	3600	0,10,20,30	1500#/side		↓		β_V	0-1/2	340°
12.1-12.4	L/C Calib.	0	90°	80,85,90,93%		6.0		L/C Pwr	2-3	220°
12.5-12.8	L/C + 6 Fans	3600	0,10,20,30°	1500#/side		↓		β_V	2-3	220°
13.1-13.4	L/C Calib.	0	90°	80,85,90,93%	15°	9.0	0°	L/C Pwr	3	10°
13.5-13.8	L/C + 6 Fans	3600	0,10,20,30	1500#/side				β_V	3	10°
13.9-13.12	6 Fans Only	2000.3000 3500.3700	0°	0				Fan RPM	3	10°
13.13-13.16	↓	3600	0.10.20.30					β_V	3	10°
13.17-13.20	3 R.H. Fan Calib.	2000.3000,3500,3700	0°					Fan RPM	3	10°
13.21-13.24	3 L.H. Fan Calib.	↓	0°	↓				↓	3	10°
14.1-14.4	L/C Calib.	0	90	80,85,90,93%			5°	L/C Pwr	2-3	340°
14.5-14.8	L/C + 6 Fans	3600	10,20,30,0	1500#/side				β_V	4	340°
14.9-14.11	6 Fans Only	2000,3000,3600	0°	0				Fan RPM	2-3	350
14.12-14.14	↓	3600	10.20,30	↓				β_V	2-3	350
15.1-15.4	L/C + 6 Fans	3600	0,10,20,30	1500#/side	30°	4.44	0°	β_V	0	---
15.5-15.7	6 Fans Only	2000,3000,3600	0°	0				Fan RPM	0	---
15.8-15.10	↓	3600	10,20,30	↓				β_V	1	355
15.11-15.14	L/C Eng. Calib.	0	0	80,85,90,93%				L/C Pwr	1-2	0°
16.1-16.3	↓	↓	90°	80,85,90%			5°	↓	1-2	300°
16.4-16.7	L/C + 6 Fans	3600	0,10,20,30	1500#/side				β_V	1	330
16.8-16.11	6 Fans Only	↓	↓	0				↓	1	350
16.12-16.14	6 Fan Calib.	3600,3000,2000	0°	↓				Fan RPM	1	350
17.1-17.4	L/C + 6 Fans	3600	10,20.30,0	1500#/side		6.0	0°	β_V	0-3	40°
18.1-18.4	↓	↓	↓	↓		↓	5°	↓	1	30°→ 90°
19.1-19.4	L.H. L/C Calib.	0	90	80,85,90,93%	0°	9.0	0°	L.H. L/C Pwr	4	25°
19.5-19.8	R.H. L/C Calib.	↓						R.H. L/C Pwr	2	35°
19.9-19.12	L/C Calib. RH & LH	0						L/C Pwr	2	35°
19.13-19.15	L/C + 6 Fans	2000	0°	80,85,93%				L/C Pwr	4	20
19.16-19.18	L/C + 6 Fans	3000 to 3300	0°	80,85,90%	0°	9	0°	L/C Pwr	4	20°
20.1-20.4	↓	3600	10,20,30,0	1500#/side	30°	2.65	0°	β_V	2	350
20.5-20.8	L/C Only	0	10°	80,85,90,93%	↓			L/C Pwr	2	330
21.1-21.2	L/C Only	0	90°	80 & 90%	45°			L/C Pwr	2	330
21.3-21.6	L/C + 6 Fans	3600	10,20,30,0	1500#/side				β_V	4	340
22.1-22.3	L/C Calib.	0	90°	80, 85, 90%	↓	4.45	0	L/C Pwr	2	330
23.1-23.3	L/C + 6 Fans	2000	0°	80,85,90%	0°	2.65	0°		1	180

TABLE I. - LIST OF TEST RUNS - Concluded

TEST RUN	CONFIGURATION	FAN RPM	β_V DEGREES	L/C POWER	δ_F	MODEL HEIGHT	α	VARIABLE	WIND VEL (MPH)	WIND DIR.
23.4-23.6		3000	0°	80,85,90%					0	---
23.7-23.9		3600							0	---
24.1-24.3		2000				4.45	5°		3	320
24.4-24.6		3000							3	320
24.7-24.9		3600							3	320
25.1-25.3		2000				9	5°		12	20°
25.4-25.6		3000							12	20°
25.7-25.9		3600							12	20°
26.1-26.4	L/C + 6 Fans		0,10,20,30	1500#/side	30°	9	0	β_V	0-4	240°
26.5-26.7	L/C Only	0	0°	80, 85, 90%				L/C Pwr	2-4	240
27.1-27.3	L/C Only	0	90°	80,85,90%		9	5°		2	230
28.1-28.4	L/C + 6 Fans	3600	0,10,20,30	1500#/side	45°	9	0°	β_V	1	30
28.5-28.7	L/C Only	0	0	80,85,90%				L/C Pwr	0	---
29.1-29.4	L/C + 6 Fans	3600	0,10,20,30	1500#/side	45°	2.65		β_V	7	350
29.5-29.7	L/C Only	0	0	80,85,90%				L/C Pwr	7-10	0°
30.1-30.4	L/C Only	0	90	80,85,90,93%	0	4.45	5°		9	15°
31.1-31.3	4 Inbd Fans	2000,3000,3600	0	0	0°	2.65	0°	Fan RPM	0	---
31.4-31.6		3600	10,20,30					β_V	0	---
32.1-32.4		3600	0,10,20,30			4.45	5°	β_V	1	260
33.1-33.3		2000,3000,3600	0				0°	Fan RPM	3	190
33.4-33.6		3600	10,20,30					β_V	3	190
34.1-34.3		2000,3000,3600	0			6	0°	Fan RPM	3	190
34.4-34.6		3600	10,20,30					β_V	3	190
35.1-35.3		2000,3000,3600	0			9	0°	Fan RPM	2	180
35.4-35.7		3600	0,10,20,30					β_V	0	---
36.1-36.4		3600	0,10,20,30			9	5°	β_V	1	240
37.1-37.4	2 Inbd Fans	3000	0,10,20,30			9	0°	β_V	0	---
38.1-38.3		2000,3000,3600	0					Fan RPM	8	30°
38.4-38.7		3600	0,10,20,30					β_V	7	40°
39.1-39.3		2000,3000,3600	0			2.65	0°	Fan RPM	9	70°
39.4-39.6		3600	10,20,30					β_V	10	50
40.1-40.4		3600	0,10,20,30			4.44		β_V	12	50
41.1-41.4		3600	0,10,20,30			6		β_V	10	100°
42.1-42.3	6 Fans Aft Wheel Fairings Off	2000,3000,3600	0			2.65		Fan RPM	1	170°
42.4-42.7		3600	0,10,20,30					β_V	1	170°
43.1-43.3		2000,3000,3600	0			9.0	0°	Fan RPM	2	160
43.4-43.6		3600	10,20,30					β_V	2	160
44.1-44.4		3600	0,10,20,30				5°	β_V	2	190
45.1-45.3		2000.3000,3600	0			6	0°	Fan RPM	2	190
45.4-45.6		3600	10,20,30					β_V	2	190
46.1-46.3	6 Fans Aft-Wheel Fairings Off	2000,3000,3600	0°		0°	4.45	0°	Fan RPM	2	180
46.4-46.6		3600	10,20,30					β_V	1	190
47.1-47.4		3600	0,10,20,30				5°		2	140
48.1-48.4			0,10,20,30			6.0	5°	β_V	1	120
49.1-49.4	6 Fans + L/C Wheel Fairing Off	3600	0,10,20,30	1500#/side		2.65	0°	β_V	2	210
50.1-50.4						4.45	0°		2	170
51.1-51.4						6.0	0°		4	170
52.1-52.4						9.0	0°		4	190
53.1-53.4							5°		3	210
54.1-54.4						4.45	5°		2	180
55.1-55.4					75°	2.65	0°		3	200
55.5-55.4			0	85,80%				L/C Pwr	1	180
55.7-55.8		3000,2000		1500#/side				Fan RPM	1	180

TABLE II. - PROPULSION DATA REDUCTION TEST POINT SCHEDULE

Data Test Point	Number of Fans	Fan Speed rpm	Fan Louver Angle β_V , deg	L/C Engine Power	L/C Nozzle Angle δ_N , deg	Ground Height, ft
1-11	6	2000	0	Off	0	2.65
1-12	↓	3000	0	↓	↓	2.65
1-13	↓	3600	0	↓	↓	2.65
1-14	↓	↓	10	↓	↓	2.65
1-15	↓	↓	20	↓	0	2.65
15-7	↓	↓	0	↓	30	4.44
9-1	↓	↓	0	↓	0	6.0
8-9	↓	↓	0	↓	↓	9.0
8-10	↓	↓	10	↓	↓	9.0
8-11	↓	↓	20	Off	↓	9.0
6-1	↓	↓	0	On	↓	2.65
6-4	↓	↓	10	↓	↓	2.65
6-2	↓	↓	20	↓	↓	2.65
7-1	↓	↓	0	↓	↓	4.44
5-1	↓	↓	↓	↓	↓	6.0
8-3	↓	↓	↓	↓	0	9.0
10-2	↓	↓	↓	↓	15	2.65
13-5	6	3600	↓	On	15	9.0
31-1	4	2000	↓	Off	0	2.65
31-2	4	3000	↓	Off	0	2.65
31-3	4	3600	0	Off	0	2.65

Angle of attack and angle of yaw are 0° for all test points.
Four-fan operation includes inboard and center fans in each wing.

TABLE III. - STATIC PRESSURE INSTRUMENTATION AT THE RIGHT-HAND INBOARD, CENTER, AND OUTBOARD FAN INLETS

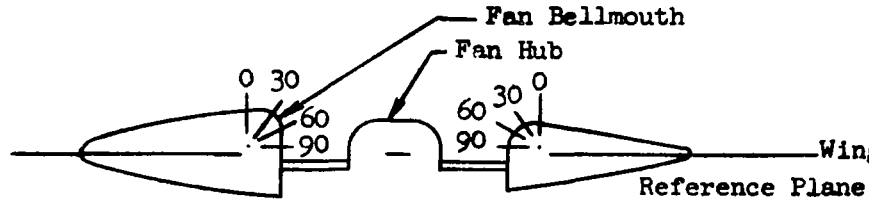

Fan Radian	Bellmouth Angular Location - deg									
	Inboard Fan			Center Fan				Outboard Fan		
θ - deg	0	30	90	0	30	60	90	0	30	90
0	123	124	125	137	138	139	140	161	162	163
20	---	---	---	156	155	154	153	---	---	---
70	---	---	---	---	---	---	---	164	165	166
90	126	127	128	---	---	---	---	---	---	---
110	---	---	---	141	142	143	144	---	---	---
160	---	---	---	---	---	---	---	---	---	167
180	---	---	129	---	---	---	---	---	---	---
200	---	---	---	148	147	146	145	---	---	---
250	---	---	---	---	---	---	---	---	---	135
270	130	131	132	---	---	---	---	---	---	---
290	---	---	---	152	151	150	149	---	---	---
330	---	---	---	---	---	---	---	---	---	134
340	---	---	---	---	---	---	---	168	169	170
Hub Angular Location - deg										
10	---	---	---	---	---	---	133	---	---	---
20	---	---	---	---	---	---	160	---	---	---
70	---	---	---	---	---	---	---	---	---	171
110	---	---	---	---	---	---	157	---	---	---
160	---	---	---	---	---	---	---	---	---	172
200	---	---	---	---	---	---	158	---	---	---
250	---	---	---	---	---	---	---	---	---	173
290	---	---	---	---	---	---	159	---	---	---
340	---	---	---	---	---	---	---	---	---	174

TABLE IV. - TOTAL PRESSURE INSTRUMENTATION AT THE RIGHT-HAND INBOARD, CENTER, AND OUTBOARD FAN EXITS

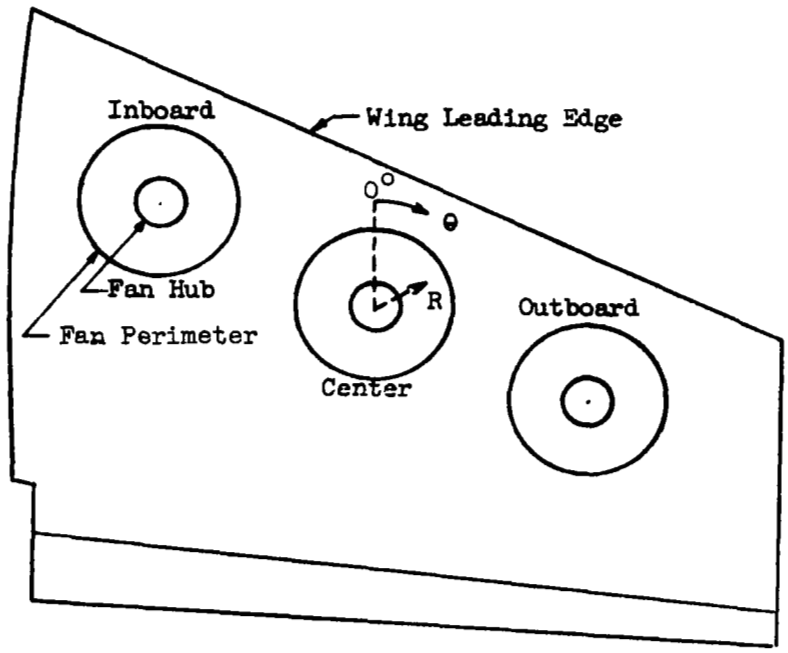

Right Hand Wing

Radius (R) inches	Fan Radian θ - deg											
	Inboard Fan				Center Fan				Outboard Fan			
	0	90	180	270	0	90	180	270	0	90	180	270
9.36	308	309	310	311	332	333	334	335	356	357	358	359
11.42	304	305	306	307	328	329	330	331	352	353	354	355
13.18	300	301	302	303	324	325	326	327	348	349	350	351
14.70	296	297	298	299	320	321	322	323	344	345	346	347
16.10	292	293	294	295	316	317	318	319	340	341	342	343
17.38	288	289	290	291	312	313	314	315	336	337	338	339

TABLE V. - HOT GAS INGESTION DATA

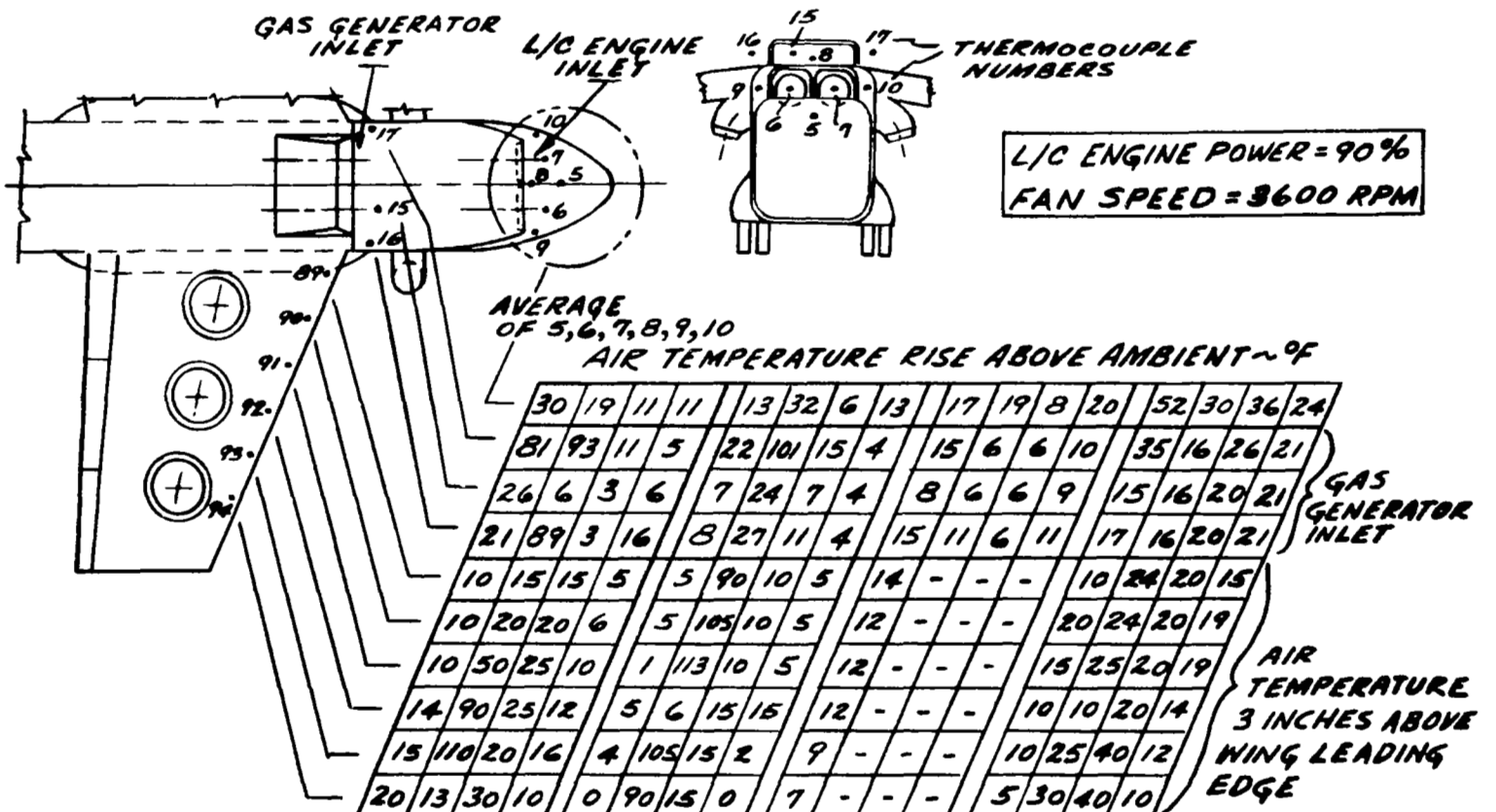

FAN LOUVER ANGLE	0°	10°	20°	30°	0°	10°	20°	30°	0°	10°	20°	30°	0°	10°	20°	30°		
L/C NOZZLE ANGLE	0°				0°				0°				0°					
MODEL HEIGHT	2.65'				4.45'				6.0'				9.0'					
WIND	2-6 MPH				5 MPH				½ MPH				0-4 MPH					
	30	19	11	11	13	32	6	13	17	19	8	20	52	30	36	24		
	81	93	11	5	22	101	15	4	15	6	6	10	35	16	26	21		
	26	6	3	6	7	24	7	4	8	6	6	9	15	16	20	21	GAS GENERATOR INLET	
	21	89	3	16	8	27	11	4	15	11	6	11	17	16	20	21		
	10	15	15	5	5	90	10	5	14	-	-	-	10	24	20	15		
	10	20	20	6	5	105	10	5	12	-	-	-	20	24	20	19		
	10	50	25	10	1	113	10	5	12	-	-	-	15	25	20	19	AIR TEMPERATURE 3 INCHES ABOVE WING LEADING EDGE	
	14	90	25	12	5	6	15	15	12	-	-	-	10	10	20	14		
	15	110	20	16	4	105	15	2	9	-	-	-	10	25	40	12		
	20	13	30	10	0	90	15	0	7	-	-	-	5	30	40	10		

TABLE V. - HOT GAS INGESTION DATA - Continued

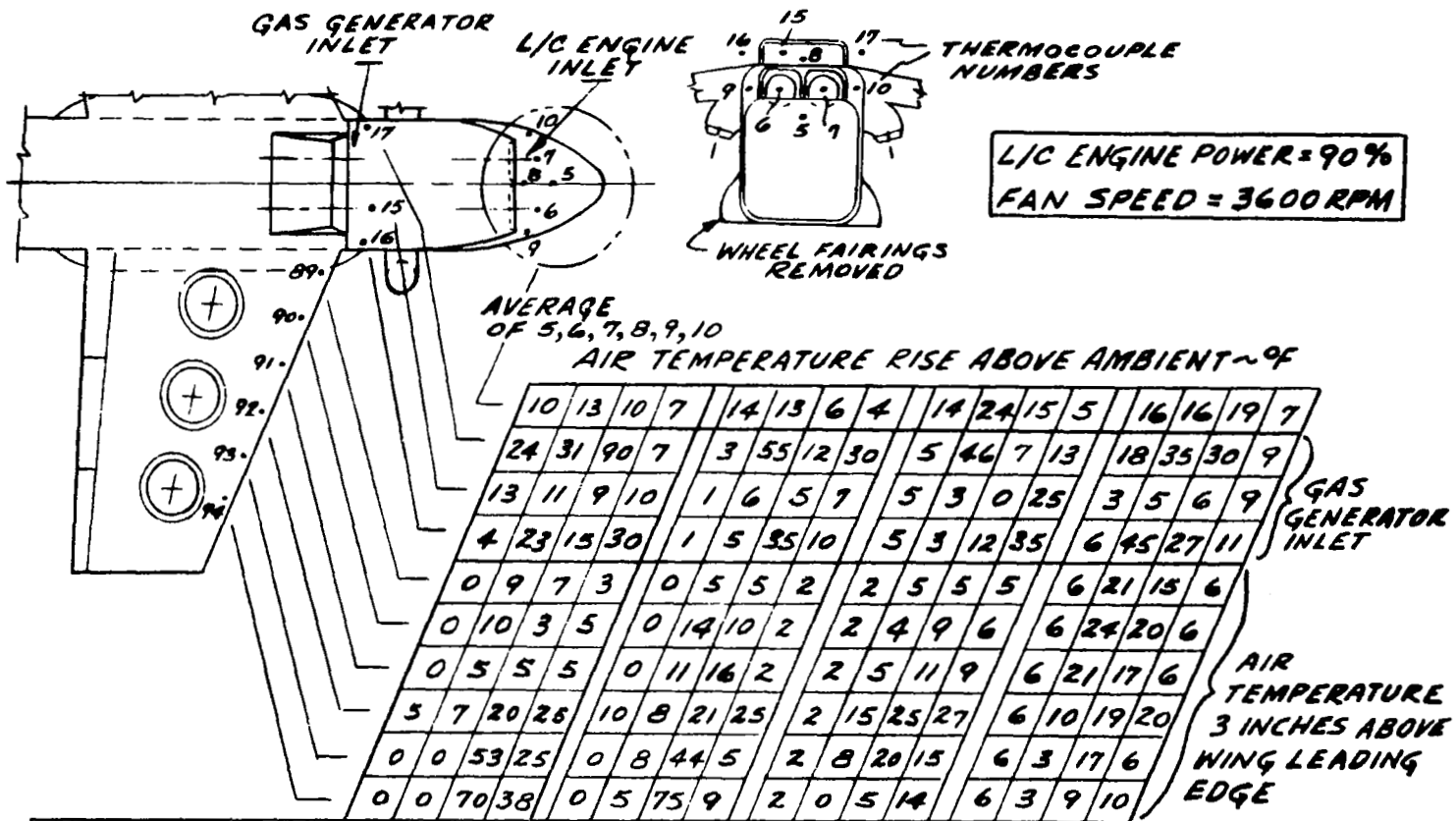

10	13	10	7	14	13	6	4	14	24	15	5	16	16	19	7
24	31	90	7	3	55	12	30	5	46	7	13	18	35	30	9
13	11	9	10	1	6	5	7	5	3	0	25	3	5	6	9
4	23	15	30	1	5	35	10	5	3	12	35	6	45	27	11
0	9	7	3	0	5	5	2	2	5	5	5	6	21	15	6
0	10	3	5	0	14	10	2	2	4	9	6	6	24	20	6
0	5	5	5	0	11	16	2	2	5	11	9	6	21	17	6
5	7	20	26	10	8	21	25	2	15	25	27	6	10	19	20
0	0	53	25	0	8	44	5	2	8	20	15	6	3	17	6
0	0	70	38	0	5	75	9	2	0	5	14	6	3	9	10

FAN LOUVER ANGLE	0°	10°	20°	30°	0°	10°	20°	30°	0°	10°	20°	30°	0°	10°	20°	30°
L/C NOZZLE ANGLE	0°				0°				0°				0°			
MODEL HEIGHT	2.65'				4.45'				6.0'				9.0'			
WIND	12 MPH				12 MPH				14 MPH				14 MPH			

TABLE V. - HOT GAS INGESTION DATA - Continued

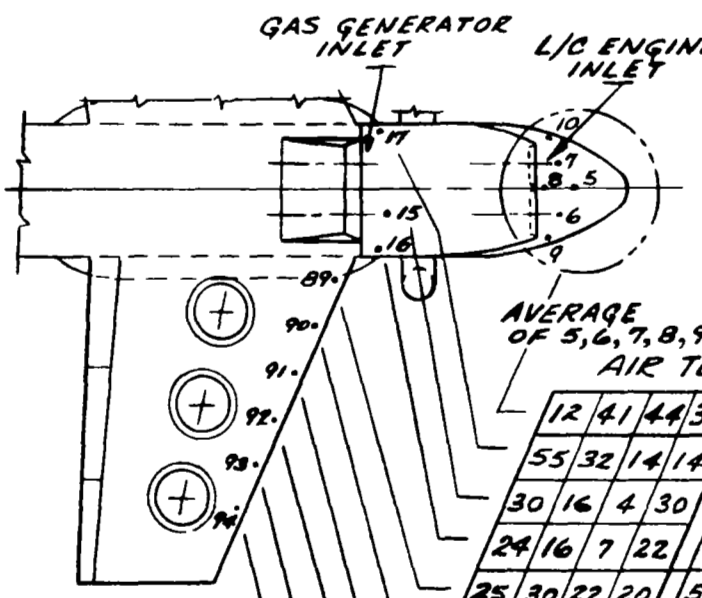

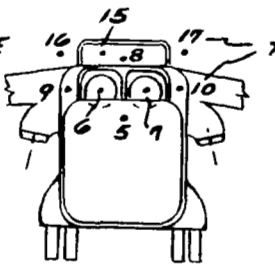

L/C ENGINE POWER = 90 %
FAN SPEED = 3600 RPM

AVERAGE OF 5,6,7,8,9,10

AIR TEMPERATURE RISE ABOVE AMBIENT ~ °F

12	41	44	34	18	25	13	1	78	32	17	33	56	14	33	5	
55	32	14	14	0	2	0	7	50	0	8	5	15	5	13	4	
30	16	4	30	6	2	4	4	85	14	5	5	40	15	10	5	GAS GENERATOR INLET
24	16	7	22	17	7	10	2	105	12	2	5	65	10	6	9	
25	30	22	20	50	30	10	6	80	10	5	5	65	10	10	9	
45	76	50	20	40	55	10	6	90	10	5	3	55	10	9	5	
-	-	-	-	40	65	10	6	95	10	3	2	45	5	5	5	AIR TEMPERATURE 3 INCHES ABOVE WING LEADING EDGE
-	-	-	-	30	-	-	-	-	-	-	-	-	-	-	-	
124	85	20	5	27	45	6	5	85	10	1	1	55	20	4	4	
120	85	0	5	45	80	6	5	90	60	1	0	50	32	1	1	

FAN LOUVER ANGLE	0°	10°	20°	30°	0°	10°	20°	30°	0°	10°	20°	30°	0°	10°	20°	30°	TEST CONDITIONS
L/C NOZZLE ANGLE	15°				15°				15°				15°				
MODEL HEIGHT	2.65'				4.45'				6.0'				9.0'				
WIND	1 MPH				1/2 MPH				2MPH				3MPH				

TABLE V. - HOT INGESTION DATA - Continued

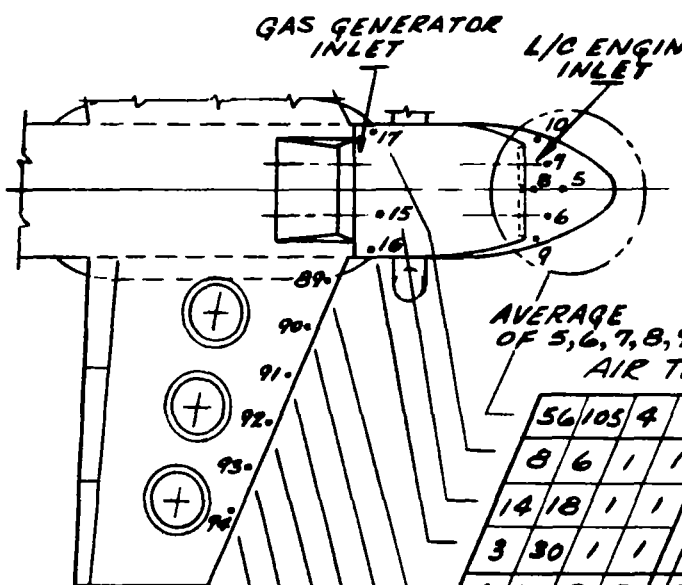

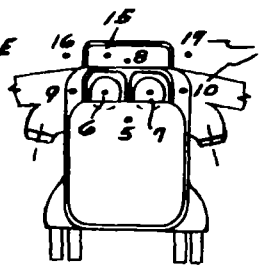

L/C ENGINE POWER = 90 %
FAN SPEED = 3600 RPM

AVERAGE OF 5, 6, 7, 8, 9, 10

AIR TEMPERATURE RISE ABOVE AMBIENT ~ °F

56	105	4	3	15	3	2	4	53	0	0	0	23	48	6	0	
8	6	1	1	42	22	5	5	80	5	3	0	5	25	3	2	GAS GENERATOR INLET
14	18	1	1	14	10	5	5	5	1	0	0	1	22	4	2	
3	30	1	1	15	5	5	5	30	1	0	0	3	32	5	2	
4	33	8	3	30	7	5	5	10	7	5	4	1	18	10	5	
3	58	8	3	29	5	5	5	9	6	5	4	1	20	18	4	
7	48	5	3	11	2	5	5	5	4	3	2	1	19	6	1	AIR TEMPERATURE 3 INCHES ABOVE WING LEADING EDGE
-	-	-	-	-	-	-	-	-	-	-	-	-	-	-	-	
83	42	3	0	4	3	5	3	9	2	2	1	1	0	4	3	
97	58	2	0	11	3	5	3	10	0	0	0	1	0	4	3	

FAN LOUVER ANGLE	0°	10°	20°	30°	0°	10°	20°	30°	0°	10°	20°	30°	0°	10°	20°	30°	TEST CONDITIONS
L/C NOZZLE ANGLE	30°				30°				30°				30°				
MODEL HEIGHT	2.65'				4.45'				6.0'				9.0'				
WIND	2 MPH				NONE				NONE				NONE				

TABLE V. - HOT GAS INGESTION DATA - Continued

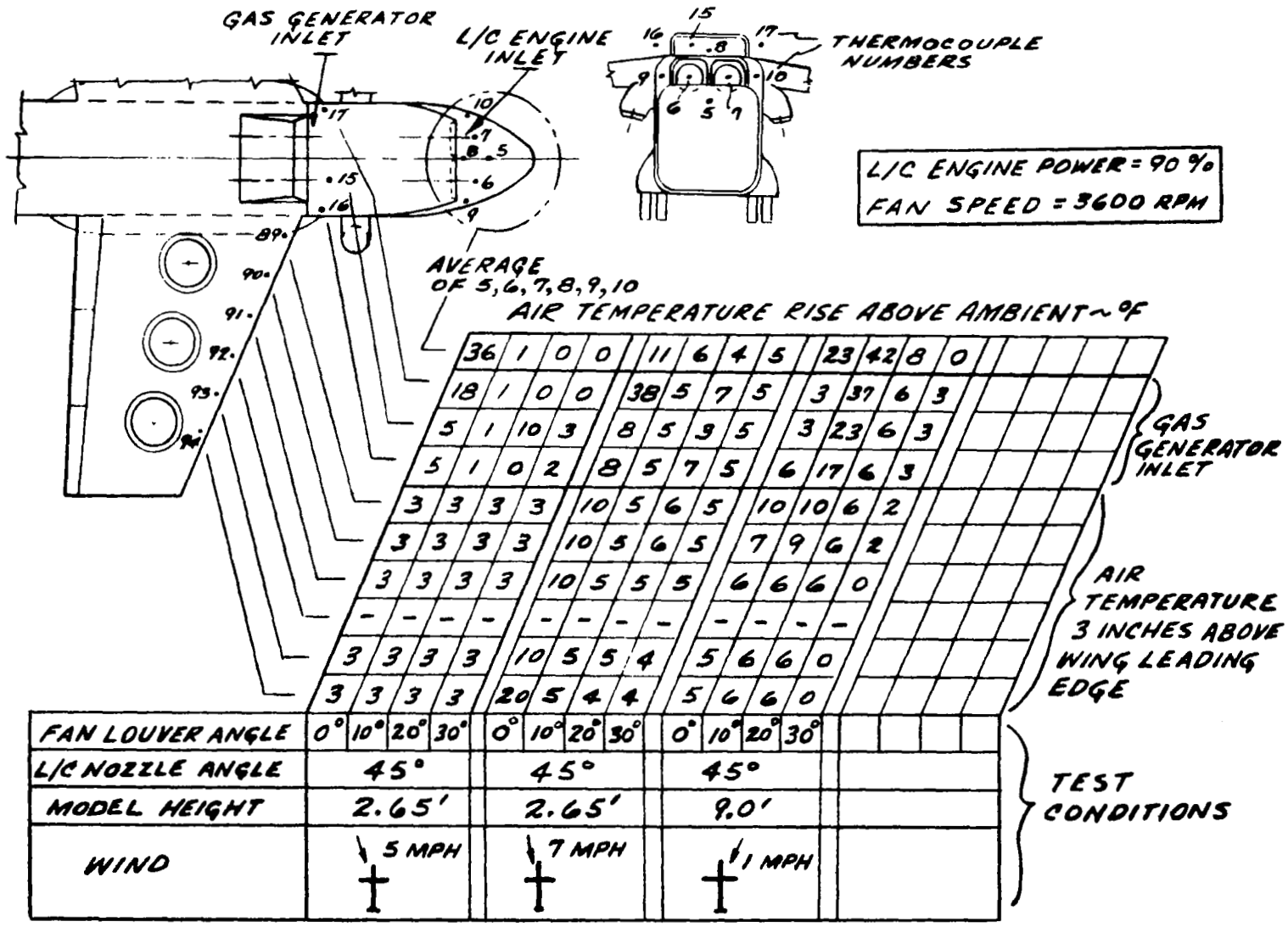

FAN LOUVER ANGLE	0°	10°	20°	30°	0°	10°	20°	30°	0°	10°	20°	30°
L/C NOZZLE ANGLE	45°				45°				45°			
MODEL HEIGHT	2.65′				2.65′				9.0′			
WIND	5 MPH				7 MPH				1 MPH			
89°	36	1	0	0	11	6	4	5	23	42	8	0
90°	18	1	0	0	38	5	7	5	3	37	6	3
91°	5	1	10	3	8	5	3	5	3	23	6	3
92°	5	1	0	2	8	5	7	5	6	17	6	3
93°	3	3	3	3	10	5	6	5	10	10	6	2
94°	3	3	3	3	10	5	6	5	7	9	6	2
	3	3	3	3	10	5	5	5	6	6	6	0
	-	-	-	-	-	-	-	-	-	-	-	-
	3	3	3	3	10	5	5	4	5	6	6	0
	3	3	3	3	20	5	4	4	5	6	6	0

TABLE V. - HOT GAS INGESTION DATA - Continued

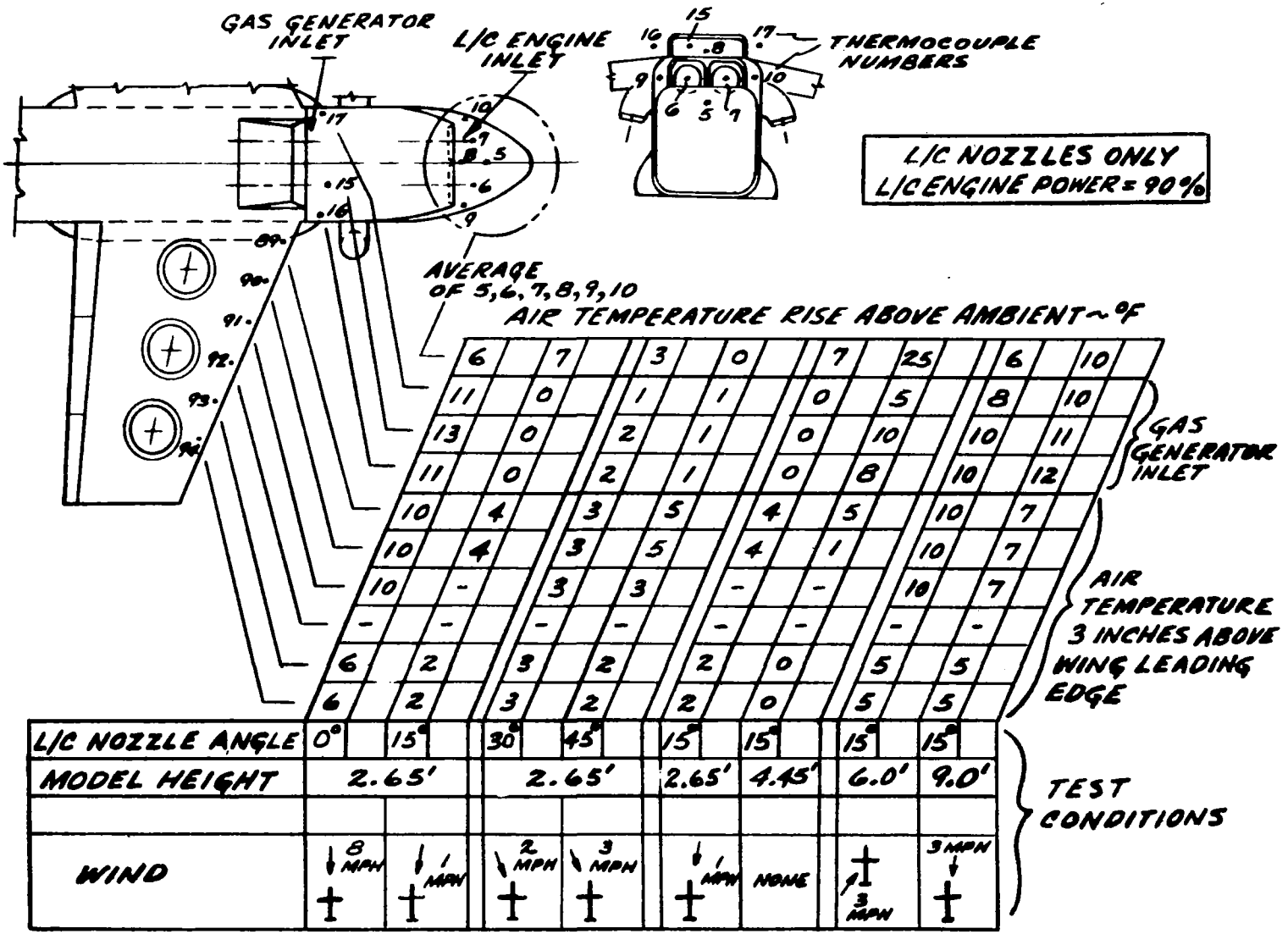

	6	7	3	0	7	25	6	10				
	11	0	1	1	0	5	8	10				
	13	0	2	1	0	10	10	11				
	11	0	2	1	0	8	10	12				
	10	4	3	5	4	5	10	7				
	10	4	3	5	4	1	10	7				
	10	-	3	3	-	-	10	7				
	-	-	-	-	-	-	-	-				
	6	2	3	2	2	0	5	5				
	6	2	3	2	2	0	5	5				
L/C NOZZLE ANGLE	0°	15°	30°	45°	15°	15°	15°	15°				
MODEL HEIGHT	2.65'		2.65'		2.65'	4.45'	6.0'	9.0'				
WIND	8 MPH	1 MPH	2 MPH	3 MPH	1 MPH	NONE	3 MPH	3 MPH				

TABLE V. - HOT GAS INGESTION DATA - Concluded

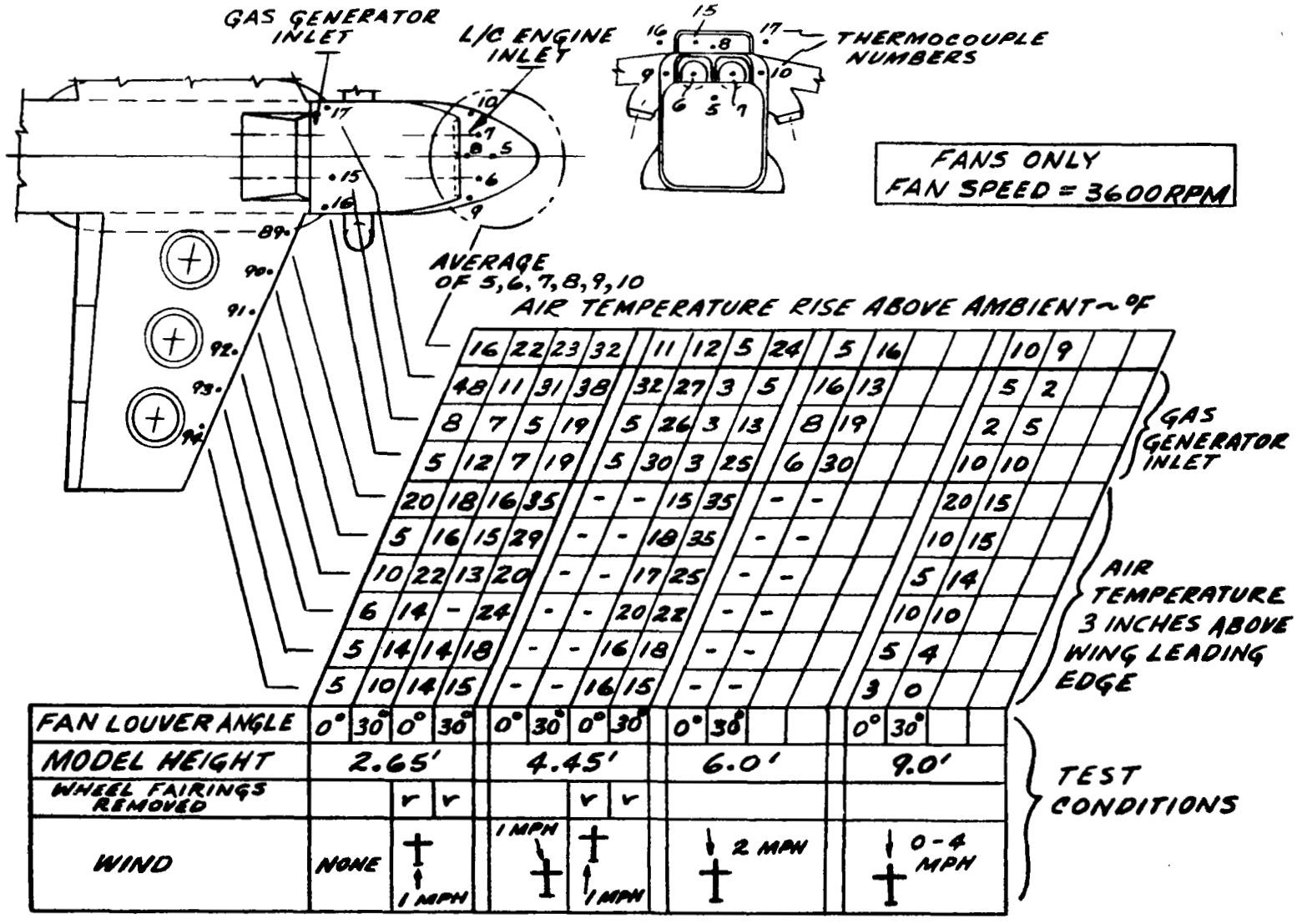

89°	16	22	23	32	11	12	5	24	5	16			10	9		
90°	48	11	31	38	32	27	3	5	16	13			5	2		
91°	8	7	5	19	5	26	3	13	8	19			2	5		
92°	5	12	7	19	5	30	3	25	6	30			10	10		
93°	20	18	16	35	-	-	15	35	-	-			20	15		
94°	5	16	15	29	-	-	18	35	-	-			10	15		
	10	22	13	20	-	-	17	25	-	-			5	14		
	6	14	-	24	-	-	20	22	-	-			10	10		
	5	14	14	18	-	-	16	18	-	-			5	4		
	5	10	14	15	-	-	16	15	-	-			3	0		
FAN LOUVER ANGLE	0°	30°	0°	30°	0°	30°	0°	30°	0°	30°			0°	30°		
MODEL HEIGHT	2.65'				4.45'				6.0'				9.0'			
WHEEL FAIRINGS REMOVED			r	r			r	r								
WIND	NONE		1 MPH		1 MPH		1 MPH		2 MPH				0-4 MPH			

TABLE VI. - FLOW FIELD PRESSURE DATA

		RAKE LOCATIONS FIGURE 8(a)						RAKE LOCATIONS FIGURE 8(b)										
	TEST RUN DATA POINTS	1.11	1.12	1.14	1.15	4.2	5.1	6.1	6.4	7.1	7.2	8.4	8.3	10.1	11.5	12.5	13.5	51.1
	PRESSURE PROBES	PRESSURE READINGS IN PSF UNITS																
	436	0	0	3	3	-3	3	14	-6	-15	-3	51	26	-6	3	-25	-6	-30
2 FT	437	-3	0	0	3	-3	3	3	-6	-15	-3	31	14	-6	5	-8	-3	-27
VERTICAL	438	-3	0	0	3	-6	3	0	0	-9	-6	54	23	-6	3	58	3	-24
RAKE	439	0	0	0	3	0	3	-16	0	0	-3	51	29	-9	5	69	8	-9
	440	3	20	6	3	19	14	16	8	11	3	71	17	6	15	22	17	3
	441	17	48	25	6	60	39	22	11	17	11	-3	26	14	30	19	31	18
	442	0	3	0	3	-3	3	3	0	-3	-3	-31	-20	0	22	55	-6	-6
2 FT	443	0	3	-3	0	0	3	3	0	0	-6	17	3	0	20	63	-6	-6
VERTICAL	444	0	6	-3	6	-3	3	14	6	17	8	-23	14	3	3	38	0	-3
RAKE	445	0	8	-3	6	6	6	16	0	33	22	99	37	14	5	-5	3	6
	446	0	3	-3	11	3	14	60	39	98	81	148	57	11	15	52	11	38
	447	17	40	20	17	59	50	218	220	234	223	182	82	28	25	85	20	89
	410	-3	0	0	0	-6	-3	117	139	48	42	94	3	-3	12	38	-17	15
	411	-3	0	0	0	-6	-3	232	254	92	83	57	0	43	27	74	-8	30
	412	-3	0	0	0	-3	-3	169	196	119	83	96	-3	160	64	71	11	42
	413	-3	0	0	0	-3	-3	41	63	75	66	105	0	288	130	11	17	39
6 FT	414	-3	0	0	0	-3	-3	-3	41	18	36	85	-26	374	180	93	25	21
HORIZONTAL	415	-3	0	0	0	-3	-3	-33	11	-12	12	82	-17	239	197	167	34	-21
RAKE	416	-3	0	0	0	-3	-3	-47	-6	-36	-6	71	-26	74	145	184	42	-36
	417	-3	0	0	0	-3	-3	-49	-6	-51	-12	74	-28	11	89	77	42	-50
	418	-3	0	0	0	-3	-3	-49	-6	-57	-12	51	-11	-14	17	0	45	-53
	419	-3	0	0	0	-3	-3	-46	-6	-48	-9	45	-6	-11	20	36	48	-48
	420	-3	6	0	0	0	-3	-46	-6	-42	-9	31	0	-11	3	41	36	-39
	421	9	31	0	0	34	11	-36	-6	-36	-9	23	-9	-11	-8	44	8	-33
	422	34	85	28	0	110	39	-20	-6	-15	-6	62	-6	-11	-10	-36	3	-15
	423	0	3	3	0	0	0	3	-6	-9	-12	-3	8	-19	-42	-52	-17	-15
	424	0	0	3	0	0	-3	3	-6	-9	-12	62	-3	-9	-17	19	-20	-12
	425	0	14	3	0	26	3	11	-6	-9	-12	68	-6	-3	-15	49	-17	-12
	426	31	74	11	0	115	25	11	-6	-12	-12	-11	-3	-6	0	36	-17	-12
6 FT	427	40	93	68	0	146	64	14	-6	-12	-9	48	-8	-9	-27	36	-14	-12
HORIZONTAL	428	37	82	110	0	126	102	8	-6	-12	-9	65	11	-3	-27	3	-11	-12
RAKE	429	40	90	40	0	141	116	0	-6	-12	-6	57	26	-3	-10	41	-11	-12
	430	34	82	6	-6	93	91	0	-6	-9	-3	57	11	0	0	69	-14	-12
	431	6	9	-9	-20	9	39	-6	-3	-6	0	17	-3	-6	5	19	-20	-12
	432	-16	-34	-23	-20	-30	0	3	-6	-6	0	45	23	-6	5	-44	-17	-12
	433	-3	-6	-31	-20	-11	-6	-3	-6	-10	-6	48	-6	-6	3	27	-20	-12
	434	20	48	0	-9	59	6	-8	-6	-24	-9	43	14	-11	-10	44	-25	-18
	435	22	56	59	8	75	33	-11	-8	-30	-9	-40	17	-11	-3	41	-25	-21
	400	0	-3	0	0	9	6	40	14	3	3	3	50	3	18	-	3	13
	401	0	-6	0	0	0	14	20	14	21	0	9	26	9	16	-	0	65
	402	-3	-9	-3	-3	-9	0	-3	-20	-3	-3	3	35	-12	0	-	0	0
LOCATION	403	0	6	-6	-3	20	3	11	17	19	9	29	-6	23	18	-	-9	16
ON	404	6	9	-27	6	23	6	23	0	12	6	6	12	9	21	-	14	-13
MODEL	405	0	0	0	0	0	0	9	-6	-3	0	3	0	-3	23	-	-9	-3
	406	0	-3	0	3	0	0	3	-6	-3	-3	9	29	-3	21	-	-3	-3
	407	0	-6	-3	0	-3	-3	-6	-6	-3	0	-3	9	-6	-3	-	-6	-3
	408	9	21	29	0	41	26	32	14	40	9	32	65	49	31	-	20	-
	409	0	-3	0	0	0	0	-3	-3	-3	-3	20	44	-3	0	-	-3	0
MODEL HEIGHT, FT		2.65	2.65	2.65	2.65	2.65	6.0	2.65	2.65	4.45	4.45	9.0	9.0	2.65	4.45	6.0	9.0	6.0
FAN RPM		2000	3000	3600	3600	3600	3600	3600	3600	3600	3600	3600	3600	3600	3600	3600	3600	3600
FAN LOUVER ANGLE, β_V		0	0	10	20	0	0	0	10	0	10	10	0	0	0	0	0	0
NOZZLE ANGLE, δ_N		-	-	-	-	0	0	0	0	0	0	0	0	15	15	15	15	0

NATIONAL AERONAUTICS AND SPACE ADMINISTRATION
WASHINGTON, D. C. 20546

OFFICIAL BUSINESS

FIRST CLASS MAIL

POSTAGE AND FEES PAID
NATIONAL AERONAUTICS AN
SPACE ADMINISTRATION

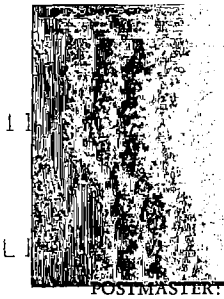

POSTMASTER: If Undeliverable (Section 15 Postal Manual) Do Not Retu

"The aeronautical and space activities of the United States shall be conducted so as to contribute . . . to the expansion of human knowledge of phenomena in the atmosphere and space. The Administration shall provide for the widest practicable and appropriate dissemination of information concerning its activities and the results thereof."

— NATIONAL AERONAUTICS AND SPACE ACT OF 1958

NASA SCIENTIFIC AND TECHNICAL PUBLICATIONS

TECHNICAL REPORTS: Scientific and technical information considered important, complete, and a lasting contribution to existing knowledge.

TECHNICAL NOTES: Information less broad in scope but nevertheless of importance as a contribution to existing knowledge.

TECHNICAL MEMORANDUMS: Information receiving limited distribution because of preliminary data, security classification, or other reasons.

CONTRACTOR REPORTS: Scientific and technical information generated under a NASA contract or grant and considered an important contribution to existing knowledge.

TECHNICAL TRANSLATIONS: Information published in a foreign language considered to merit NASA distribution in English.

SPECIAL PUBLICATIONS: Information derived from or of value to NASA activities. Publications include conference proceedings, monographs, data compilations, handbooks, sourcebooks, and special bibliographies.

TECHNOLOGY UTILIZATION PUBLICATIONS: Information on technology used by NASA that may be of particular interest in commercial and other non-aerospace applications. Publications include Tech Briefs, Technology Utilization Reports and Notes, and Technology Surveys.

Details on the availability of these publications may be obtained from:

SCIENTIFIC AND TECHNICAL INFORMATION DIVISION

NATIONAL AERONAUTICS AND SPACE ADMINISTRATION

Washington, D.C. 20546